ABSTRACT

Title of Document:	1/f NOISE AND LUTTINGER LIQUID PHENOMENA IN CARBON NANOTUBES David Andrew Tobias, Doctor of Philosophy, 2007
Directed By:	Associate Professor Michael S. Fuhrer and Professor Christopher J. Lobb, Department of Physics

Carbon nanotubes (CNTs) provide an ideal medium for testing the behavior of one-dimensional electron systems and are promising candidates for electronic applications such as sensors or field-effect transistors. This thesis describes the use of low frequency resistance fluctuations to measure both the properties of the one-dimensional electron system in CNTs, and the sensitivity of CNT devices to their environment.

Low frequency noise was measured in CNTs in field effect transistor (FET) geometry. CNTs have a large amount of surface area relative to their volume and are expected to be strongly affected by their environment, leading to speculation that CNTs should have large amounts of 1/f noise. My measurements indicate that the noise level is in the same range as that of traditional FETs, an encouraging result for possible electronic applications. The temperature dependence of 1/f noise from 1.2 K to 300 K can be used to extract the characteristic energies of the fluctuators

responsible for the noise. The characteristic energies allows for the elimination of structural and electronic transitions within the CNT itself as possible sources of 1/f noise in CNTs, leaving the motion of defects in the gate dielectric, or possibly strongly physisorbed species, as the likely culprits.

Another form of low frequency noise found in CNTs is random telegraph signal (RTS), which manifests as the alternation between two current states at a stable voltage bias. In CNTs, this phenomenon occurs due to the tunneling of electrons into and out of the CNT from a nearby defect, and thus provides a way to probe the tunneling density of states of the CNT itself. The tunneling density of states in turn provides information on the strength of the electron-electron interaction in CNTs. Due to the one-dimensional structure of CNTs their electronic state is expected to be a Luttinger liquid, which should manifest as a power-law suppression of the tunneling density of states at the Fermi energy. The power law exponent is measured in both the temperature dependence and energy dependence of the tunneling rates. In agreement with theory, the power-law exponent is significantly larger in semiconducting CNTs than found in previous experiments on metallic CNTs. The RTS can also be used as a "defect thermometer" to probe the electron temperature of the CNT. The effect of the bias voltage on the electron temperature provides a means to determine the energy relaxation length for the electrons in the CNT.

1/f NOISE AND LUTTINGER LIQUID PHENOMENA IN CARBON NANOTUBES

By

David Andrew Tobias

Dissertation submitted to the Faculty of the Graduate School of the
University of Maryland, College Park, in partial fulfillment
of the requirements for the degree of
Doctor of Philosophy
2007

Advisory Committee:
Associate Professor Michael S. Fuhrer, Chair/Co-Advisor
Professor Christopher J. Lobb, Co-Advisor
Professor Richard Greene
Professor James R. Anderson
Professor Romel Gomez

Dedication

To my father and my uncle: James and William Tobias.

Acknowledgements

I feel fortunate to have worked with wonderful people while at the University of Maryland. My first year here I realized that you learn the most from solving the homework with other students and a parallel certainly exists in the lab. I would like to thank all of the students that have helped me while here at Maryland. This list is long as many people have made Maryland a great place while I was here.

Christopher Lobb called me while I was still an undergrad at Case and asked whether I was interested in coming to Maryland, so I asked if I could work in his lab for the summer before starting classes in grad school. That was the beginning of working for him and Frederick Wellstood in the sub-sub basement of the Center for Superconductivity Research. Later I switched to nanotube research, where I was fortunate to have Michael Fuhrer become my co-advisor. All three are both excellent scientists and great advisors. Any graduate student would be lucky to work with them and the wonderful environment in their labs starts with them. They have made me a better scientist, speaker and writer. I would also like to thank my committee of Bob Anderson, Richard Greene and Romel Gomez.

I first worked with Matthew Kenyon on the single electron transistor microscope. He initiated me into the rites of working in the lab: from lithography to plumbing to left coast thinking. Hadley Lawler and Hanhee Paik brought new dimensions to working in the sub-basement and knowledge of the Korean language (mostly from Hanhee). After switching to nanotubes, Tobias Durkop introduced me to growing nanotubes and provided insight on how to always get your way for a lunch destination. Todd Brintlinger taught me how to “find and wire” the tubes and taught

me to play pool. Yung-Fu Chen was a constant source of information on what to expect from my devices and how to understand them, and possessed a truly kind soul. Gokhan Esen provided invaluable help with running the cryostat and taking measurements, and was an excellent deskmate and commiserator. Finally, Masahiro Ishigami joined me in investigating the low frequency noise in nanotubes, and added energy and vocabulary to the second floor of the physics building.

Special thanks go to Paola Barbara and Alexander Tselev at Georgetown for providing the samples that were used for the data in this thesis. No one can ever be thanked enough for samples.

Doug Bensen and Brian Straughn helped with all sorts of experimental difficulties. Belta Pollard and Margaret Lukomska helped with smoothing out traveling and purchasing. Jane Hessing is a blessing to the grad students at Maryland and has helped me more times than I can remember. Bob Dahms and Jesse Anderson have also gone beyond the call many times. The electronics and machine shop have also helped me fix my experiments.

I was fortunate to be a classmate with Samir Garzon. He taught me most of what I know about quantum mechanics and I wouldn't have passed the qualifier without him. Joshua Higgins joined me in the Center after being a class mate and has been a great friend since. Betsy Pugel has more fire than ten physicists need.

In addition to the people that worked directly with me on my projects, I was blessed to work in the sub-basement with a cohesive group of people that made physics a truly collaborative experience. The center is a great place to work due to the opportunity to walk into any lab and find someone there to help you out. It also

makes Maryland feel like a smaller place. Erin Fleet, Guy Chatraphorn, Gus Vlahacos and Aaron Nielsen helped give me a push at the start with their SQUID microscopy knowledge. Su-Young Lee was the most tenacious physicist and also the funniest. Doug Strachan provided provocative conversation and fundamental knowledge of superconductivity and dip testing. Branimir Vasilic showed me how to transfer helium and what in physics was trivial. Matt Sullivan was a MacGyver of experimental physics, and always there to throw the disc. Monica Lilly was the greatest undergraduate to ever work in a lab.

The quantum computing team helped me despite their need to constantly fight terrorism. Andrew Berkley was a post-doc from birth and pushed me to know more about what I was doing. Huizhong Xu followed that up by somehow being an even more amazing scientist and a great hot dogger. Sudeep Dutta showed me how great our lab was and how fortunate I am to be at Maryland. Rupert Lewis and Tauno Palomaki were even able to crack jokes while carrying the burden of fighting crime.

After switching to Fuhrer's lab I was fortunate to continue my streak of good co-workers. Stephanie Getty helped to make me a part of the group and Anthony Ayari proved that French people can have a good sense of humor, too. Dan Lenski and Enrique Cobas have answered too many questions about computers. Adrian Southard got me onto a soccer field again. Tarek Ghanem introduced me to Tabir. Alexandra Curtin was great for all sorts of arguments and for frisbee weekends. Sungjae Cho reminded me of my beginning as a grad student. Finally Kristen Burson made sure these acknowledgements got written.

Thanks to Jianhao Chen for making samples that were used in the low frequency noise measurements done by Masa. Winston Yang was a wonderful summer addition to the lab and a motivated youngster with a bright future. Elba Gomar Nadal brought an outsider's view to the physics department and was a great lunch, hiking and beer-drinking partner.

I also had many great roommates as a student at Maryland. Aaron Nielsen brought me into a "luxury" townhouse where I lived with DJ Patil, David Sweet, Yao-Chin Chao, Sarah Boettcher and Evelyn Boettcher over my grad school years. Living with someone creates a kind of friendship that can not be developed any other way and these are great friends that have lead to salmon fests, bhangra and to a trip to the other side of the world.

I would like to thank my family for supporting my decision to get a PhD. If I ever doubt my luck in life, I remember them.

Finally, I would like to thank Silvia for putting up with me through the stress of finishing my degree.

Table of Contents

List of Tables

List of Figures

Chapter 1 Introduction to carbon nanotubes

1.1 Carbon nanotube overview

Carbon nanotubes (CNTs) are hollow tube-shaped structures with all of the carbon atoms bonded together by sp^2 bonds in a honeycomb lattice identical to that of graphene. Conceptually, the CNT may be thought of as a single sheet of graphite (termed graphene) curved into a seamless cylinder. These structures were first identified by Ijima[1]. Initially the CNTs were exclusively multi-walled, meaning that they consisted of several concentric cylinders. Future researchers were able to develop methods capable of producing single-walled CNTs of varying lengths[2-4], and some CNTs have been grown that are centimeters in length[5, 6]. CNTs have diameters from just under a nanometer[4] to dozens of nanometers[1] and hence have very large aspect ratios.

CNTs are characterized by many impressive properties. Individually they have extremely high mechanical rigidity and toughness, leading to many hypothetical applications for ropes and fibers[7], including the famous (or infamous) space elevator[8]. Networks of CNTs have been found to have numerous interesting properties including the ability to form fire resistant material[9] and liquid crystal suspensions[10]. CNTs also have a powerful Van der Waals attraction[11] with surfaces allowing them to be used as an adhesive material between paint and plastics[12].

One of the main interesting properties of CNTs chemically and electronically is that every atom is a surface atom, and is electronically “in series” with every other atom in the CNT. This could be useful for creating chemical sensors that are able to detect very low amounts of contaminants[13]. This also leads to concerns about fluctuations and noise in CNTs[14]. CNTs can also be functionalized by many interesting molecules[15], including DNA[16], in the hope of enabling bottom-up construction of micro- and nano-structures.

CNTs also have fascinating electrical properties that derive from their graphene origin, as discussed below. CNTs are either semiconducting or metallic[17-20], depending upon the relative direction of the CNT axis with respect to the graphene lattice. Obviously this and their nanoscale size makes them a speculative candidate for future electronics technologies, but as of now the difficulty of producing, orienting and contacting the CNTs has slowed the realization of this application. However, individual single electron transistors[21] , high mobility transistors[22] and other electronic devices have been realized using CNTs.

In one dimension, electrostatic interactions between electrons are strong, and the electrons form a correlated state termed the Luttinger liquid[23-25] (LL). This state of the electrons differs in many ways from that found in bulk conductors where the electrons are able to re-arrange themselves easily to reduce the energy of the interaction amongst them. This state should only exist in 1-D materials and thus CNTs offer an excellent opportunity to study LL physics.

1.2 Electronic band Structure

The ability of CNTs to form metallic and semiconducting devices derives from the band structure of graphene[26-28]. As mentioned above, CNTs can be thought of as strips of graphene sheets that are rolled up to form a seamless cylinder. The CNT will have different properties depending upon its helicity and diameter. Graphene is a honeycomb lattice, a two dimensional hexagonal Bravais lattice, with a basis of two carbon atoms as seen in Fig. 1-1. The distance between nearest neighbors in the carbon lattice is 0.142 nm.

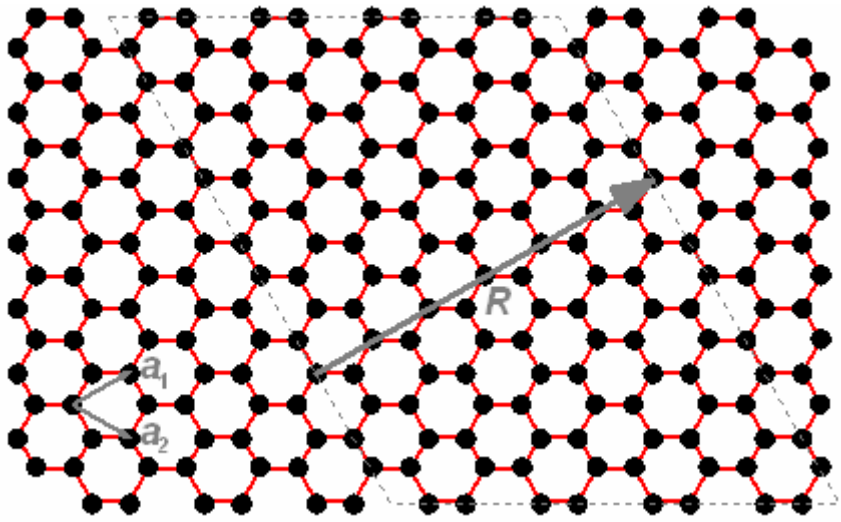

Figure 1-1. Hexagon lattice for a graphene sheet. The basis vectors are indicated in the bottom left and a rolling vector for cutting the sheet into a strip in the middle. When rolled into a cylinder the strip would form a CNT.

Since the method of rolling the CNT up from a graphene strip determines the properties of the resulting CNT, the vector that points from an atom to the atom it will

roll into is called the rolling vector, $\mathbf{R} = n\mathbf{a}_1 + m\mathbf{a}_2$, where n and m are integers and $\mathbf{a}_1$ and $\mathbf{a}_2$ are the graphene unit lattice vectors; this vector also defines the circumference of the CNT. The strip is defined by the dashed lines perpendicular to the beginning and ending of this vector as in Fig. 1-1. The result of rolling up the sheet is shown in Fig. 1-2.

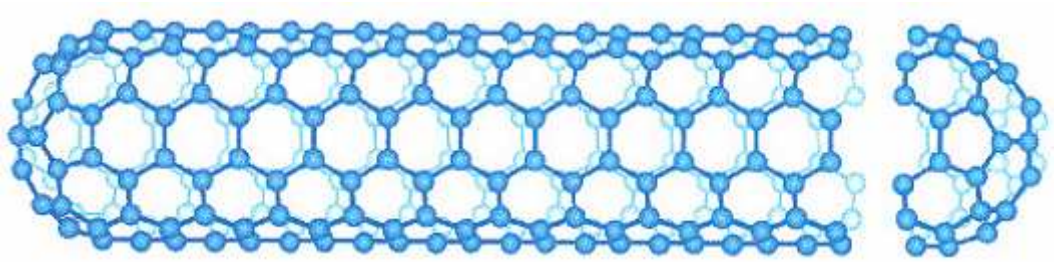

Figure 1-2. A single walled CNT. This CNT has (n,m) = (5,5), and is metallic (see text). (courtesy R.E. Smalley)

The electronic structure of the CNT may be well approximated by starting with the band structure for graphene[29] and quantizing it so that the electronic wave-function is single valued around the circumference of the CNT. The quantization condition is $\mathbf{R}\bullet\mathbf{k}=2\pi i$ where i is an integer and $\mathbf{k}$ is the wave vector. The result is that the two-dimensional band structure for graphene is cut along a series of equally spaced parallel lines to form a number of one-dimensional subbands.

The graphene band structure itself may be approximated as linear[29]:

$$E(\mathbf{q}) = E_F \pm \frac{\sqrt{3}\gamma_0 qa}{2} \tag{1.1}$$

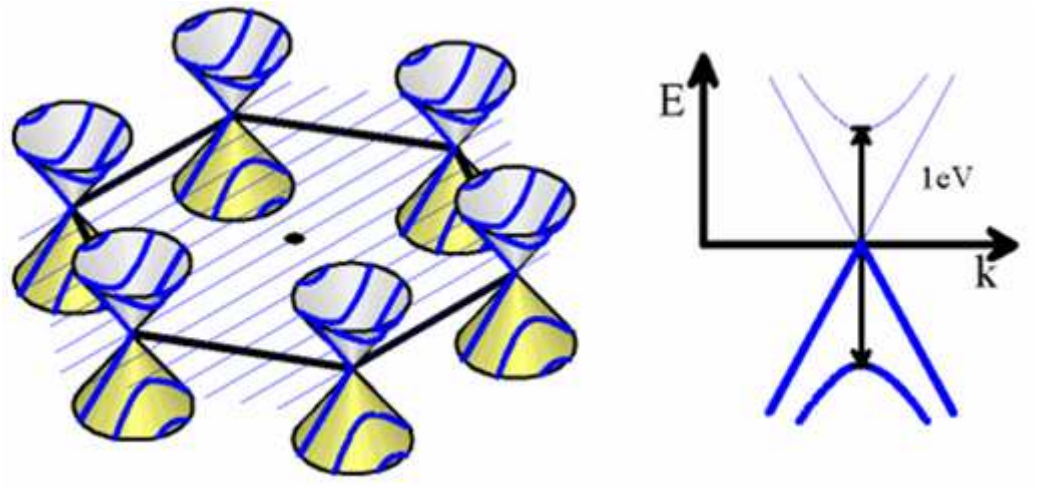

Figure 1-3. Metal CNT band structure. Slices through the band structure for graphene that determine the band structure for a metallic CNT. The lowest two subbands are depicted in the band diagram at right.

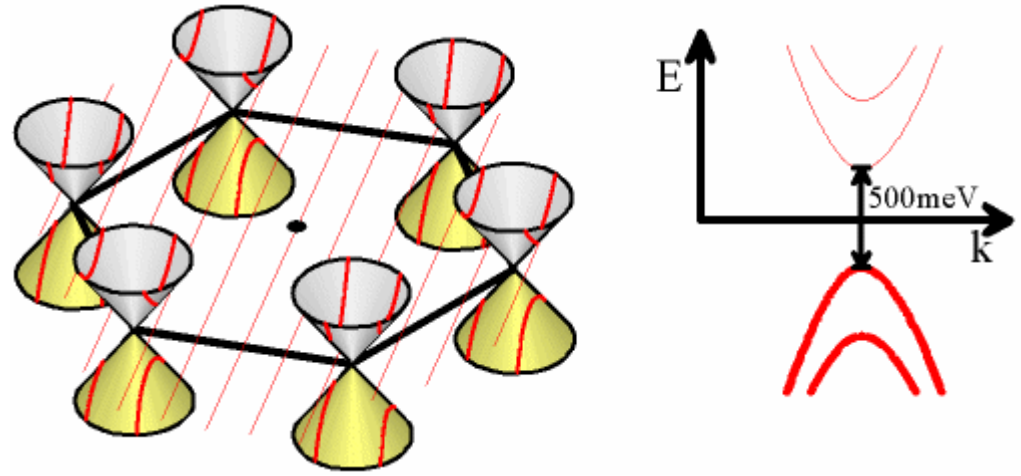

Figure 1-4. Semiconducting CNT band structure. Slices through the band structure for graphene that result in a semiconducting CNT. The lowest two subbands are depicted in the band diagram at right.

where **q** = **k** - **K** is the wave vector measured from the **K** point, γ_0 the nearest-neighbor tight-binding integral, and *a* the graphite lattice constant. Thus the band structure for graphene looks like a grid of cones with the tips at the vertices of the hexagonal Brillouin zone as show in Figs. 1-3 and 1-4. Since the bands only cross the Fermi surface at this point, the **K** point, only those CNTs which have $\mathbf{R}\cdot\mathbf{K}=2\pi i$ will be metallic. All other CNTs will have a bandgap and be semiconducting. This condition can be expressed as $n - m = 3q$ where q is an integer.

The values calculated via this method, e.g. the Fermi velocity, band gap, etc., agree very well with experiment, especially for larger diameter (d > 1 nm) CNTs, so we will use this approximation.

The dispersion relation of the lowest-lying subbands can be written:

$$E(k) = \sqrt{\Delta^2 + (\hbar v_F k)^2} \tag{1.2}$$

where $\hbar$ is Planck's constant, v_F the Fermi velocity of graphene, and $\Delta = 0$ for metallic CNTs, and for semiconducting CNTs

$$E_g = 2\Delta = \frac{2\gamma_0 a}{\sqrt{3}d} \approx \frac{830\,\text{meV}}{d\,[\text{nm}]} \tag{1.3}$$

where d is the diameter of the CNT.

1.3 Electronic device properties

A field effect transistor (FET) may be constructed from a CNT by contacting the CNT with two metallic (source and drain) electrodes, and employing a third metallic electrode, separated from the CNT by a dielectric, as a gate (Chapter 2 will

discuss some fabrication methods for CNT FETs in detail). Experimentally, it is difficult to determine the wrapping vector for an individual CNT. However, once a FET is constructed from an individual CNT two types of behavior are observed, which are identified with metallic and semiconducting CNTs[19, 30].

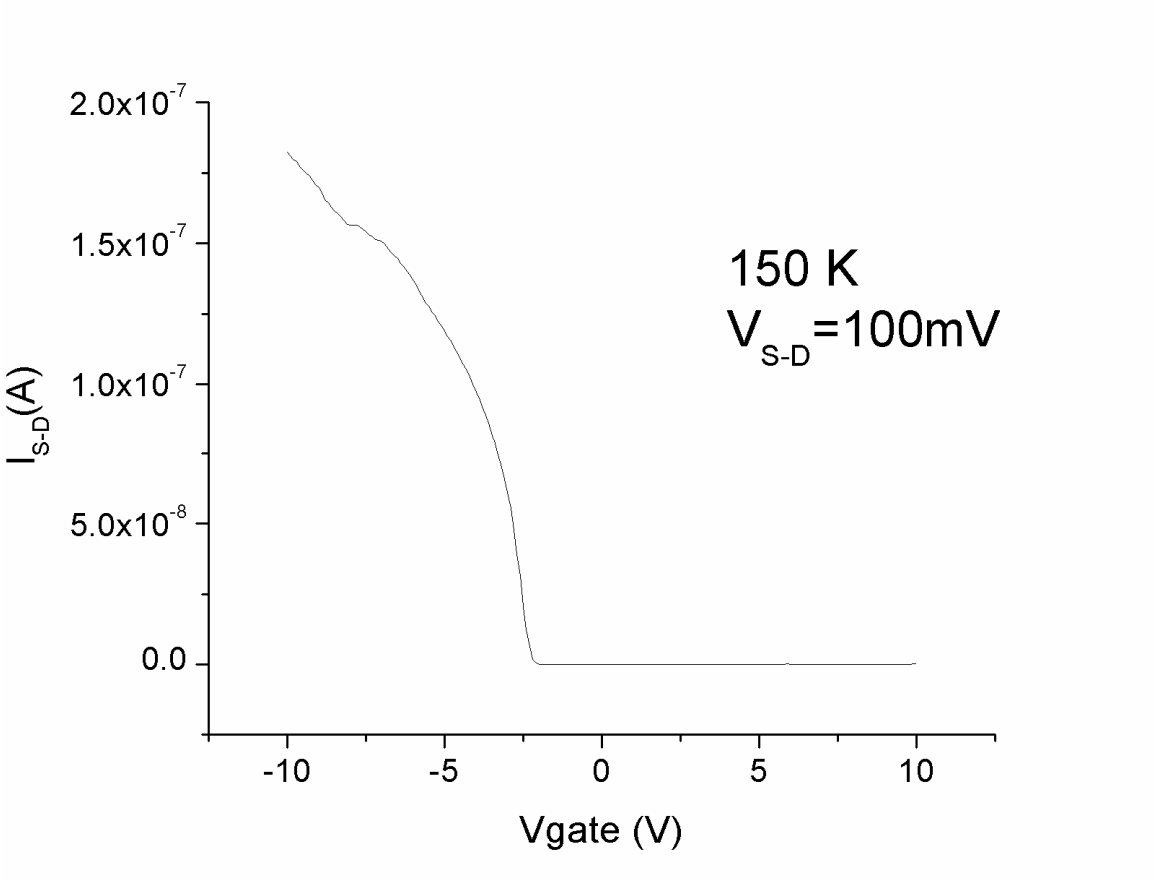

Figure 1-5. Current vs. gate voltage for a CNT in field effect transistor geometry.

Fig. 1-5 is a typical data curve from a semiconducting CNT FET. The current depends strongly on gate voltage, being finite for negative gate voltage (p-type FET behavior) and dropping to near zero for positive gate voltage. Metallic CNT FETs

show nearly constant conductivity vs. gate voltage. All of the work in this thesis was done on semiconducting CNTs.

In my dissertation I will explore low-frequency electronic noise in CNT FET devices and the insights it gives about the behavior of electrons in one-dimensional systems. In Chapter 2 I will present the basics of CNT growth and device fabrication, followed by an explanation of the experimental setup. In Chapter 3 I will review the state of knowledge on $1/f$ noise in traditional systems and in CNTs. This will provide the theoretical and experimental background needed for Chapter 4 where I will present the work of our group on the temperature dependence of $1/f$ noise in CNT FETs.

Chapters 5-7 will investigate a different type of low-frequency noise, the random telegraph signal (RTS), in CNTs. RTS in CNTs resulting from the tunneling of an electron between the CNT and a nearby defect will be used to study the Luttinger liquid state in CNTs. Chapter 5 will introduce the expected Luttinger liquid state for electrons in CNTs, followed by previous experimental work on Luttinger liquids in metallic CNTs and then a description of previous work using RTS to extract information on the correlated electron system of semiconducting materials. Chapter 6 presents the use of RTS to determine the temperature of the electron system and the energy relaxation length of electrons in CNTs. Chapter 7 analyzes the gate-voltage and temperature dependence of the RTS to extract information about the Luttinger liquid state in semiconducting CNTs.

The information in Chapter 4 and in Chapters 6-7 is currently being prepared in the form of two publications, respectively, to be submitted to peer-reviewed

scientific journals. The material on room temperature noise in Chapter 4 has been published.[31]

Chapter 2 Sample fabrication and measurement

Carbon nanotubes (CNTs) grow robustly in many situations where high temperature and carbon meet. CNTs have even been synthesized from heated plant matter[32] (including hemp!). The details of nanotube growth are still not fully understood but I will give a brief overview of the main techniques used to grow carbon nanotubes and then a description of the chemical vapor deposition (CVD) method that was used to produce all of the CNTs that are discussed in this thesis.

Device fabrication consists of growing the CNTs on SiO_2/Si substrates, and using photolithography or electron-beam lithography (EBL) to establish contact to the CNTs with metal electrodes. Afterwards the completed CNT devices are placed in a cryostat for measurement of their electrical properties at low temperature.

2.1 Growth methods

Synthesis methods for production of small-diameter (single- or few-walled) CNTs share in common a source of atomic carbon, a nano-particle catalyst (typically a transition metal or alloy of transition metals), and high temperature. Laser ablation[3] and arc discharge[1, 4] both use graphite as the source of carbon atoms. In the arc-discharge technique, a high current between a carbon cathode and an anode in an inert gas, e.g. helium, creates carbon-containing plasma, and if catalyst metal is added to the graphite electrodes, CNTs grow from tiny droplets of metal coalescing from the plasma. The laser ablation technique involves striking a piece of graphite

with intense laser pulses. Again, the graphite is impregnated with transition-metal catalyst to produce single-walled CNTs. One of the drawbacks of these techniques is that the CNTs are generally produced in bundles as opposed to individual CNTs. This is a major drawback if one hopes to investigate the electrical properties of an individual CNT. The CNTs also must be removed from the growth chamber, put in a liquid suspension or solution, and then spun onto a chip before electrical measurements can be made. The CVD method allows CNTs to be grown directly on a silicon chip.

2.2 Chemical vapor deposition

Chemical vapor deposition is initiated by creating nano-particles of a metal catalyst on the surface of an oxidized silicon chip.[2, 33] In my work, iron nano-particles were obtained by dipping a silicon chip in a ferric nitrate solution and then into hexane to force the ferric nitrate to precipitate out on the surface of the chip. The density of the ferric nitrate is important for determining the density of nanotubes that will be present on the chip after growth, values can range from 0.1 - 100 μg/ml with lower values typical for single CNT devices and higher values used to obtain dense films of CNTs.

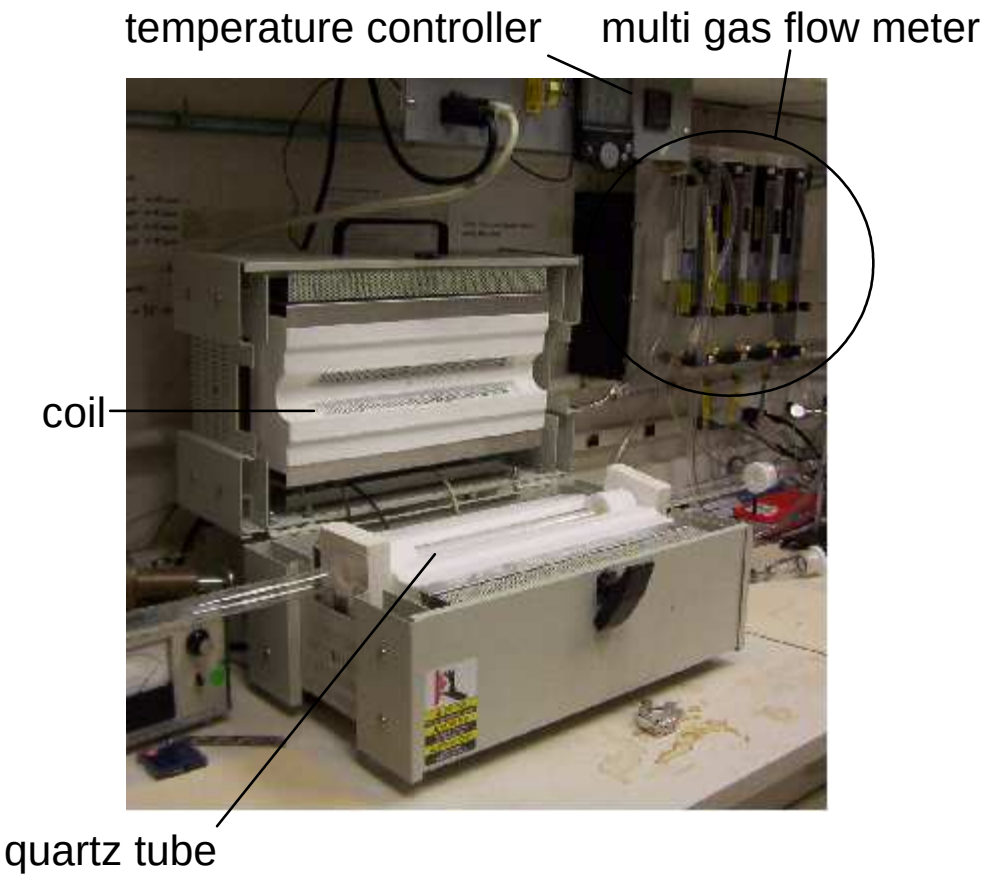

Figure 2-1. CVD furnace for CNT growth in the Fuhrer laboratory. The flow meters on the wall control the amount of carbon containing feedstock gases through the system. The silicon chips are placed inside the quartz tube and after the oven lid is closed the coils heat the oven to 850° C for the nanotube growth. Image courtesy Y. Chen.

After the chips are catalyzed, they are placed onto a quartz boat and set in a quartz tube oven; the growth recipe that I used is outlined in Table 1. The oven (see Fig. 2-1) is heated to 850° C while flowing argon through the tube. At this stage, or shortly after introduction of hydrogen during growth, the ferric nitrate particles are reduced to iron. Once the oven has reached its final temperature, carbon-containing

feedstock gases (methane, ethylene) and hydrogen are fed through the quartz tube. The ratio and flow rate of the gases (see Table 1) are adapted from the Dai group[34] and have been optimized to produce long CNTs. In general the nanotubes will be oriented along the direction of the gas flow, but numerous exceptions can be found on any given chip, including CNTs that form arcs, circles or are perpendicular to the gas flow direction.

Table 2-1. Typical recipe for CNT growth.

Growth Recipe	**Gas**	**Flow (sccm*)**	**Temp (°C)**	**Time (minute)**
Purge	Ar	730	Room Temperature	5
Heat	Ar	730	RT ⟶650	15
Soak	Ar	730	650	5
Heat	Ar	730	650⟶730	2
Soak	Ar	730	730	3
Heat	Ar	730	730⟶800	3
Soak	Ar	730	800	3
Heat	Ar	730	800⟶850	5
Soak	Ar	730	850	10
Nanotube Growth	H_2	1900	850	10
	CH_4	1300		
	C_2H_4	86		
Cool Down	Ar	730	850⟶200	wait until cool

*sccm=standard cubic centimeters per minute

2.3 Locate and contact

The CVD growth method described above produces nanotubes distributed randomly on the surface of the chip. The next step of the process is to create alignment markers on the surface of the chips to serve as guides for locating and

creating contacts to the CNTs themselves. An alternative process[35], described in the next section, uses patterned catalyst and photolithography aligned to the catalyst locations. Photolithography is a more reliable and quicker process than EBL, but EBL does have the advantage of allowing maximal flexibility in creating devices of any length up to the length of the CNT.

A standard e-beam process, depicted in Fig. 2-2, was used to create the grids on the surface of the chip and is depicted in Fig. 2-3. This involves spinning resist layers on a chip followed by baking them on a hot plate. First the methylmethacrylate (MMA) is spun on at 4500 rpm for 45s and baked for 5 min at 150° C, and then the polymethylmethacrylate (PMMA) is spun at 6000 rpm for 45s and baked for 5 min at 150° C. A modified scanning electron microscope (SEM) is then used to create a pattern in the resist layers; this is caused by the electron beam weakening the bonds in the polymer structure of the resist. After writing, the chip is developed in methylisobutylketone / isopropanol (MIBK/IPA) (3:1) for around 30 s to remove the written areas. Finally the chip is placed in a vacuum chamber where the resist acts as a stencil mask for the thermally-deposited metals used to create the pattern. The two layers of resist help create undercut; the MMA develops faster creating a tiered structure seen in Figure 2-2e. The undercut separates the metal on the surface of the resist from the metal on the SiO_2 surface, allowing the unwanted metal to be removed cleanly during lift-off. MMA is also more soluble in acetone which allows for better lift-off after deposition. Lift-off is accomplished by soaking the chip in acetone to remove the remaining resist and the metal on top of it.

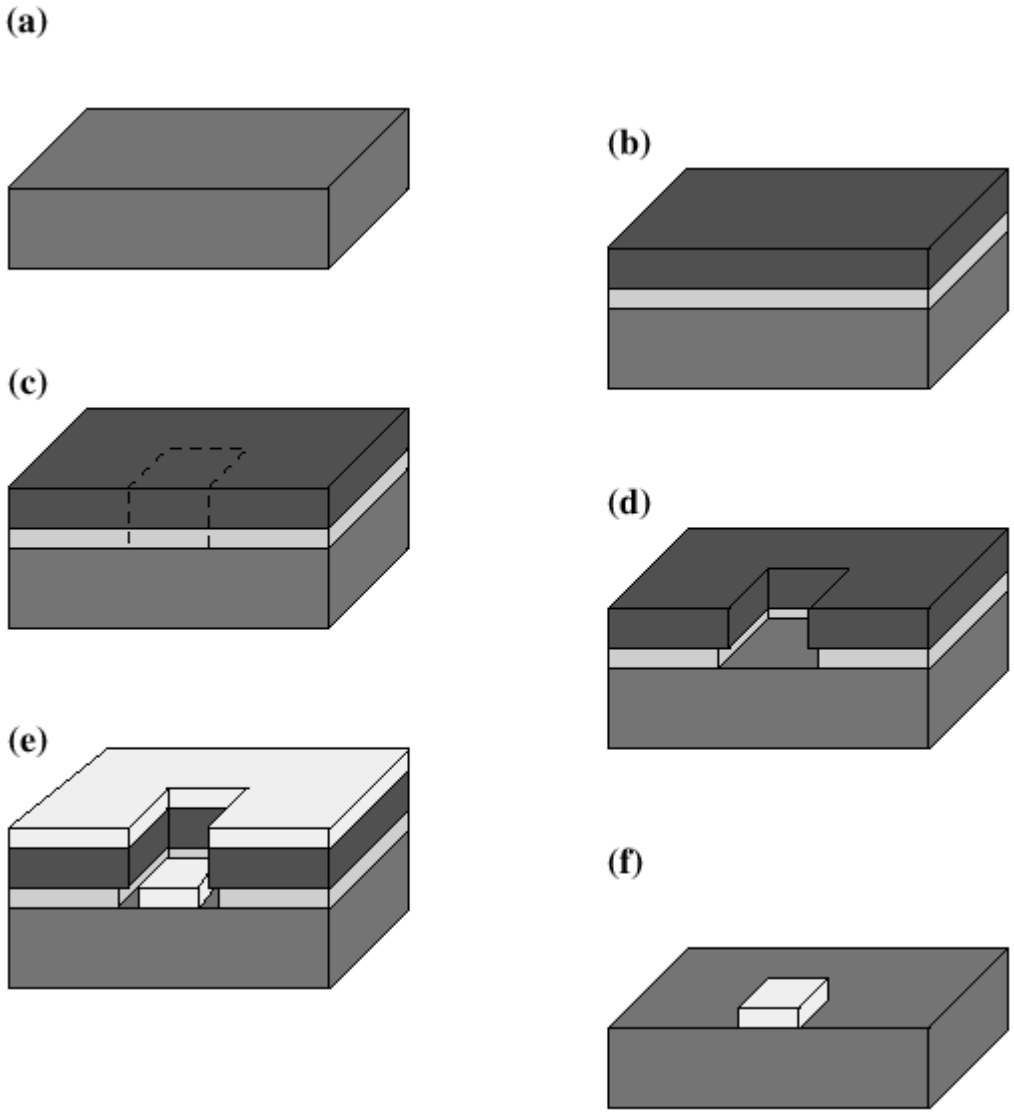

Figure 2-2. E-beam lithography process. (a) New Si/SiO_2 chip. (b) Chip coated with MMA and PMMA (c) Section of resist exposed in the SEM (d) After exposed section is developed in MIBK. (e) Metal film deposited on chip (f) After lift-off. (Courtesy Tobias Durkop)

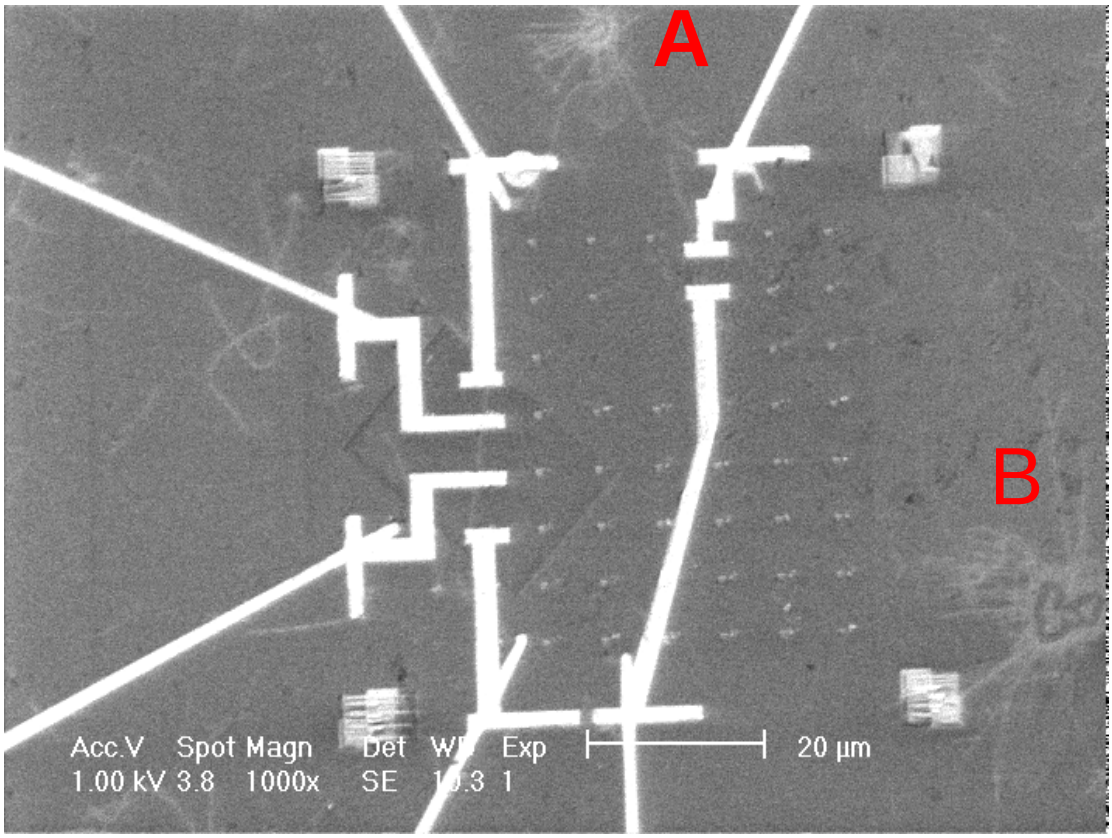

Figure 2-3. Electron micrograph of the square alignment marker pattern (array of small squares and symbols) and the electrodes (larger features leading off the edge of the image) for the individual CNTs. The four large markers in the corners are used during the second stage to allow for proper aligning of the two e-beam stages. Nanotubes can be seen individually and forming star-shaped patterns radiating from clumps of catalyst in the top middle of the image and the extreme lower right indicated by letters A and B.

The alignment mark pattern can be used to locate CNTs to contact electrically. The SEM can be used in this “find” step to locate nanotubes with reference to the grid[36]. After the CNTs are located relative to the alignment marks, EBL resist must

then be spun and baked on the chip again and the computer assisted drawing (CAD) program can be used to create electrode patterns that are referenced to the grid. Typically the metal deposited on devices in our group is Cr/Au with 1nm of Cr and 30nm of Au.

The EBL technique allows for creating metallic electrodes at any given separation (up to the length of the nanotube) whenever a CNT is found near the grid markers, this can be seen in Fig. 2-3. The device should be re-imaged after the leads are made to make sure that only one nanotube is in the junction area, as in Fig. 2-4, due to the fact that CNTs are often more visible after being contacted by metal; some CNTs may have been overlooked in the initial imaging.[36] At minimum, two electrodes contact the CNT. The heavily doped silicon substrate under the SiO_2 acts as a third or "gate" electrode, creating a field-effect transistor (FET) geometry. Satisfactory electrical contact to the gate can be made either by creating a scratch somewhere on the surface of the chip and using an ultrasonic wire bonder to attach a wire to the scratch or to silver paint placed on the scratch, or by contacting silver paint that is touching the side of the chip. The wire bonder is also used to make electrical connections to the lithographically-patterned electrodes on the chip.

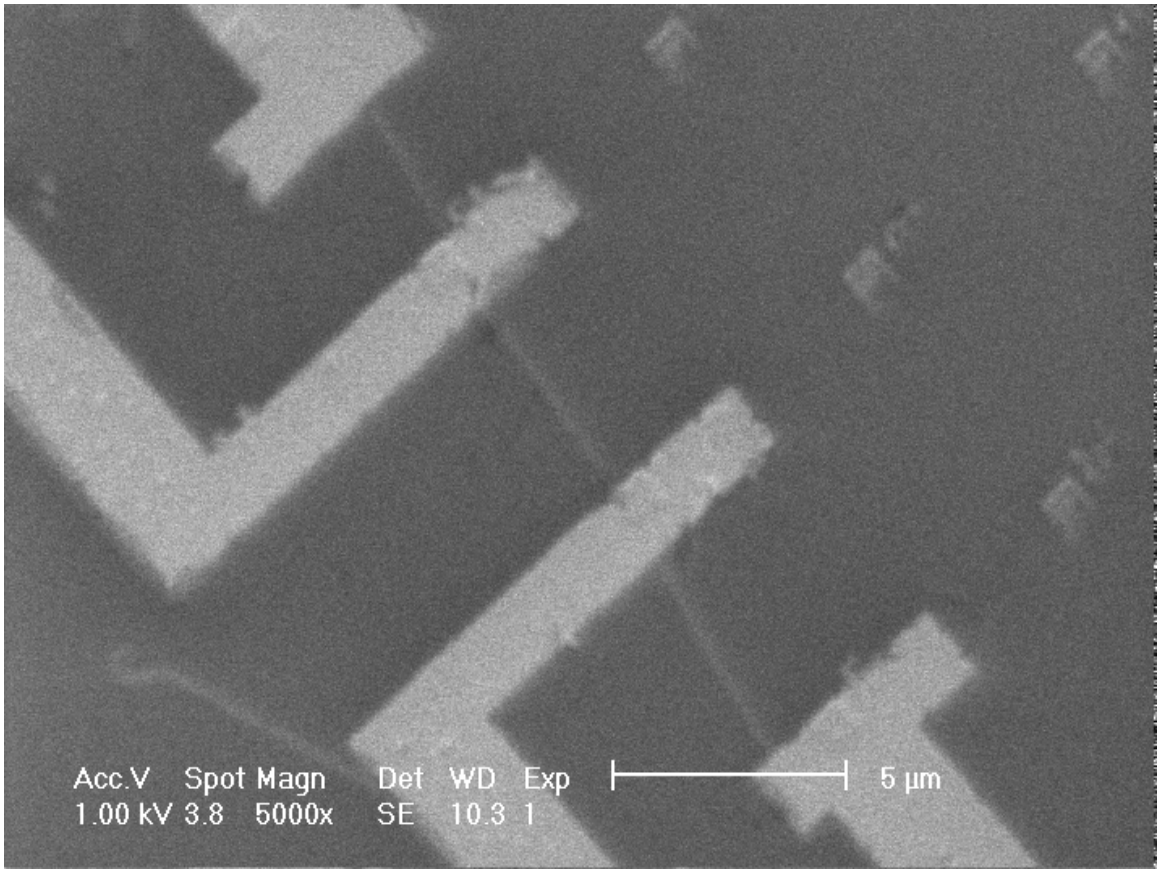

Figure 2-4. Close up image of a CNT under contacts. The individual grid markers can be seen as well as an extra tube that almost created a two-tube device. The devices need to be imaged after creation to ensure that a single tube was contacted in the junction.

2.4 Georgetown technique

The entire process outlined above is called the “find-and–wire” approach to creating devices. If patterned catalyst is used, electrodes can be created aligned to the catalyst, where one expects the CNTs to be, and then the chip can be inspected to see if the CNTs were contacted by the electrodes. This has been called the “wire-and-

find" approach, and was used by the group of Paola Barbara at Georgetown University[35] to create some of the devices studied in this thesis.

The wire-and-find technique utilizes a patterned growth method that allows for the growth of nanotubes only at certain locations on the chip. The other attractive feature of the process is that it is done solely with photolithography which removes the need for an SEM (costly apparatus!). The first step involves creating a photolithographic pattern for the catalyst islands. The chip is then immersed in catalyst solution, which can only reach the surface of the chip through the photolithographic mask. When the mask is removed with acetone, the catalyst is only left in small islands on the chip's surface. After growing CNTs, another photolithography step is done by aligning to the first pattern. This step puts electrodes down that are matched to the catalyst island locations. The electrodes for the CNT samples used in this study were Pd/Nb metal. Pd has a high work function and a good wetting interaction with the tubes[37] so it is a good choice for FET devices, the Nb was deposited to allow for superconductivity measurements done by the Georgetown group[38].

2.5 Experimental Setup

This thesis concerns electrical measurements made on CNT devices in the field effect transistor (FET) configuration. The conductance measurements are made in two-probe configuration which is acceptable given the devices' high resistances (>100 KΩ). It is also difficult to make four probe measurements of nanotube devices

due to their complicated interaction with contacts[39]. Commonly the electrons will completely leave the CNT and enter the contact, making the flow of current through a four-probe device more like three two-probe devices in series.

The DC drain and gate voltages are sourced from a National Instruments BNC-2090 data acquisition device (DAQ), as depicted in Fig. 2-5. The source current is measured by an Ithaco 1201 current preamplifier which converts the current to a voltage that is measured by either a National Instruments board for telegraph signal measurements or a Stanford Research Systems SR785 spectrum analyzer for low-frequency noise measurements. The control of the DC voltages for the device and gate bias and the spectrum analyzer and A/D board were accomplished using programs created in LABVIEW.

All of the measurements were done inside of a Desert Cryogenics ^{4}He flow cryostat. The accessible temperature range is 1.2 K to 325 K.

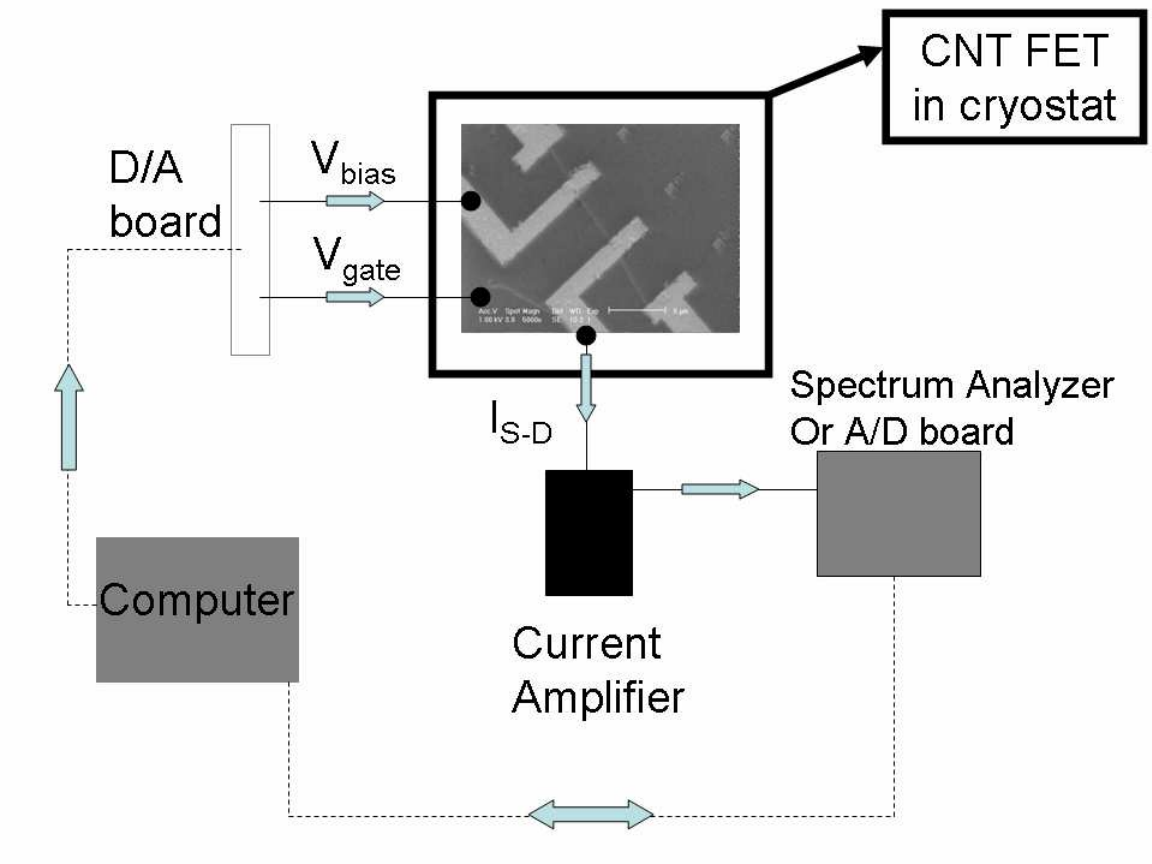

Figure 2-5. Schematic of the electronic setup used in the cryostat. The computer controls the bias and gate voltages as well as the data collection parameters. For low-frequency noise the spectrum analyzer is triggered and the frequency span is set by the computer, for telegraph signals the computer takes in time series from the A/D board. V_{bias} is the bias voltage and $I_{S\text{-}D}$ in the current flowing from the source to the drain.

Chapter 3 1/*f* noise

1/*f* noise is the part of the spectrum at low frequencies where the noise power versus frequency approximately exhibits 1/*f* dependence. 1/*f* noise is found in such a wide range of physical phenomenon that it cries out to many people for a universal cause. How can traffic flow and ocean tides and symphonic music all have 1/*f* noise inside? However we are left with the simple fact that despite its bizarre universal presence no universal theory can account for it.[40] Even more discouragingly, instances where theory and experiment are able to merge the most satisfactorily occur where the mechanism clearly is of a non-universal nature[40].

For years 1/*f* noise in condensed matter systems was not commonly studied. This attitude prevailed up until the 1970's when some people noted that, despite the advances of solid state physics, it was difficult to explain the noise that appeared in a truly simple circuit comprised of a metal film and a voltage bias.[40] The spectral current noise power of such a circuit has a well-understood frequency-independent contribution from the thermal or Johnson noise that dominates at high frequencies, however at low frequencies the noise typically exhibits a 1/*f* spectrum.

In this chapter I will explain the basics of noise and introduce 1/*f* noise. Then I will present a theoretical framework within which the temperature dependence of the 1/*f* noise can be related to the energy spectrum of the fluctuators that are responsible for the 1/*f* noise.

3.1 Introduction to noise

We first consider the circuit in Fig. 3-1 which depicts a sample to be tested connected to a current amplifier.

When the voltage bias is zero the frequency spectrum of the voltage noise across the resistor will be white (frequency independent) and have a magnitude proportional to the magnitude of the resistance. This noise is called thermal or Johnson noise and is caused by the thermally distributed velocities of the charge carriers. It is found in any resistive element and in many other systems that can be thought of as involving energy loss to a random process (e.g. water flow through a pipe). Johnson noise is given by

$$S_I(f) = 4k_bT / R \tag{3.1}$$

Here k_b is the Boltzmann constant and S_I is the current noise power per unit frequency (A^2/Hz), T is the temperature and R is the resistance.

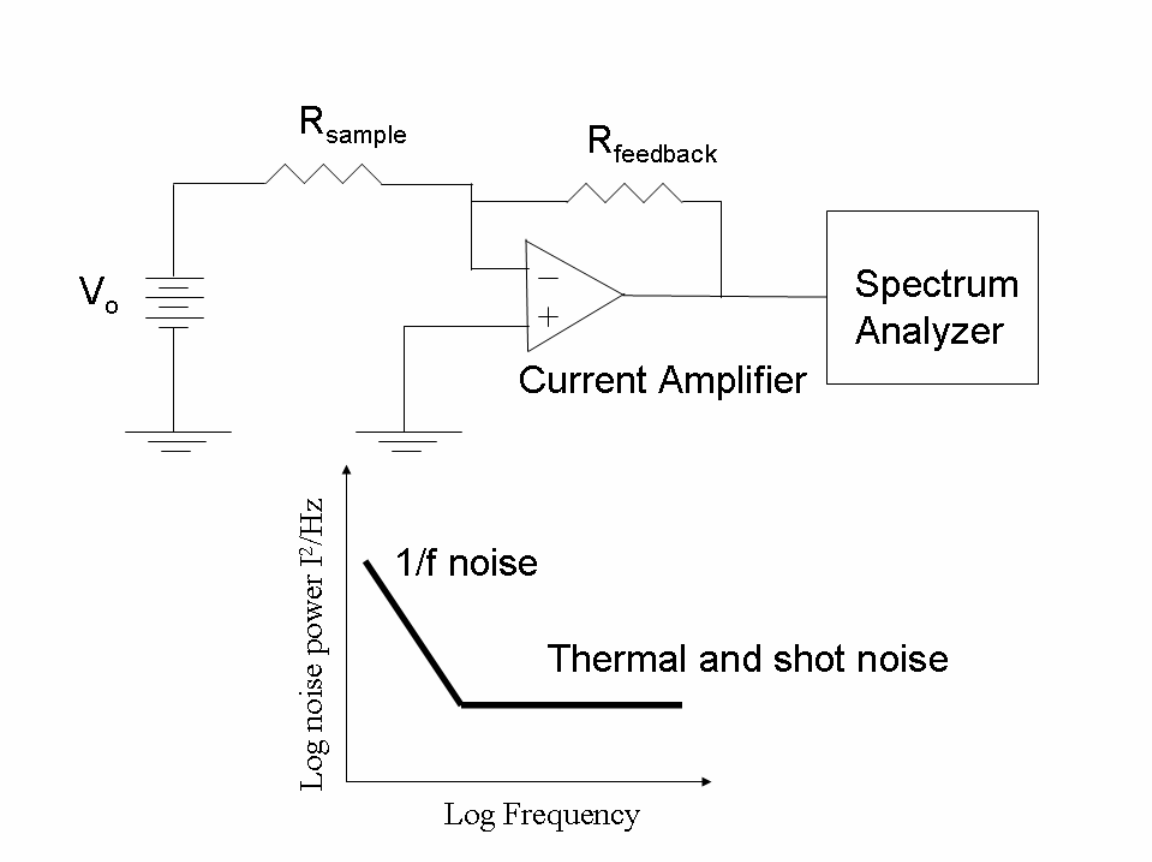

Figure 3-1. Noise circuit. This schematic illustrates the basic setup used for noise measurements. The op-amp is shown in a trans-impedance configuration which converts the current to a voltage for the spectrum analyzer to perform a fast-fourier transform (FFT) on. The bottom graph is an illustration of the three main types of noise to be expected in such circuits.

Once the voltage is non-zero two other types of noise appear. One is called shot noise and is caused by the finite size of the electrical charge, which leads to statistical fluctuations in the current crossing a junction, for example, electrons moving through the leads connected to the nanotube sample. This noise is also white and is commonly given by

$$S_I(f) = 2eI \tag{3.2}$$

where e is the electron charge and I is the current through the device. The dominant noise at low frequencies, however, will have a $1/f$ frequency dependence and its nature is still poorly understood for the majority of systems.

Unlike Johnson noise or shot noise, there is no equation that is derived from physical principles that can predict the magnitude of the $1/f$ noise in a conductor. A strictly phenomenological equation that I will frequently use as a tool was proposed by Hooge[41, 42]

$$S_V(f) = AV^{2+\beta} / f^z \tag{3.3}$$

In this equation, known as Hooge's law, S_V is the voltage noise power (V^2/Hz), A is the noise magnitude (and is dimensionless as long as β=0 and z=1), V is the bias voltage and f is again the frequency where the noise is being measured. The quadratic dependence of the noise on voltage indicates that the fluctuations are not current driven but are actually due to $1/f$ fluctuations in the value of the resistance[40]. Hooge set $A = \zeta/N$, where N is the number of carriers, to attempt to create a universal parameter, ζ, for $1/f$ noise where the size of the sample led to different values of A. If β is zero and z is one, ζ is dimensionless.

Hooge proposed that ζ was a universal quantity that would describe many $1/f$ processes in simple metals and semiconductors. Initial analysis was heartening: Many semiconductors showed values of ζ near 2×10^{-3}. Unfortunately it was found that the value can vary greatly even amongst samples fabricated in the same

batch.[42] Choosing the value of N to use in the equation can also be difficult; i.e. it is not clear how many of the carriers are participating in the noise process. It is also hard to separate out the contact-dependent portion of the $1/f$ noise. However the quadratic voltage dependence and the inverse dependence of the noise on the number of carriers (noise inversely proportional to the volume of the system) are commonly observed in $1/f$ systems. Bulk conductors commonly have a noise that is inversely proportional to their volume and gated transistors can be seen to have a noise that varies with the gate voltage, indicating that the number of charge carriers is determining the noise magnitude.[43]

It should be noted that Hooge's law is strictly phenomenological and that many exceptions are known: $1/f$ noise processes can be current driven in some systems, z may differ from one, and the noise can be a surface effect in some systems, removing the N dependence[40]. Furthermore it is obvious at some very low frequency the noise must stop following this behavior or the total noise power integrated over all frequencies will diverge, which is unphysical. Hooge's law does however prove to be a useful tool in many situations and will be referred to frequently.

3.2 Semiconductors and transistors

Pure homogeneous semiconductor materials have been studied extensively. In semiconductors ζ values vary from 10^{-3} to 10^{-6} for Si, Ge, GaAs and other common semiconductors that have been measured.[42] Unfortunately the uncertainty for any

given material is usually about one order of magnitude due to variability between samples. Assuming that $\beta \cong 0$ and $z \cong 1$, we can see that the equation from Hooge, Eq. 3.3, becomes

$$S_I(f) = AI^2/f = \frac{\zeta}{N} I^2/f \tag{3.4}$$

which is a powerful way to parameterize the noise for comparison purposes. Measurements taken at different biases, currents or frequencies can be used for comparing the magnitude of the noise.

In transistor devices a good deal of work has been done to discern whether or not the source of the noise is fluctuations in carrier number or carrier mobility.[43] Since the observable is conductance fluctuations and conductance is $\sigma = \mu ne$, where μ is the mobility and n is the number of carriers; it is not immediately clear which is the source (or if both are the source), but each assumption makes a different prediction for the way the noise should change with the gate voltage. For number fluctuations the value of ζ should vary with gate voltage but for mobility fluctuations it should remain constant. It appears that for many semiconductors, n type transistors exhibit number fluctuations and p type transistors have mobility fluctuations.[43] In the next chapter data and discussion will be presented for nanotube transistors.

3.3 Basic noise model

Dutta and Horn present a theory that connects the most commonly used model for $1/f$ noise with the energy spectrum of the fluctuators responsible for the noise.[40]

I will start off by presenting the relevant beginning model and then will show the modifications to it to make it more physically plausible. The process is outlined pictorially in Fig. 3-2.

First I begin with the most basic of fluctuators, the two-level system. A two-level fluctuator will have a Lorentzian spectrum[44]

$$S(\omega) \propto \frac{\tau}{\omega^2\tau^2 + 1} \tag{3.5}$$

where ω is the angular frequency and τ is the characteristic time of the process. If we integrate this function over a distribution of two-level fluctuators we get

$$S(w) \propto \int \frac{\tau}{\omega^2\tau^2 + 1} D(\tau) d\tau \tag{3.6}$$

where D(τ) is the density of states for the fluctuators. To clear up some confusing notation,

$$\begin{aligned} &D(\tau) \equiv \frac{dn}{d\tau}, D'(E) \equiv \frac{dn}{dE} \\ &D'(E) \times \frac{dE}{d\tau} = D(\tau) \end{aligned} \tag{3.7}$$

where *n* is the density of electrons. The density of states is an operator that takes a derivative with respect to *E* or τ, this should not be taken to mean that $E=\tau$.

Unfortunately by varying the distribution of fluctuators this equation can be used to produce many kinds of frequency spectrums. Assuming that the fluctuators are inhomogeneous, and in particular the they are distributed as

$$D(\tau) \propto \tau^{-1} \tag{3.8}$$

leads to a noise spectrum that is

$$S(\omega) \propto \omega^{-1} \tag{3.9}$$

We are now left with the problem of justifying this distribution of fluctuators. A first step is to think of the fluctuators as being caused by a thermally activated process. Then $\tau = \tau_o \exp(E/k_B T)$ and the required energy distribution would be D′(E) = const for all energies. For example if noise in a semiconductor were caused by trapping and detrapping in the oxide, which modulated the carrier density, we would expect this kind of thermally activated process. Thus if over a wide range of energies all trap energies were equally probable, we would have a consistent explanation.

Unfortunately these assumptions lead to a linear dependence of the spectral noise power on temperature, which is usually not seen in semiconductors (or many other conductors, namely most metals). The flat distribution of the energies of the traps also cannot extend to arbitrarily low and high energies, which will be the topic of the next section.

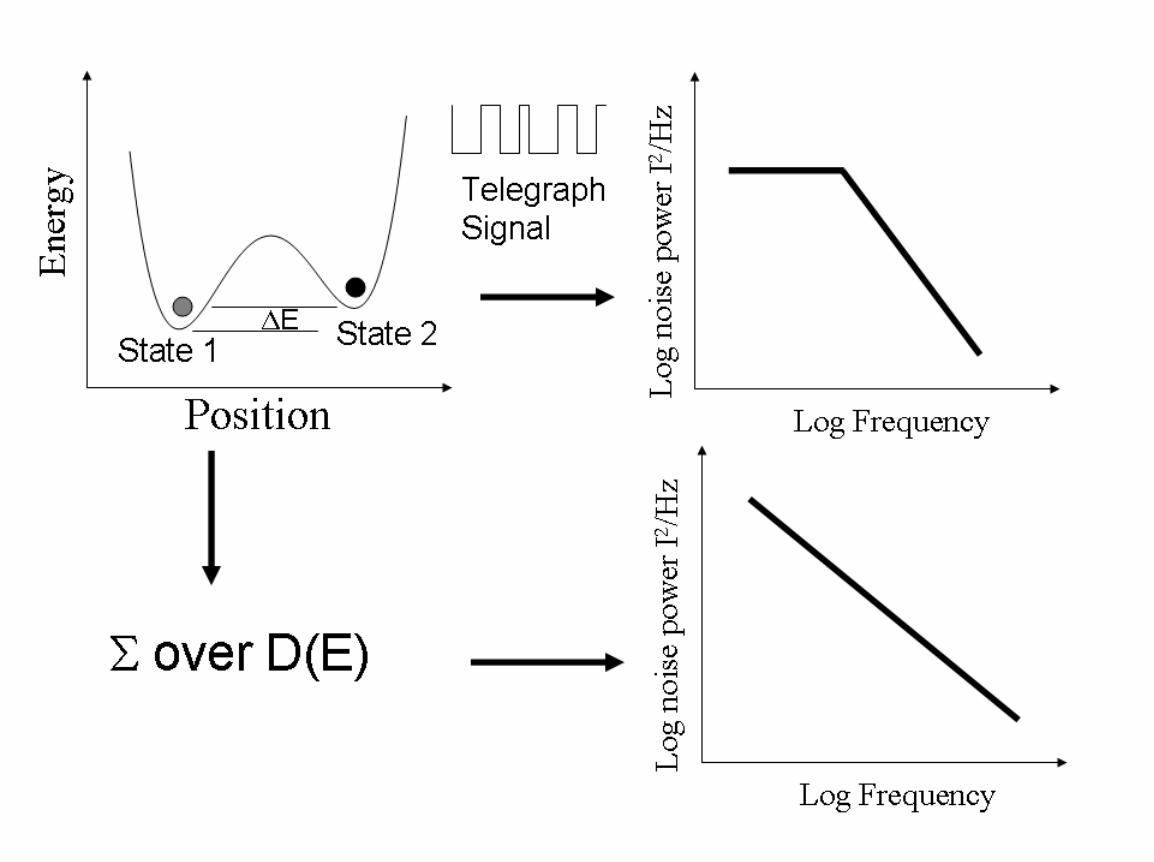

Figure 3-2. 1/f noise formation. This schematic depicts how the noise from many two-level systems can be summed to create a 1/*f* spectrum. The transform of the telegraph signal from a two level system is a Lorentzian, it has a flat spectrum followed by a knee and then a $1/f^2$ dependence. If these are summed over an appropriate distribution of energies the result is a 1/*f* spectrum.

3.4 Theory for temperature dependence

A better model for noise would not force the distribution of energies to be flat for all values, a clearly non-physical requirement. To correct the unphysical nature of the assumption of an infinitely wide and flat distribution of fluctuators being

responsible for the noise, Dutta and Horn inserted a spectrum of two level fluctuators that is limited in energy distribution. This alteration removes the strictly 1/*f* nature of the noise by creating an exponent that should range between 0.8 and 1.4 and should also vary slowly with temperature and frequency[45, 46]. The most significant result is that the spectrum of the fluctuators can be directly related to the noise power,

$$S(\omega,T) \propto \frac{k_B T}{\omega} D'(E') \tag{3.10}$$

where $E'=-kT\ln(\omega\tau_0)$. This is the first term of a Taylor series expansion of Eq. 3.6, with $D'(E')$ allowed to be a smoothly varying function of E′. This allows for the observation of the energy of the fluctuator that corresponds to the noise features at a given temperature through

$$E'_p \approx -k_B T_p \ln(\omega\tau_0) \tag{3.11}$$

This shows that a maximum at any temperature value, T_p, is correlated with a maximum in the energy of the fluctuators, E'_p. τ_o is the characteristic attempt time for the fluctuators of order 10^{-14} s (i.e. inverse of a typical phonon frequency). The ln term is of the order 30 for frequencies between 0.1 and 100Hz. The exponent of the 1/*f* noise also varies with frequency and temperature, but the deviation from unity is proportional to $1/\ln(2\pi f\tau_o)$ and is therefore small and hard to measure experimentally. Data from Dutta and Horn[40] is shown in Fig. 3-3 and illustrates the peak in noise and then extracts a peak energy for the fluctuators that are responsible for that noise in Fig. 3-3c.

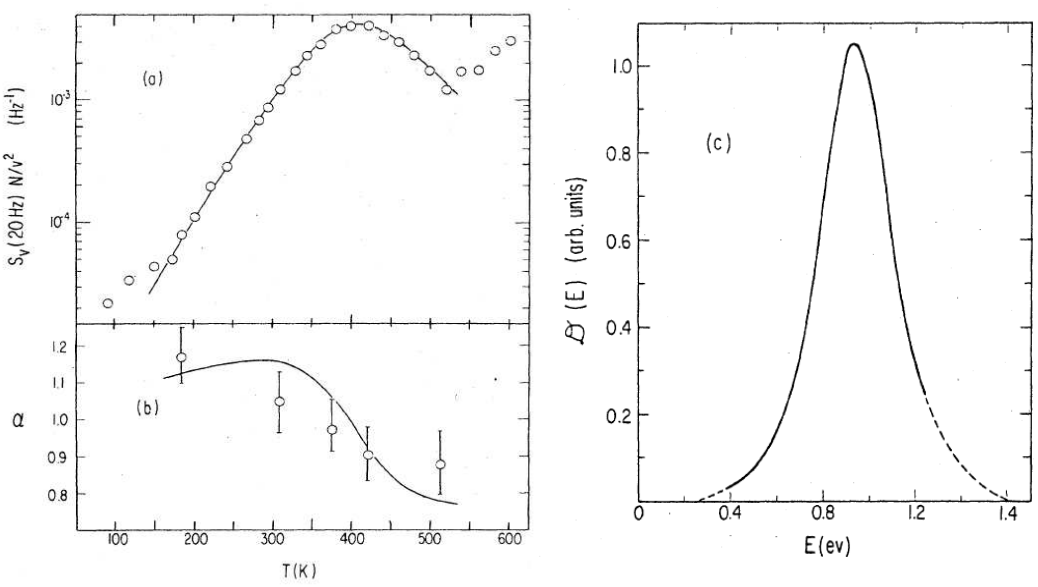

Figure 3-3. Graph from Dutta and Horn[40] illustrating the temperature dependence of the noise in a Ag metal film. The line is the theoretical prediction for the data and the points are the experimental values. (a) The data exhibits a peak in noise at a temperature around 400 K. (b) The theory also predicts a small shift in the power of the 1/*f* dependence with temperature. The predicted shift is from $1/f^{1.1}$ and $1/f^{0.8}$. The y-axis is the exponent, denoted as z in this chapter (c) This is the calculated density of states corresponding to the noise data in (a). The noise peak corresponds to a peak in the noise at an energy around 0.9 eV.

3.5 Previous results in nanotubes

Nanotubes present an interesting medium for studying 1/*f* noise for several reasons.[13, 14, 31, 47-49] The strong sp^2 bonded carbon atoms in the nanotube

lattice should not be able to move around easily, eliminating a source of noise commonly considered in typical bulk metals. The nanometer diameter of the material presents the first straightforward opportunity to measure the phenomenon of 1/*f* noise in a 1-D conductor. The nanotube also has all of its atoms as surface atoms, which has led to the prediction that one-dimensional systems should intrinsically have more 1/*f* noise than their higher dimensional counterparts[14]. Nanotubes also have a one-dimensional current, so any contaminant or adsorbate that interacts with an atom on the tube is interrupting the flow of current. In contrast, in 3-D systems the removal of a single atom in the bulk of the material will have a negligible impact on the conductivity of the device. Finally 1/*f* noise is considered to be a bulk effect in most materials due to its 1/*N* dependence on the number of carriers in the system - the most famous paper in the field is titled "1/*f* Noise is no surface effect"[41] - but nanotubes can be viewed as a material that is all surface. This has led to several papers on the magnitude of the noise in individual carbon nanotube devices and some of the relevant past work will be discussed here.

The first work on nanotube 1/*f* noise was from the Zettl group.[14] Their data indicated that the noise in the devices was strongly connected with the total device resistance for samples including bulk collections of CNTs (3D), "mats" or thin films of CNTs (2D) and devices constructed from individual or perhaps small bundles of CNTs (1D). They determined that $A/R=10^{-11}\Omega^{-1}$ which for typical single tube devices gives a value for A of 10^{-7}. This value is extremely high, four to ten orders of magnitude higher than that for most typical resistors. This led the group to conclude that nanotubes may indeed be fulfilling the prediction that 1-D conductors would be

unusually noisy due to all of the atoms being surface atoms. The paper attempted to create an estimate for γ by taking the number of carriers as the number of atoms. This led to a value for γ=0.2 which is 100 times as high as Hooge proposed for semiconductors, and up to 10,000 times as high as is commonly seen in high quality semiconductor devices. This was further validation for the view that nanotubes (and perhaps all 1-D systems) are exceptionally noisy, but the calculation of the number of carriers as being equal to the number of carbon atoms in the device is probably inappropriate; it would certainly overestimate the carrier number in semiconducting CNTs.

In the next chapter I will present our group's results on noise in nanotube transistors, first at room temperature and then as a function of temperature.

Chapter 4 Temperature dependence of 1/f noise in carbon nanotube transistors

This chapter will present the results of measurements performed on individual semiconducting CNTs in FET geometry. The most extensive measurements were taken on two FET devices provided by our Georgetown collaborators; the fabrication procedure for these devices is described in Chapter 2.

In the first three sections I will present the analysis techniques used to extract the noise parameters. In section 4, I will describe the results of the initial work done by our group on CNTs in FET geometry at room temperature and all the data will be from Ishigami *et al*[31]. In the last section I will discuss the behavior of the noise parameter γ at temperatures from 1.2 to 300 K, and the implications the data has for the origin of the $1/f$ noise in the devices.

As discussed in the last chapter, perfect $1/f$ noise would require a perfectly flat spectrum of fluctuators $D(E)$ at all energies E. If this were true the pre-factor γ in equation 3.4 would show a linear dependence on temperature. However, if the spectrum of fluctuators $D(E)$ is smoothly varying, it results in a temperature dependence for the $1/f$ noise with the same functional form as $D(E)$, as indicated by equation 3.10.

All the data presented in this chapter (except section 4.4 which is from a separate set of devices) were taken on two CNT devices from the Georgetown group.

The data for all the plots in this chapter was taken on a 3 um long CNT with a diameter of 1.4 nm and will be referred to in the thesis as Sample 1. Data from the second device only appears in the final results in section 4.5 and is also 3um long CNT with a diameter of 1.9 nm and will be referred to in the thesis as Sample 2.

Table 4-1. Device Characteristics

Device	Diameter (nm)	Contact Metal	Device Length (μm)
Sample 1	1.4	Pd/Nb 3.5 nm / 215 nm	3
Sample 2	1.9	Pd/Nb 3.5 nm / 215 nm	3

4.1 Noise signal

Several methods are available to determine the noise parameter associated with a given noise spectrum. As a reminder from the last chapter we want to determine *A* where

$$S_V(f) = AV^2 / f^z$$
$$S_I(f) = AI^2 / f^z \quad (4.1)$$

if β=0. The two equations demonstrate the fluctuations can be measured as a function of either electrical parameter, in this thesis the current noise is always being measured. All of the data were generated on a spectrum analyzer that simply performs an analog-to-digital conversion of the incoming signal and then performs a fast Fourier transform (FFT) on the digital signal.

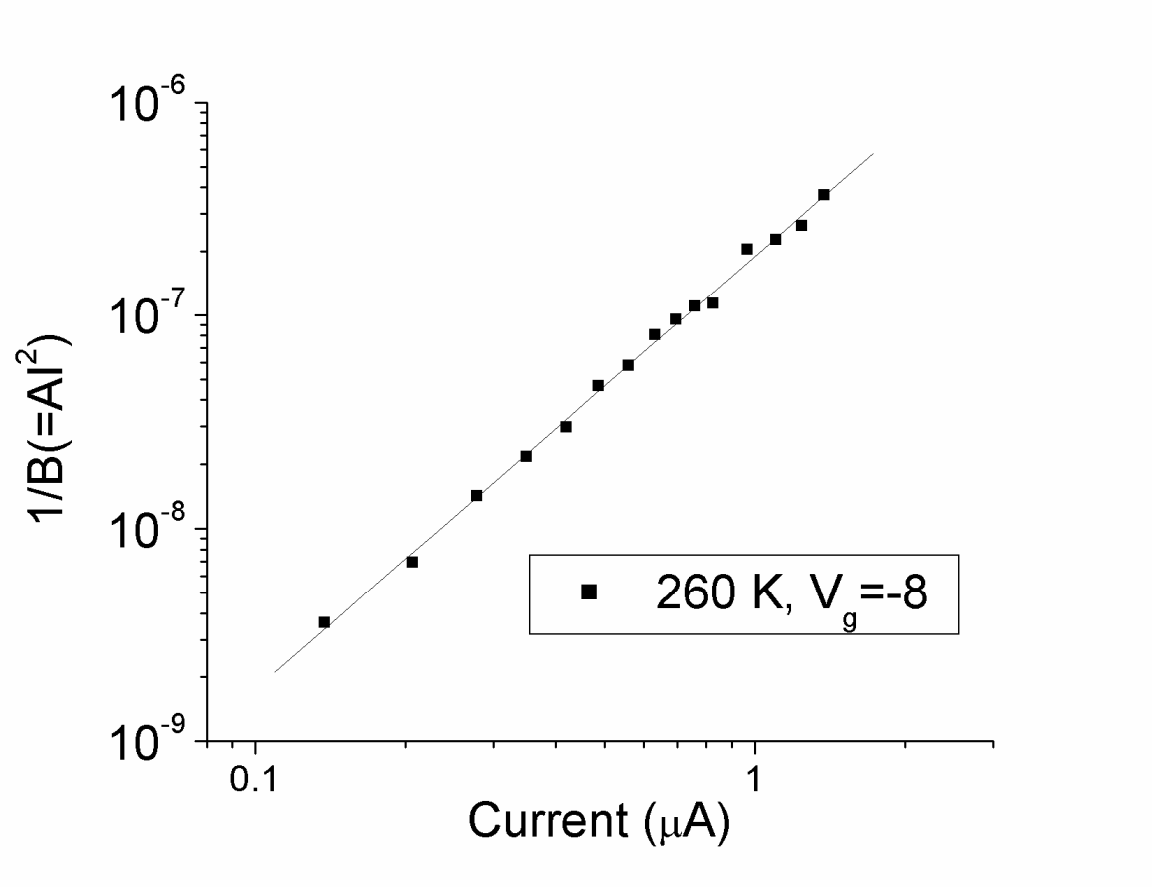

Figure 4-1. Dependence of noise on current bias. Numerator of the Hooge equation plotted vs. current to check on the expected squared dependence of the noise. The slope is 2.03 ± 0.03 on data from sample 1.

As a first check to see if our data follows Hooge's law, I will show that the noise spectral power is indeed quadratic in current, which is expected for resistance fluctuations.

$$\frac{1}{S_I} = f / AI^2 = Bf \tag{4.2}$$

Eq. 4.2 is a simplified version of Hooge's law (Eq. 3.3) where $\beta = 0$ and $z = 1$. A plot of $1/B$ vs. current should display an I^2 dependence. This is done in Fig. 4-1 for sample 1 at 260 K and $V_g = -8$ V.

It is also useful to think about a form of Hooge's law more suitable to transistors,

$$S_I(f) = AI^2/f^z = \frac{\zeta}{N} I^2/f^z = \frac{\zeta}{C_G V_G/e} I^2/f^z \tag{4.3}$$

where the last step is applicable if the bias voltage is held constant and the gate is varied in the linear regime of the transistor, so that $N=C_G V_G/e$.

Next, I will turn to a careful examination of the frequency dependence; i.e. can the frequency dependence be described as $1/f^z$? If z varies from unity then the constant A is no longer dimensionless, which means variation in A will depend on the frequency of the measurement. In many of the spectra I have taken at the same bias temperature and bias voltage the exponent varies from 0.9 to 1.1 between scans at different gate voltages, making it difficult to decide whether it is acceptable to ignore the variation when trying to determine the prefactors A or ζ. Furthermore the data is sometimes influenced by the presence of telegraph signal whose spectrum is

$$S_i(f) = \frac{bI^2}{1+\left(\frac{f}{f_o}\right)^2} \tag{4.4}$$

where b is a constant. Hopefully the magnitude of this noise is small, or a region in frequency space can be found where its effects are negligible. I will go through the

data analysis methods that I used to try to gain confidence that the trends observed in the variation of A with temperature and carrier number are real.

4.2 Data analysis techniques

I attempted to analyze the noise spectra by several methods described below. Each method assumes a certain functional form for the spectra, and so may introduce systematic errors in the dependence of the noise pre-factor on temperature. I will discuss the advantages and drawbacks of each method.

4.2.1 Power-law method

A first way to think about extracting the value of A for a given noise spectrum is to plot the noise power vs. frequency on a log-log plot as in Fig. 4-2. Then the slope $d(\ln S_I)/d(\ln f)$ gives the value of z, and the value of AI^2 is the given by S_I at f = 1 Hz. Since the value of z varies for different noise plots, the constant A is no longer unitless. This may cause problems for the comparison of different spectra; for example, the temperature dependence would in principle depend on the measurement frequency. The value of A is also very sensitive to the errors in the slope.

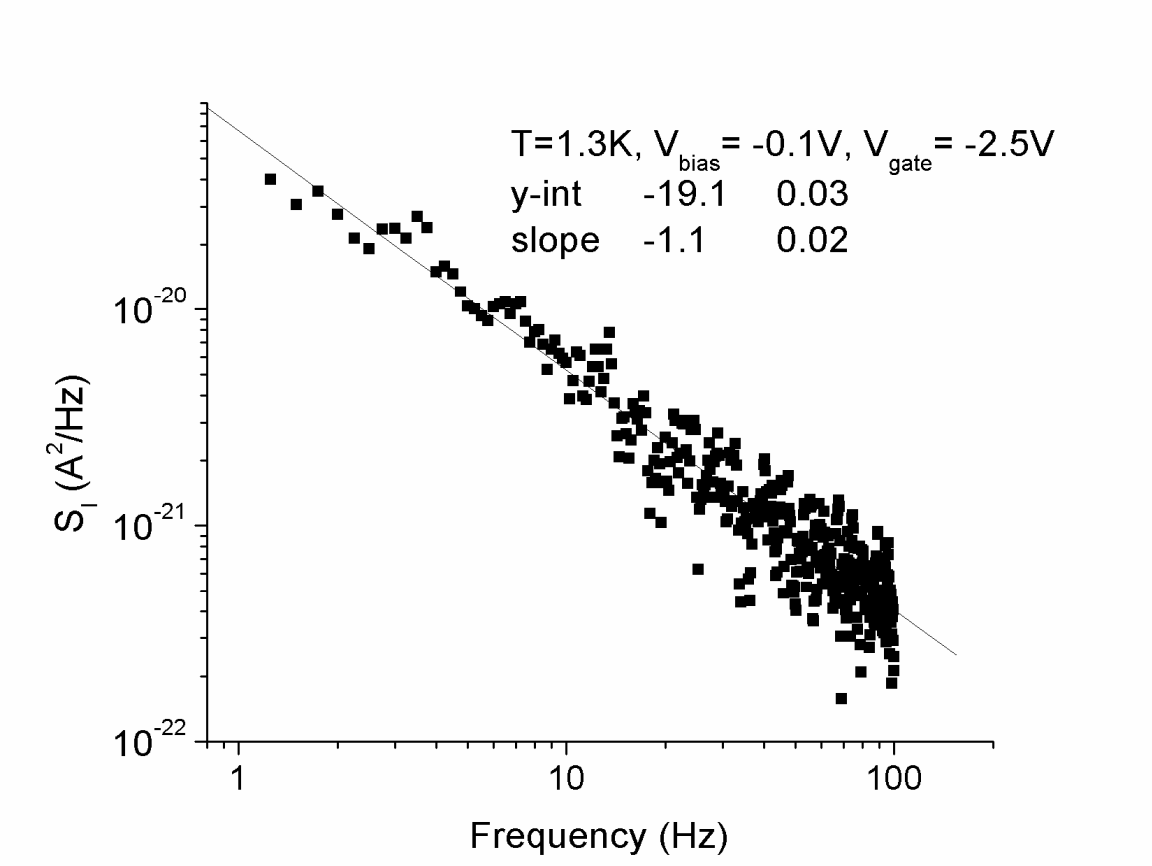

Figure 4-2. Current noise versus frequency. The log-log plot allows for a linear fit to extract the values of A and z for the spectrum. Here $A = 2.67 \times 10^{-8}$ and $z = -1.11$

4.2.2 Inverse noise method

Another useful way to display the data is to plot the reciprocal of the noise power versus frequency as in Fig. 4-3. Since this should now be a proportional relation if the exponent $z = 1$, the parameter A is straightforward to extract; the reciprocal of the slope is AI^2. The advantage of fitting the data with a line is that it forces all of the plots to have $z = 1$ and therefore have a dimensionless A. This means that comparison should be on a more equal footing. The difference between this and

the power law method, and a crucial factor to consider in fits in general, is that the data will be weighted differently in these different methods. The default for most fitting programs is to assume that there is a constant percentage uncertainty in the data entered into the routine. Taking the reciprocal of the data without altering the uncertainty will lead to different values for the fits.

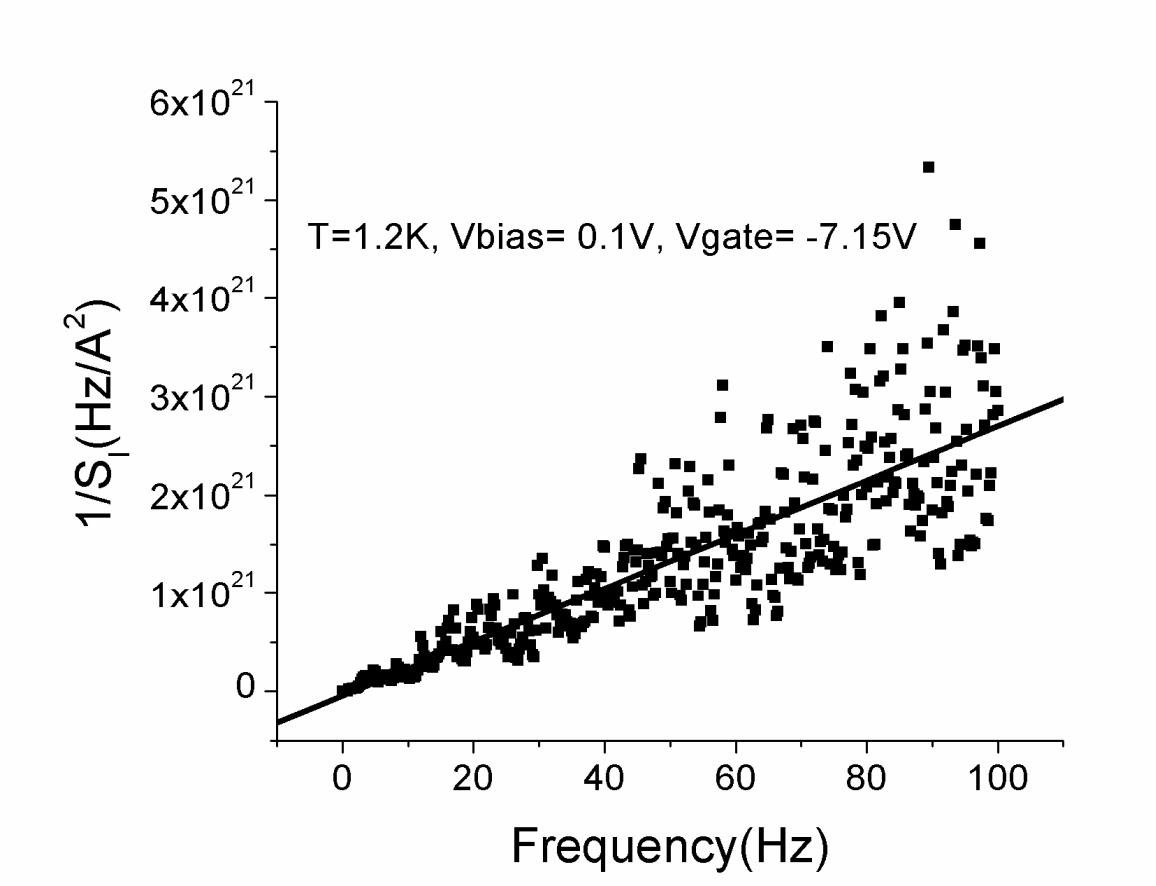

Figure 4-3. Plot of 1/SI versus frequency. Here the frequency dependence becomes linear and fitting a proportional relation to the data forces z =1. For this spectrum A = 1.36×10^{-8}.

4.2.3 Inverse noise plus telegraph method

Some of the noise spectra appear to have a Lorentzian-like component, which could be due to telegraph noise from a single fluctuator. If this is the case then it would be desirable to account for the telegraph contribution by fitting a sum of the telegraph noise spectrum and the 1/*f* spectrum to the data set[31], i.e.

$$S_i(f) = \frac{AI^2}{f} + \frac{BI^2}{1+\left(\frac{f}{f_o}\right)^2} \tag{4.5}$$

I attempted this in the following manner. In the fit the value of the knee frequency in the telegraph Lorentzian and the magnitude of the 1/*f* and telegraph noise are allowed to vary but the value of *z* is fixed at 1. This is for two reasons: If the value of *z* is allowed to vary the fitting process commonly fails to converge and the data needs to be successfully fit over a large range of data for the exponent's deviation from one to be fit accurately. There is an additional difficulty that, in introducing an additional component of the noise in the fit, that there will be a systematic reduction in the magnitude of the 1/*f* noise obtained in the fit (because the best fit to the noisy data set will always include some positive Lorentzian term). Figs. 4-4 and 4-5 show this technique being applied to the reciprocal of the noise power and to the noise plotted directly.

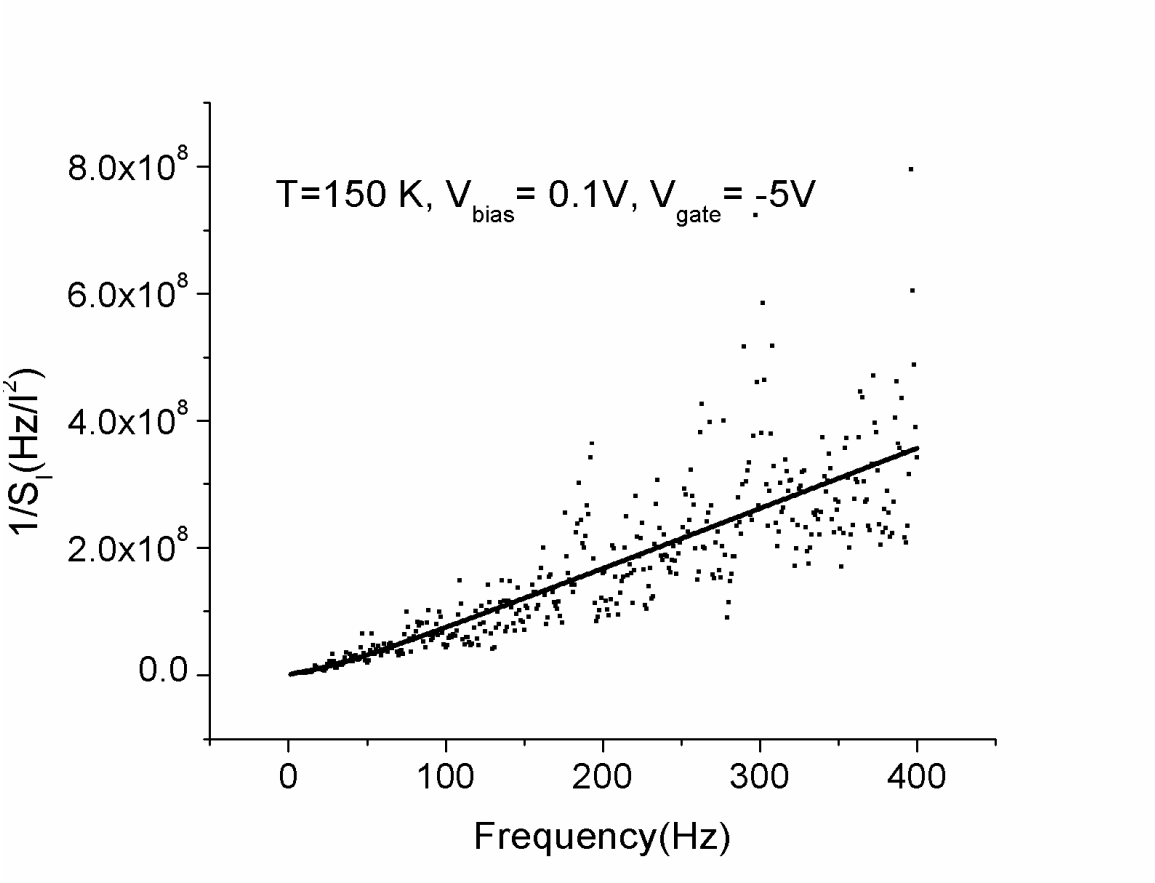

Figure 4-4. A nonlinear fit for 1/noise versus frequency. The added telegraph term has a knee at 10 Hz and its effect is best seen by the fits bend at low frequencies.

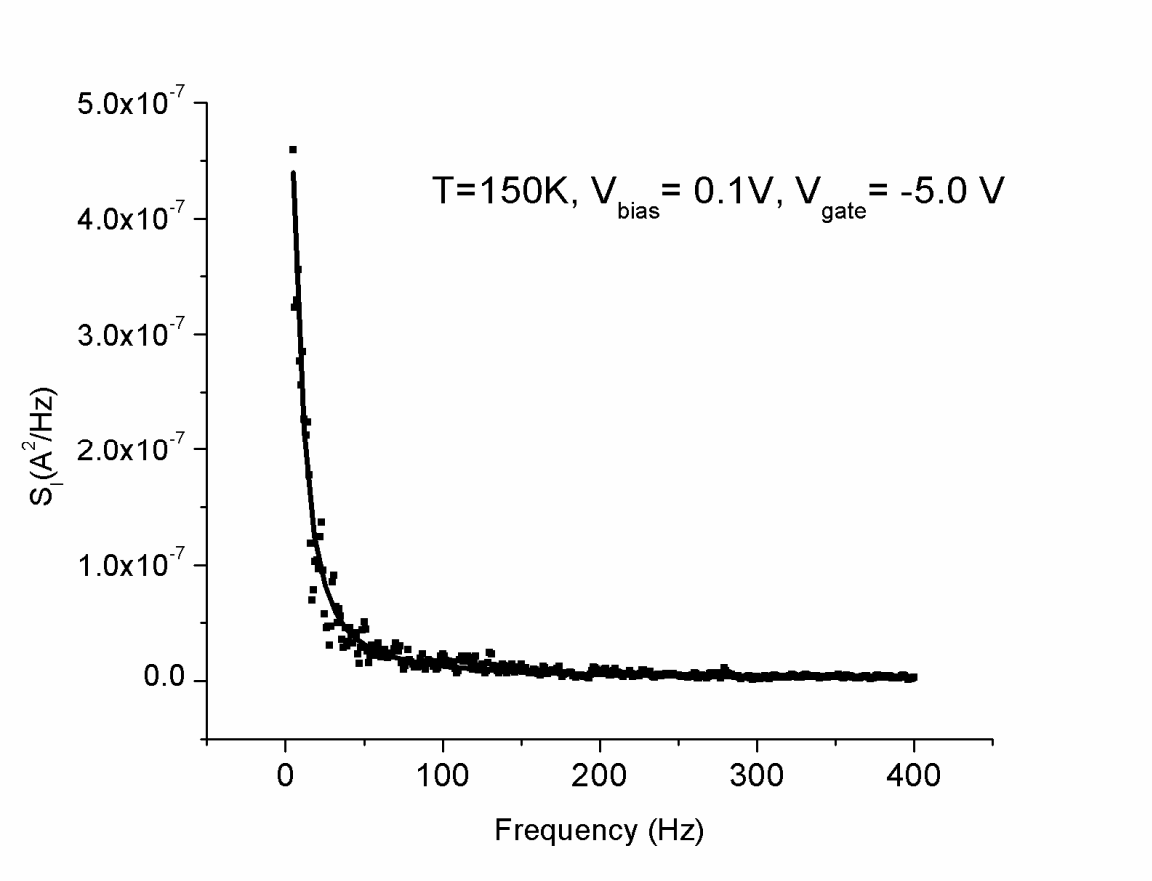

Figure 4-5. Noise power versus frequency with a nonlinear fit. Same data as for the reciprocal fit Fig. 4-4.

4.2.4 “Show all the data” method

Because of the difficulties discussed for the methods above, I developed a new method that uses each data point of the spectrum as an independent measure of A that is shown in Fig. 4-6. For each point I determine a value of $1/A = I^2/fS_I$; this way each data point in the spectrum produces a value for $1/A$ instead of the spectrum as a whole. Then I can examine the dependence of $1/A$ at a particular frequency on gate

voltage and temperature, and determine whether there is a significant dependence on the frequency.

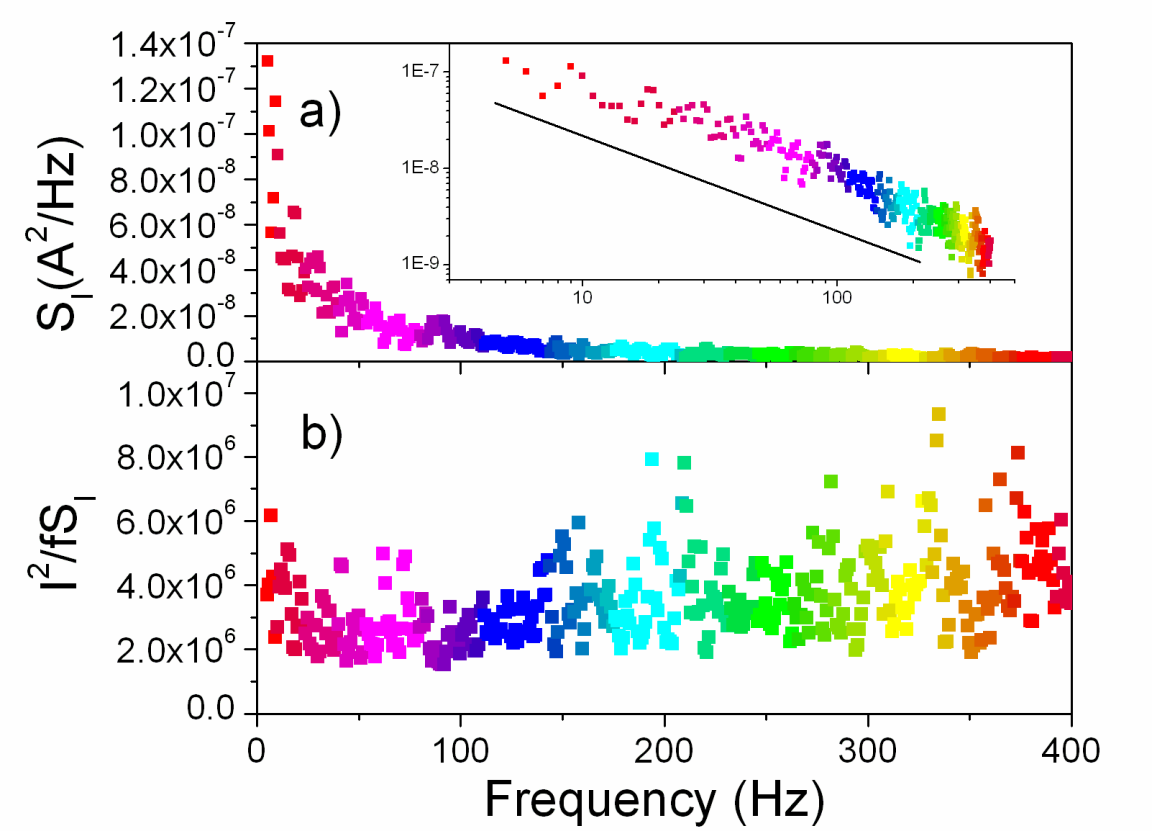

Figure 4-6. "Show all the data" plot. a) Spectrum of 1/f noise from a CNT FET at a bias voltage of 100 mV, a gate voltage of -8 V, and a temperature of 150 K, shown on linear-linear scale (main panel) and log-log scale (inset). The solid line in the inset indicates a slope of -1. b) Presentation of the noise spectra with the values recalculated to give the value of the constant $1/A = (I^2/fS_I)$ at each frequency, as discussed in the text. Colors indicate the value of the frequency the data is taken at and the points are separated by 1 Hz.

4.3 Gate dependence

The observed gate dependence of the nanotube noise is best plotted as 1/*A* versus gate voltage. Since the graph is linear it is easy to extract the value of γ from

$$AI^2/f^z = \frac{\zeta}{N} I^2/f^z \Rightarrow 1/A = \frac{C_G V_G/e}{\zeta} \tag{4.6}$$

This dependence indicates that the transistor is in the linear regime where the gate voltage linearly increases the number of carriers in the nanotube. By comparing the 1/*A* vs. gate curve with the current vs. gate curve in Fig. 4-7 it is clear that the current is not linear with gate voltage while the inverse of the noise magnitude is. This is an indication that the data is described by Hooge's law, as seen in Eq. 4.6 it is expected that $1/A \propto N$. This is also strong evidence that the fluctuations are in mobility, not carrier number.

Specifically, a model of random potential fluctuations[50] that has been used to explain the noise in short, Schottky-barrier-dominated CNTs[51] predicts a much stronger dependence of 1/*A* on V_g. Thus we can eliminate charge fluctuations in the dielectric as a source of noise in our CNT devices, at least in the linear regime.

Data were taken at different temperatures to determine the evolution of ζ. Another benefit of our use of ζ is that it also compensates for changes in the threshold voltage at different temperatures and for the change in the Fermi energy versus gate voltage; this is due to using the rate of change of 1/*A* vs V_g as seen in Eq. 4.6.

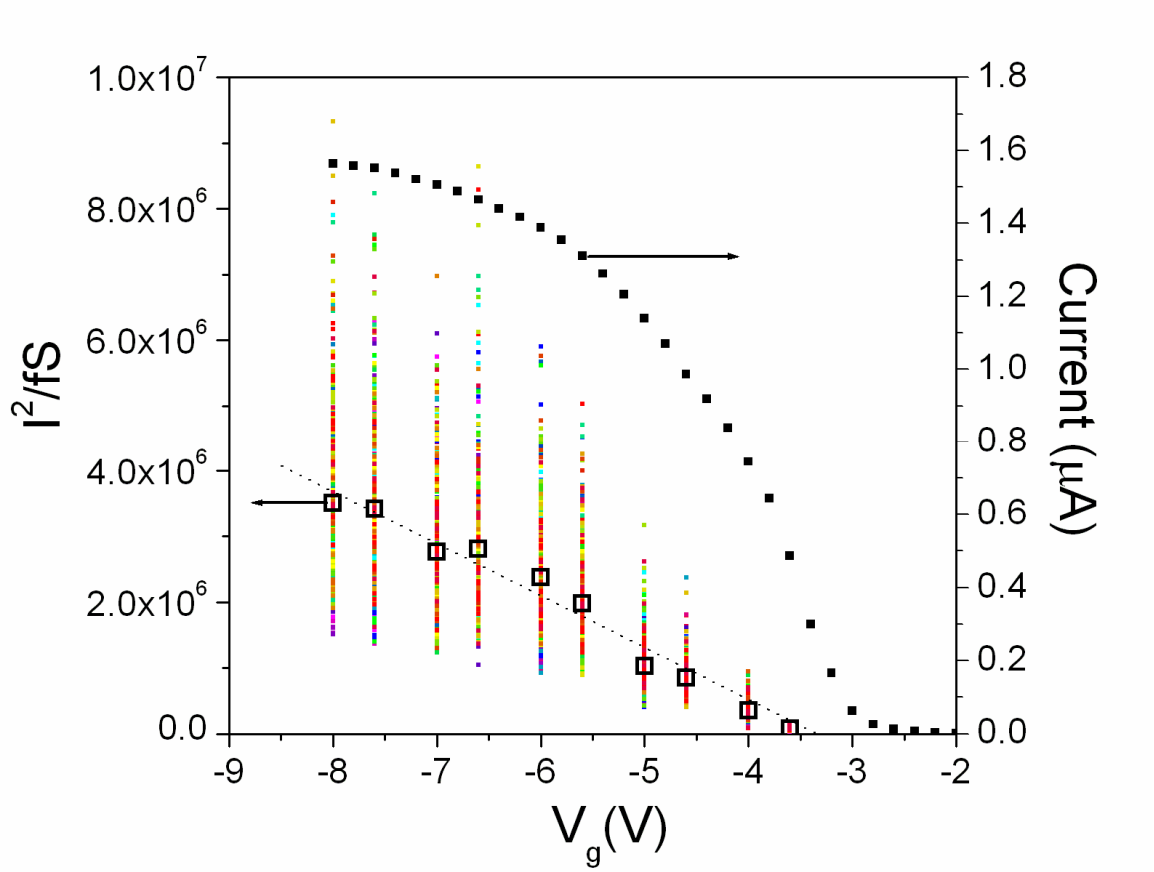

Figure 4-7. Reciprocal of the noise prefactor 1/A = I^2/fS_I (colored squares) and current (filled squares) versus gate voltage for sample 1 at 150 K. Current data are taken with drain voltage of 100mV. The 1/*A* data are color-coded according to frequency as in Fig. 4-6. The open squares indicate the mean values of 1/*A* at each gate voltage, and the dotted line is a linear fit to these points. The standard deviation of the mean for these points is smaller than the size of the squares used to indicate the mean value. Note that larger 1/*A* values correspond to less noise. A benefit of plotting the data using this technique is that all of the data from the spectra are presented.

The main benefit of the show-all-the-data method is that all the data from the noise spectra can be displayed in a 1/*A* versus gate voltage graph, and is all used to

determine the value of ζ. The method does assume implicitly that $z = 1$, however the value is predicted to only vary slightly even for a non-constant $D(E)$ as discussed in Chapter 3. The particular frequency range does not significantly alter the magnitude of the value of ζ. This can be seen by observing the color coding of the data. The frequency range chosen does not affect the value of the slope obtained from the $1/A$ vs Vg plot.

4.4 Noise in semiconducting devices at room temperature

Two papers on $1/f$ noise in individual semiconducting devices came out concurrently in 2006, one from Maryland[31] and another from the IBM group[51]. Both papers revealed several significant aspects of the noise in CNTs and both found that the reciprocal of the noise amplitude is linear with gate voltage. In this section I will explain the results of the Maryland[31] paper and both of the plots, Figs. 4-8 and 4-9, are taken from that paper.

Assuming that the transistor is in the linear regime we again use Eq. 4.6. We calculate the capacitance $C_g = c_g L$, where c_g is the gate capacitance of the device per unit length, L is the length of the CNT and V_g is the applied gate voltage. For our CNT devices, $c_g \cong \frac{2\pi\varepsilon_0\varepsilon_{sub}}{\ln(2t/d)}$ with ε_{sub} the dielectric constant of the oxide, t the thickness of the oxide and d is diameter of the CNT.

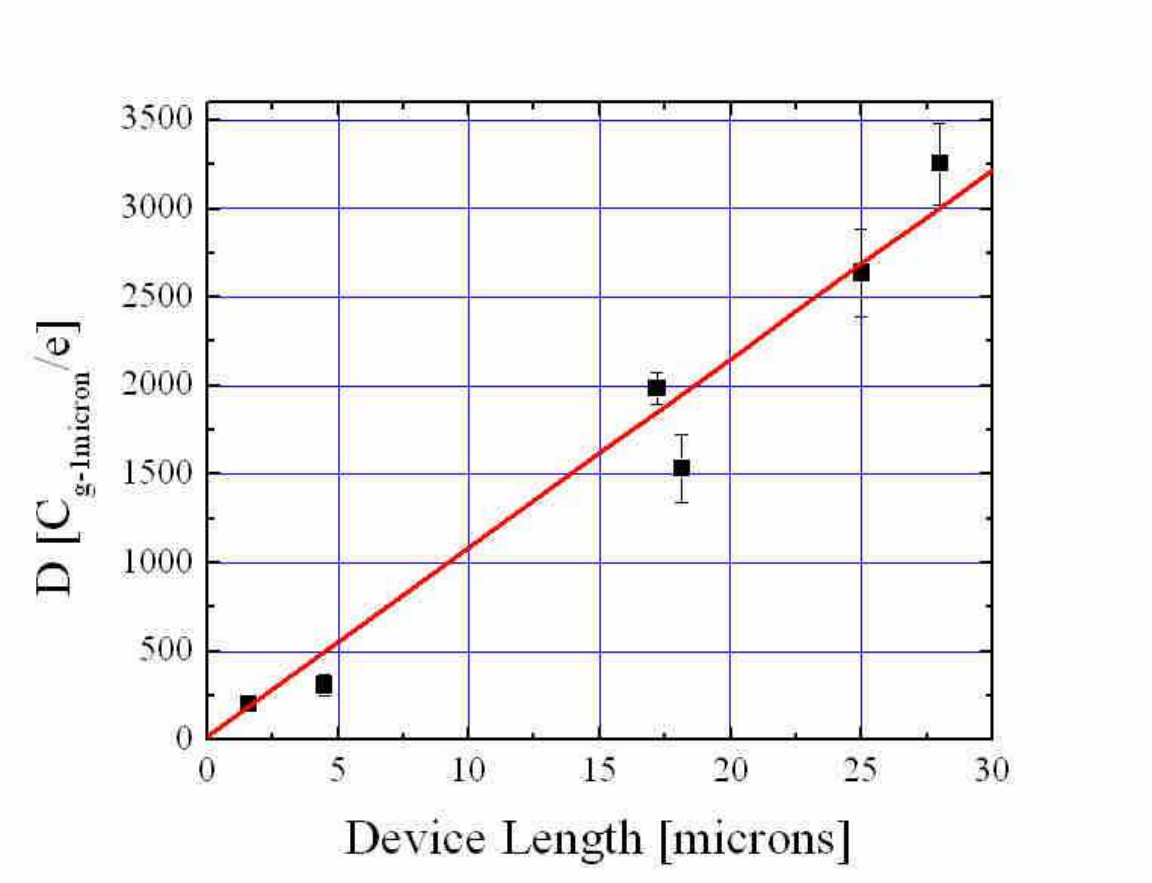

Figure 4-8. Noise data from Ishigami *et al.*[31] Measurements taken on devices at a range of lengths to demonstrate that the source of the noise is the channel resistance not the contact resistance. If the noise was being sourced at the contacts it would be expected that the low length limit would be dominated by a contact term, while the longer CNTs would be dominated by noise from the CNT. However, the behavior is linear over the entire range indicating that the main source of noise is the CNT.

After seeing that the noise parameter $1/A$ varies linearly with the gate voltage as I have also shown for my data in Fig. 4-7, the experiments verified that the noise being measured in the two contact geometry is dominated by noise created in the CNT and not noise from the contacts. This was done by plotting the quantity D =

$c_g L/e\gamma$ vs. length for several different devices with lengths ranging from 2 to 30 μm, shown in Fig. 4-8. The linear behavior verifies that the noise is coming from the fluctuations of the length-dependent resistance of the CNT. The value for ζ obtained from this is 9.3×10^{-3}, comparable to traditional FET devices. This means that nanotubes are not excessively noisy; but since they do have far fewer carriers than normal semiconductors individual CNT devices will have larger *A* values. All of this data was taken in ultra-high vacuum (UHV).

Data were taken on the same device in UHV and ambient pressure to test the prediction that physisorption of gases was a possible cause of noise in CNT. The results of this indicate the reverse phenomenon from that expected if physisorption were the source of noise: The CNT is actually noisier in UHV as shown in Fig. 4-9. It is important to remember when looking at the graph that $1/A$ is the reciprocal of the $1/f$ noise magnitude, so larger values indicate less $1/f$ noise.

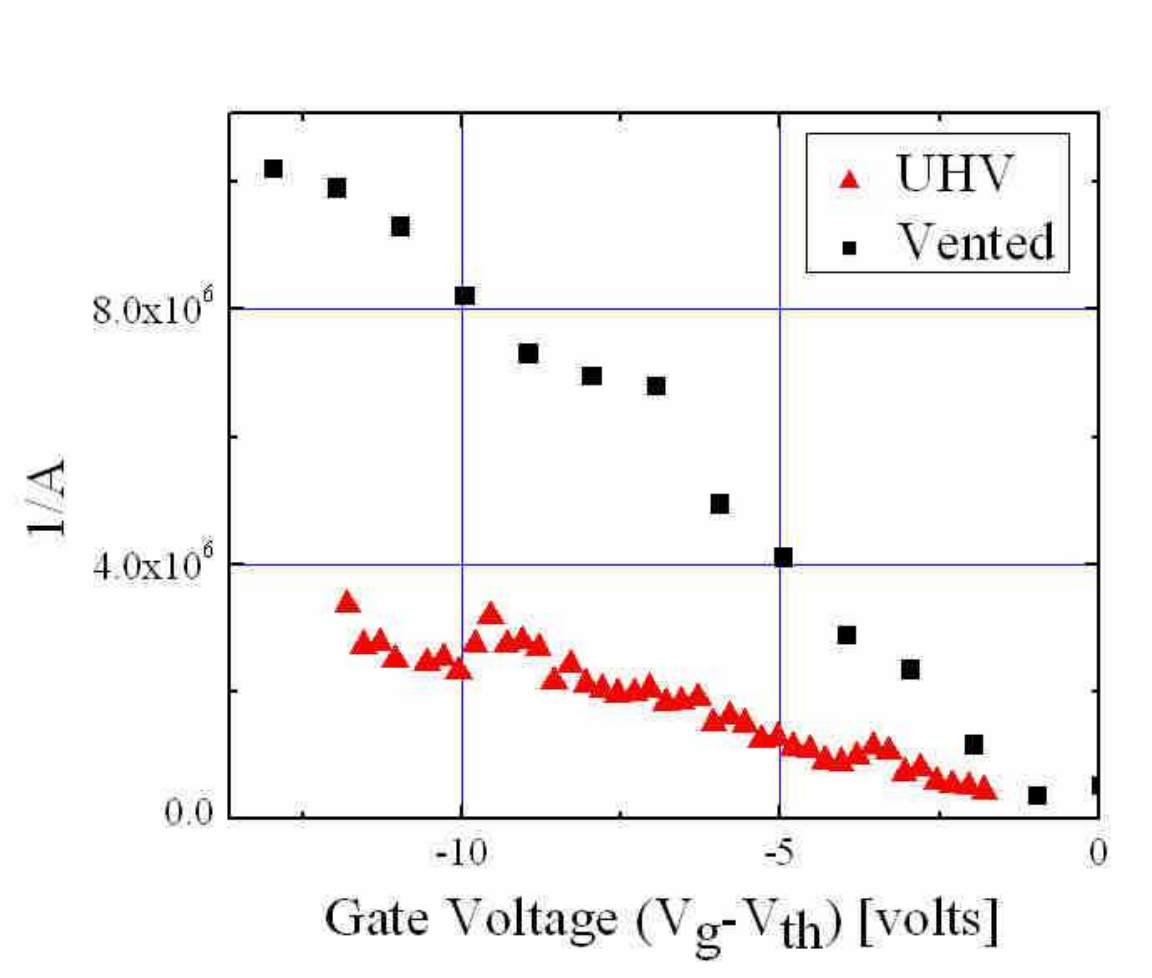

Figure 4-9. Comparison of inverse noise amplitude $1/A$ vs gate voltage $V_g - V_{th}$ for the same semiconducting CNT device in UHV and in air from Ishigami *et al*.[31] at room temperature. The amplitude of the $1/f$ noise in air is three times smaller than in UHV.

4.5 Temperature dependence

Fig. 4-10a shows the temperature dependence of ζ for two CNT devices. Device 1 has a diameter of 1.4 nm, and Device 2 has a diameter of 1.9 nm. The

Hooge's constant ζ, where $A=\zeta/N$, has an exponential dependence on temperature from 1.2 K to 150 K, with a change of about an order of magnitude, and is much less temperature dependent at temperatures greater than 150 K. As described in the previous chapter, we can use the temperature dependence of ζ to gain information about the density of states of the fluctuators that are causing the 1/f noise. This is done by using the Dutta and Horn result that $E_p = -\ln(2\pi f\tau_0)k_B(T) \approx 0.4$ eV for $f = 1$ Hz and $\tau_0 = 10^{-14}$ s (this value is introduced in Ch. 3 and Eq. 3.11)) and T =150 K. The noise versus temperature data then indicated that the fluctuators responsible for the 1/f noise are mostly at and above 0.4 eV. The Dutta and Horn model also connects the exponential dependence of the noise to an exponential rise in the density of states responsible for the 1/f noise.

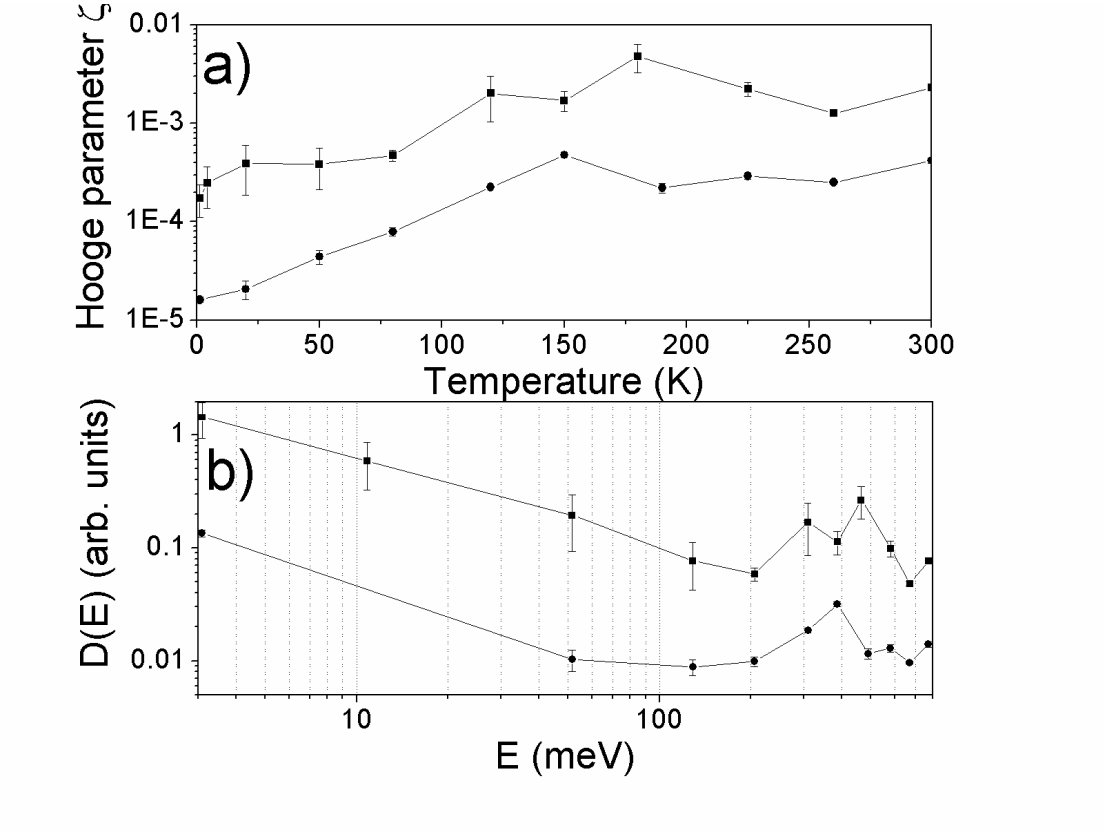

Figure 4-10. Noise vs temperature (a) Temperature dependence of the Hooge parameter ζ for two CNT devices. The data points are calculated using the slope from <1/*A*> vs *Vg*, as shown in Fig. 4-7. The significant upward trend between 1.2 K and about 150 K is seen in both samples. (b) Distribution of activation energies of the fluctuators *D*(*E*) responsible for 1/*f* noise, calculated as described in text. Filled squares and circles correspond to Device 1 and Device 2 respectively, in both (a) and (b)

For another way to plot the data that allows for an easier identification of the peak we can use a formula from the previous chapter,

$$S(\omega,T) \propto \frac{k_B T}{\omega} D'(E') \tag{3.10}$$

which means that ζ/T is proportional to the density of states, since ζ is also a measure of the magnitude of the noise. This is plotted in Fig. 4-10b. This is the same data set as in Fig. 4-10a, but this more clearly shows the location of the peak.

It is not surprising to see a spread between the two traces for the different samples, even though they were prepared identically, with the same contacts and similar lengths. Individual defect contributions for the two devices could be very different, as random structural defects could vary greatly between the tubes. The local density of defects in the oxide should also play a strong role in determining the strength of the $1/f$ noise.

The main feature of Fig. 4-10 is the peak in $D(E)$ at $E \cong 0.4$ eV. This feature is responsible for the majority of the room-temperature noise. The characteristic energy scale allows us to rule out some possibilities for the source of the noise. The energy scale is comparable to the bandgap ($\cong 0.5$ eV and $\cong 0.37$ eV for Devices 1 and 2 respectively) and therefore we can rule out electronic excitations (e.g. defect ionization, etc.) within the CNT itself as the major noise source; such mechanisms should have characteristic energies less than or equal to half the bandgap. As discussed above, we also rule out potential fluctuations due to the motion of charged defects in the dielectric. Structural fluctuations of defects in the CNT lattice itself are also ruled out, as they have very high characteristic energies. The energy is $\cong 10$ eV for Stone-Wales defect formation[52, 53] which involves one of the hexagons of the lattice losing a carbon atom to become a pentagon.

Unfortunately the characteristic energy $\cong 0.4$ eV does not provide enough information to pinpoint what is causing the noise. However, the fact that the noise

magnitude is comparable to conventional MOSFETs suggests that the noise may in fact result from similar processes in CNT-FETs, i.e. motion of defects in the dielectric or at the dielectric/CNT (or dielectric/vacuum) interface. Still, other processes, such as binding and unbinding of strongly physisorbed species cannot be ruled out; the binding energies for CO_2 and H_2O, for example, lie in this range[51, 54]. Though our measurements are carried out in helium gas with an extremely low partial pressure of atmospheric components, it is possible that previously-adsorbed water is still present on the SiO_2 surface and could be responsible for the noise.

To summarize, we have measured the Hooge parameter $\zeta(T)$ at temperatures between 1.2 K and 300 K. The room temperature value, $\zeta(300\text{ K}) \sim 10^{-3}$, we observe is comparable to $\alpha(T = 300\text{ K})$ found in traditional FETs indicating that CNT-FETs are not afflicted by inherently large noise at room temperature. I use $\alpha(T)$ to estimate the distribution of activation energies of the fluctuators $D(E)$ responsible for the noise*;* $D(E)$ shows two features: a rise at low energy with no characteristic energy scale, and a broad peak at energy of order 0.4 eV. By using the theory presented in Chapter 3, I determined that the latter feature is responsible for the room temperature noise. Electronic excitations and structural fluctuations within the CNT itself can be ruled out as the source of this feature. Fluctuations within, or at the surface of, the amorphous dielectric are likely responsible for the room temperature $1/f$ noise in CNT-FETs on SiO_2, though some physisorbed species (e.g. H_2O, CO_2) have similar binding energies[54] and could be responsible for the room-temperature noise.

To further test whether the noise is coming from the oxide, the oxide layer under a CNT could be etched away. A particularly illuminating experiment would

create four leads on one CNT, measure the noise in the two devices created this way, and then etch out the oxide under one of the devices. This would eliminate tube to tube variation and make sure that the etching process didn't damage the CNT. Other possibilities include testing devices on different substrates and treating the surface with chemicals that should passivate the traps in the substrate.

As a result of the work here at Maryland[31] and IBM[51] it is now clear that semiconducting CNT devices have a noise level very similar to that of traditional semiconductors. The value for γ is in line with many other materials and devices, and the high values for A obtained by early experiments[14] was merely an indicator of the small number of electrons in the material, not an indicator of an extraordinarily noisy material.

Chapter 5 Introduction to 1-D physics and telegraph signal

CNTs are an ideal laboratory for studying one-dimensional (1-D) electron behavior. This behavior is expected to differ from that in three-dimensional systems due to the inability of electrons to re-arrange themselves to minimize electron-electron interactions.[55-57] This chapter will begin by motivating the need for a new description of the electron state in CNTs. Then it will introduce the technique we intend to use to study the phenomenon in semiconducting CNTs. The chapter will conclude by explaining how the hysteresis in CNTs makes it possible to uncover the state of the electrons in semiconducting CNTs.

5.1 Drude and Luttinger

The initial successful description of electrons in solids was produced by Drude[58, 59]. This model for electron behavior assumes that the electrons do not interact at all with each other, termed the independent electron approximation. In fact it is assumed that the electrons only interact with the ion cores through hard core scattering processes, resulting in a characteristic scattering time and length for a given conductor. This assumption proves to be very good for most metals where the distance between electron-electron scattering events can be in the millimeter range.[59] This is the origin of the term electron gas, since the electrons are behaving like gas molecules in the ideal gas model. The addition of another electron, for example through tunneling, to the electron gas is possible at the energy of the highest

occupied state, as the other electrons will easily be able to re-arrange themselves to eliminate interactions. This means that there are excited states present just above the highest occupied electron state; there is no energy gap in the density of states for adding an electron, termed the tunneling density of states (TDS). Superconductors are a good example where electron-electron interactions result in a correlated electron state which exhibits an energy cost to add another electron to the system; adding an unpaired electron to the superconductor requires giving the electron an additional energy above the energy of the highest occupied state.[60] It is important to keep in mind the distinction between the density of states D(E) for the system and the tunneling density of states (TDS). The TDS measures the energy distribution of excited states for the sudden addition of one electron to a system initially containing N electrons, i.e. a transition from $N \rightarrow N+1$ electrons, while D(E) corresponds to the energy distribution of single-particle states of a system with N electrons. For non-interacting electron systems the two densities of states are equivalent, but for interacting systems they can be very different. This chapter will deal will almost exclusively with the TDS and not D(E) for electrons already in a system.

It may seem obvious that there will be situations in which ignoring the electron-electron scattering is no longer feasible. Shrinking the number of dimensions in the system should begin to cause problems to the concept of the electrons being free from interacting with each other. A first modification of this theory is the Fermi-Liquid theory[59, 61, 62]. In this theory the electrons do have some small interaction with each other; however, it is assumed that this interaction can be treated as a small perturbation to the original free electron gas states. This results in the requirement of

using an effective mass to calculate the new wave-vectors and energies, but the TDS is still free-electron like; there is a one-to-one correspondence between non-interacting electron states and the new interacting "quasiparticle" states.

In one dimension it seems reasonable that this approach should fail. The electrons will have to interact strongly with each other as they are confined to stay along the line defined by the 1-D conductor. In this situation Tomonaga and Luttinger predicted that the electrons would form an interacting electron state where the perturbative terms used in the Fermi-Liquid theory would diverge[63], this state is the Luttinger liquid state[55-57] (Tomonaga actually originated the concept of the new state, but only for a restricted set of conditions, Luttinger showed that it should occur in any arbitrarily weakly interacting 1-D electron state). The Luttinger state was first described in the 60's but no experimental attempts to measure the signatures of this state were successful (or at least published) until 1995 for constricted AlGaAs/GaAs heterostructures[64-68] followed closely in 1999 for CNTs[69, 70].

As opposed to the independent electron assumption, perhaps visualized as a few ping-pong balls bouncing around the Grand Canyon, the Luttinger liquid model could be thought of as the executive desk toy, where each electron knows exactly what the rest are doing, as depicted in Fig. 5-1. This will obviously create a different TDS spectrum than in the previous model, as each electron will have formed a coordinated lowest energy with all the other electrons in the system and each electron will have to be disturbed in order for an extra electron to enter the system. The result is that a finite energy is required to add an electron to the system; at $T = 0$ it is

impossible to add an extra electron to the system at exactly the Fermi level, and the TDS has a power law behavior.[63]

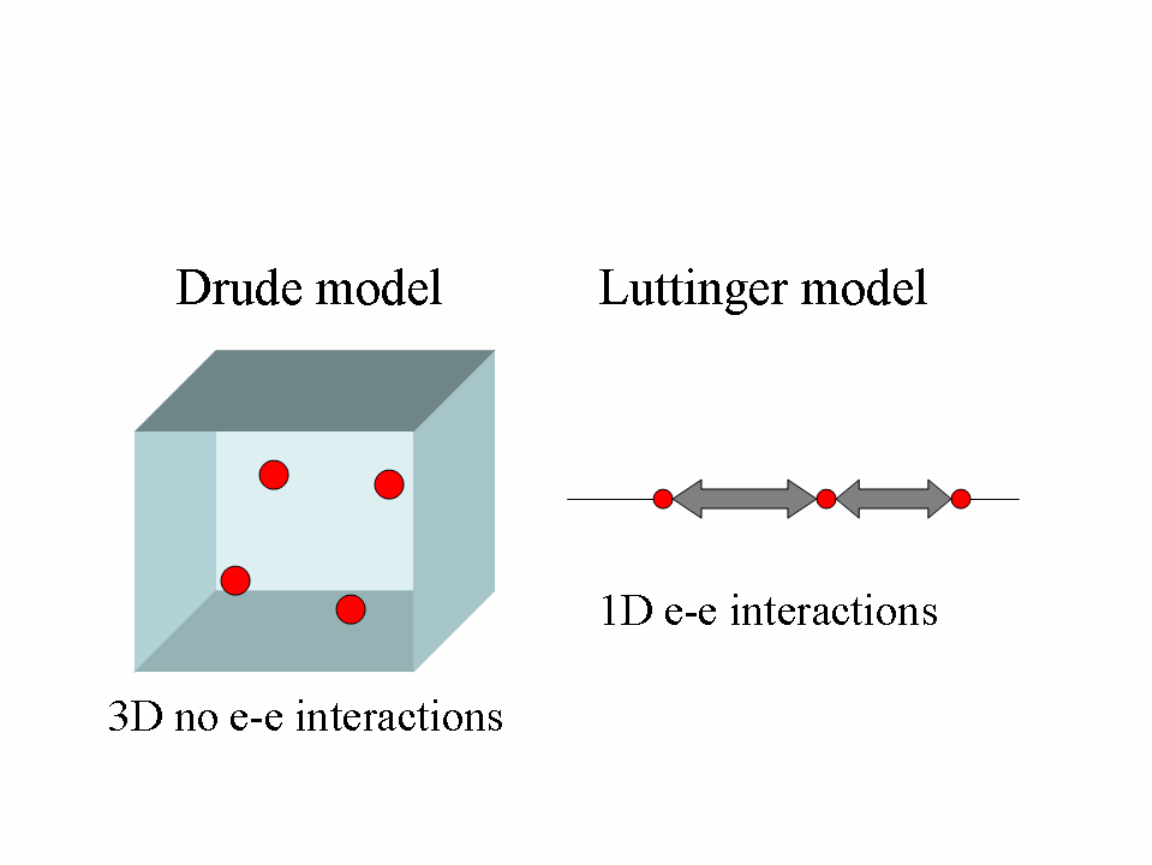

Figure 5-1. Drude vs Luttinger. This is a visual depiction of the electron behavior in the two different models. In the Fermi gas the electrons act independently from one another, but in the Luttinger model electron-electron interactions should cause a bosonic state to form that would alter the physics of the system.

This power-law behavior, $TDS(E) \propto (E-E_f)^{\alpha}$ is depicted in Fig. 5-2. This can be measured experimentally in a tunnel junction between the Luttinger liquid and a Fermi liquid or another Luttinger liquid; such a junction shows a power-law behavior

for the zero-bias conductivity versus temperature and differential conductance bias voltage[63], $G(T) \propto T^{\alpha}$ and $dI/dV \propto V^{\alpha}$.

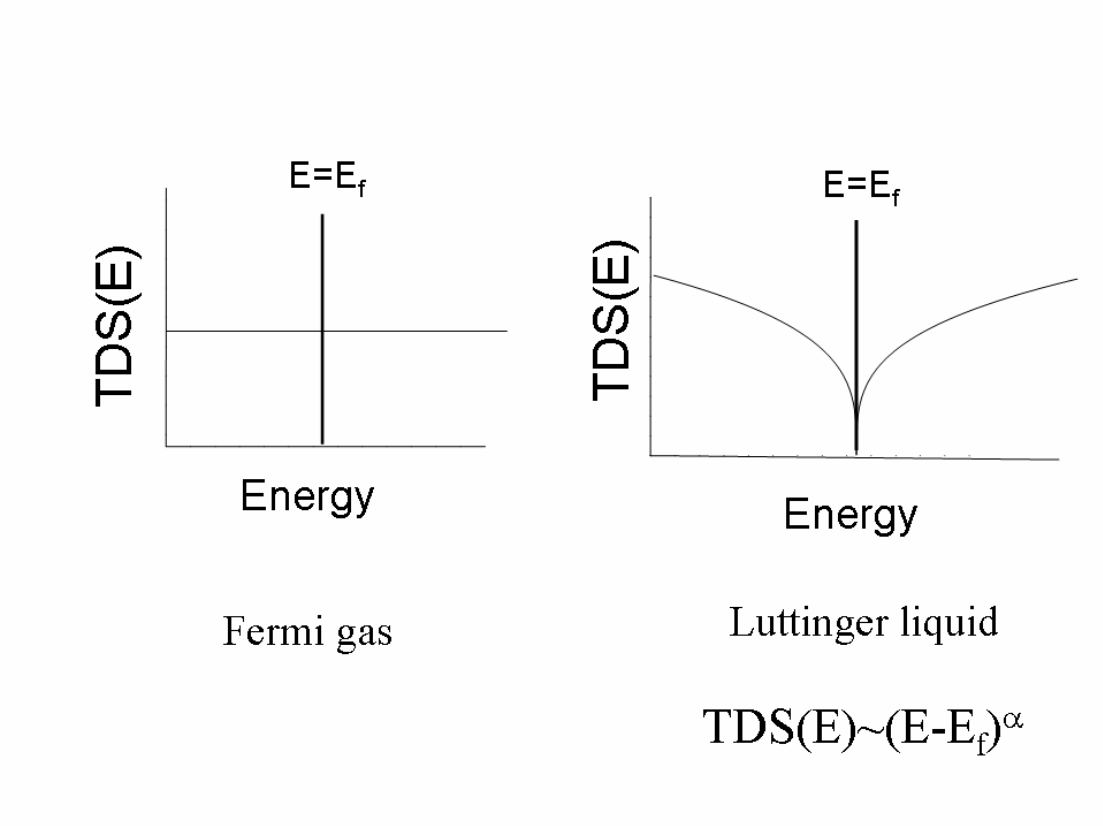

Figure 5-2. Tunneling density of states. The left graph depicts the availability of TDS just above the Fermi energy in a system described by Fermi statistics. On the right is a graph of the TDS for a Luttinger system, with its characteristic dip at energies near the Fermi Energy. This TDS leads to tunneling observables for the zero bias conductivity versus temperature $G(T) \sim T^{\alpha}$, and for the conductivity versus bias voltage, $dI/dV \sim V^{\alpha}$.

There is a further complication for determining the TDS. The unitless parameter α that describes the experimentally measurable effects is determined by the

interaction parameter *g*, a unitless variable that describes the amount of electron interaction in the system. *g* should always be the same for a given one-dimensional system, but α depends on the geometry of the experiment, i.e. whether the electron is tunneling into the "end" of the one dimensional system or the "bulk". This will be illustrated in the next section where I describe the initial experiment on the Luttinger state in CNTs. g ranges from 1 to 0 with smaller values indicating stronger interactions.

5.2 Previous measurements in carbon CNTs

The original measurements performed on the Luttinger state in CNTs were performed by Bockrath *et al*.[69] on metallic CNTs in two different geometries: metal electrodes on top of or below the CNT. The significance of doing this is that different tunneling behaviors are observed for the two contact situations. When metal leads are first placed on the chip and then CNTs are placed on top of the leads, the device is referred to as having bottom contacts. This contact geometry usually results in higher contact resistance due to a weaker coupling between the CNT and the metal contact. In essence the CNT is just resting on top of the metallic lead. This results in the electrons having the opportunity to tunnel into any part of the CNT that is lying above the contact, or the "bulk" of the CNT.

When the CNTs are first placed on the chip and then metal leads are created on top of the CNTs, as in the devices used in this thesis, the devices are said to have top contacts. In this situation the presence of the metal electrode "cuts" the CNT

electronically; electrons in the CNT impinging on the metal electrode have essentially zero probability of continuing under the electrode in the CNT. Thus the electronic current from electrode to CNT essentially remains entirely within the metallic lead until it is forced at the last moment to exit the lead and tunnel into the CNT, and the geometry approximates tunneling into the "end" of the Luttinger liquid. This picture is born out by low temperature measurements of the charging energy of devices in both configurations[71, 72]; CNTs with top contacts have energies determined by the length of the CNT between the leads while CNTs with bottom contacts have a charging energy determined by the entire length of the CNT. The equations for the exponent in the two different geometries are[73, 74]

$$\alpha_{end} = \frac{\frac{1}{g} - 1}{4}$$
$$\alpha_{bulk} = \frac{\frac{1}{g} + g - 2}{8} \qquad (5.1)$$

As a result of performing both temperature dependent (zero bias conductivity vs. T), as in Fig. 5-3, and bias voltage dependent (dI/dV vs. V_{bias}) measurements on CNTs of both geometries; Bockrath *et al*. were able to extract values for the exponents in both geometries α_{bulk} = 0.3-0.4 and α_{end} = 0.5-0.7. The values are in good agreement with theory which predicts $g \approx 0.28$ and $\alpha_{bulk} = 0.24$ and $\alpha_{end} = 0.65$. Fig 5-3. is a plot from Bockrath *et al*.[69] depicting the power law behavior of the conductivity, which allows for the extraction of the values for α and g. Later experiments were able to see this behavior in crossed metallic CNTs[25, 75], providing another example of bulk tunneling. Another experiment with a kinked

metallic CNT[25] saw behavior of end-end tunneling from one 1-D system to another.

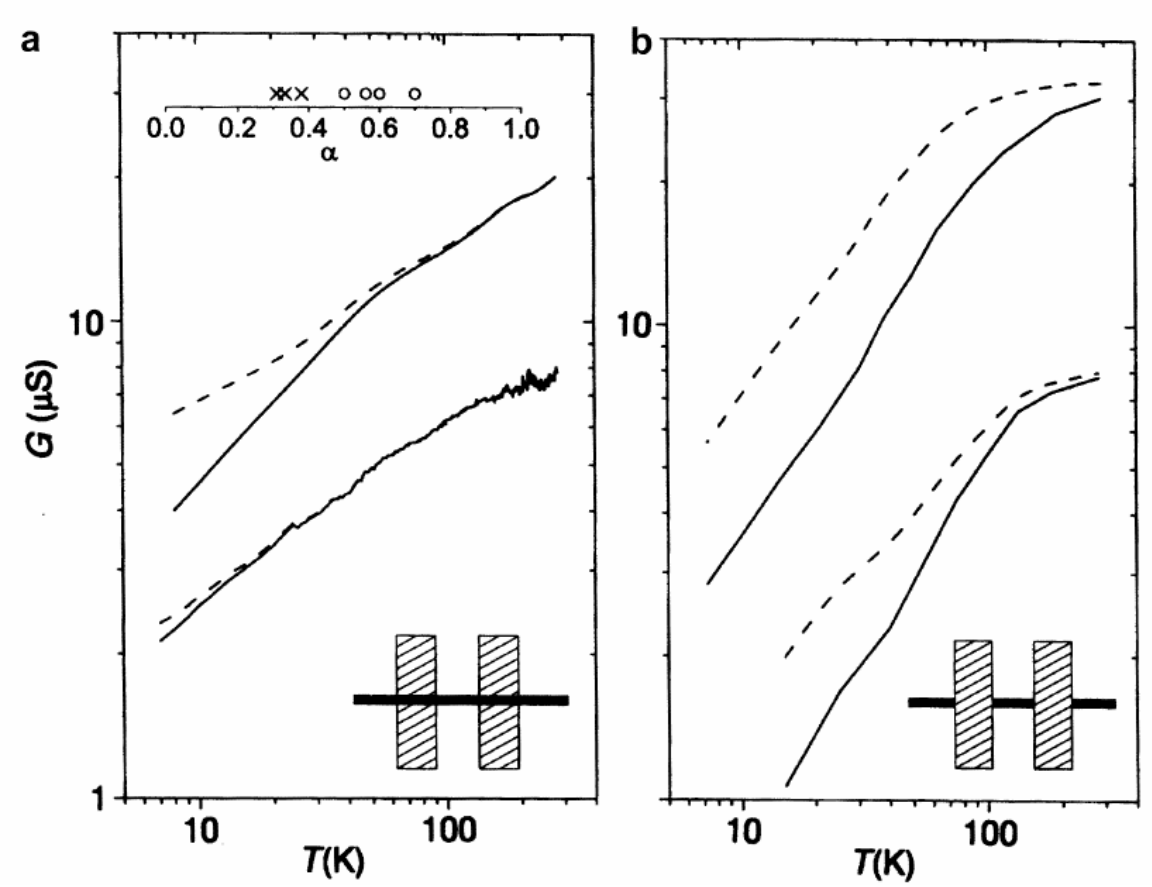

Figure 5-3. Plot from Bockrath *et al*.[69] showing the Luttinger liquid dependence of the conductance G against temperature T. The plot on the left shows tunneling into the bulk with the leads under the CNT and the plot on the right shows the opposite scenario with the leads on top. The effects of the lead placement are discussed in the text. The log-log plot shows the power-law dependence expected for Luttinger liquids, with the solid lines representing the data and the dashed lines taking into account a correction for Coulomb charging at low temperatures. Open circles in the inset indicate α values for end contacted samples and crosses indicate values for bulk contacted samples.

It might not be obvious why attaching 3-D metallic leads to a metallic CNT results in a tunnel junction even at high temperatures. The exact nature of the barrier in these and many other experiments on CNTs remains unclear. However, the fact that some processes can produce contacts with no (or almost no) barrier[37, 76, 77] indicates that the barrier is an extrinsic property of metal-CNT junctions. It is fortuitous that this accidental barrier has good properties for studying the energy-dependent tunneling into CNTs; the barrier itself must have relatively energy-independent transmission.

Unfortunately semiconducting CNTs can't be studied using the same techniques. Semiconducting CNTs form contacts which are more complicated than metallic CNTs, although a direct measurement in the vein of Bockrath *et al*. has been tried on multi-walled CNTs[78]. Schottky barriers[79] may form for semiconducting CNTs and have temperature, bias-voltage, and gate-voltage dependences of their own. Semiconducting CNTs also can be doped by nearby contaminants. This doping level will also have its own temperature dependence. These effects will mask the possible Luttinger effects on tunneling dependence. The rest of this chapter will set up a path to avoid the need to consider metallic contacts for probing the Luttinger liquid in semiconducting CNTs.

Other experiments have also measured the Luttinger parameter with photoemission studies on bundles of CNTs[70]. What is missing is a direct method of measuring the tunneling in a single CNT device without mixing in the effects of the

contacts. In the next two sections I will outline how telegraph noise and hysteresis in CNTs allow us to observe the tunneling of individual electrons into the CNT.

5.3 Hysteresis in CNTs

Many semiconducting CNTs in an FET geometry show hysteresis in the current versus gate voltage curve.[80] This effect has been used to make memory elements from CNT devices and, since it involves the transfer of electrons from traps to the CNT, it is a useful tool to study tunneling into the electron system of the CNT. First I will discuss how it was used as a memory device and how that indicated it could be used for my purposes.

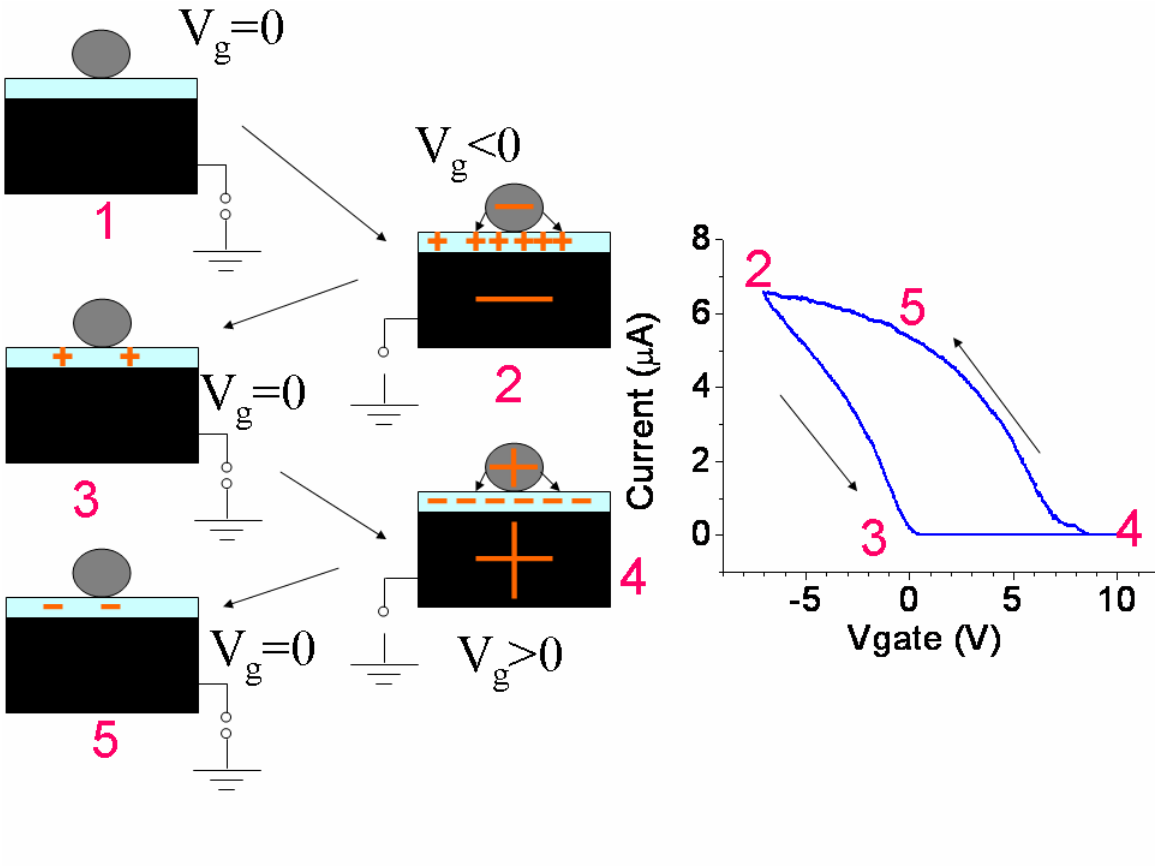

Figure 5-4. Semiconducting CNT hysteresis. This is a depiction of the stages of hysteresis in the I-V_g curve for a CNT-FET. The charge traps around the CNT-FET act as an additional gate for the circuit, and their long life creates a memory effect for the current state of the device. As can be seen if the gate voltage is swept to a negative value, holes will be present in nearby traps. If the gate voltage is returned to zero then the current will be suppressed by the field created by these traps. The opposite effect is seen if the gate voltage is swept to positive gate voltages.

As can be seen in Fig. 5-4, there is a large hysteresis in the I-V_g graph for CNTs. To think about what the source of this might be it is useful to think about the

strength of the electric fields near the CNT when gate voltages of -10V are applied to one of the devices.

$$E = V_g / KR_t \ln(\rho_g / \rho_t) \quad (5.2)$$

Where ρ_t ~ 1 to 2 nm is the CNT radius, $\rho_g \simeq 500$ nm is the dielectric thickness, and $K = 3.9$ is the dielectric constant of SiO_2. This gives us field strengths in the range of 0.1 to 1 V/nm which is on the order of the breakdown field of SiO_2 (about 0.2 V/nm, but varies depending upon quality and growth technique for the SiO_2). This suggests that a likely explanation for the hysteresis is charge reordering from traps near the CNT to the CNT.[80] It might be thought the charge rearrangement occurs between two traps near the CNT and not actually with the CNT itself. However, this would result in the hysteresis loop having the opposite sign: Positive gate voltage increasing the threshold voltage indicates that the electrons are actually entering and leaving the CNT. If the hysteresis were due to charges moving from trap to trap in the substrate we would expect the opposite sign for the hysteresis loop.[80]

In effect, the moving charge is acting as an extra gate voltage, meaning that the field the CNT is affected by is not just that applied through the gate, but also that created by the charge dislocated from the traps. This means that the hysteresis is caused by a number fluctuation. If instead the charges moving around created a mobility change by altering the scattering process in the CNT we would expect a completely different type of behavior to be seen in the I-V_g curves. Instead of having a horizontal shift of the curves, the threshold voltage would remain constant and the conductivity would shift up and down as the moving charges altered the mobility of the device.

This can be used as a memory device by placing the gate voltage at V_g=0 since the current state will depend upon whether the gate voltage was ramped up or down to get to that point.[80] The high current and low current states are both very long lived (~10,000s) another important attribute for a memory bit. The state can be written, erased, read and rewritten repeatedly.

The important part of the story for my thesis is that this hysteresis implies that there is tunneling occurring between two different number states of the CNT, and that if this tunneling happens on an appropriate time scale we can measure the tunneling rates to gauge the TDS in the CNT. This will be an indication of whether the electrons in the semiconducting CNT are following the Luttinger liquid or Fermi gas model.

5.4 Random telegraph signals

If the bias voltage and gate voltage are left constant, the same tunneling that results in hysteresis can instead give rise to a random telegraph signal (RTS) as in Fig. 5-5. This means that the system switches back and forth between (hopefully two) discrete states. These sorts of signals have been used in the past to understand the behavior of other novel electron systems.[81] Here I will discuss the concepts necessary to proceed from the observation of a two-state RTS to an understanding of the TDS in the CNT.

In particular RTS has been used to discern the electronic state of a transistor built from a two-dimensional electron gas (2DEG)[81], with an electron assumed to

be tunneling from a defect to the two-dimensional gas which allowed for the confirmation of the theoretical prediction for the electronic state of the electron system. This experiment by Cobden *et al*.[81] was a direct inspiration for the work in the next chapters of this thesis, not only due to their use of telegraph signal to provide insight into the electron system of a novel material, but also in terms of understanding the evolution of the TDS with temperature. In this 2-D system the TDS at the Fermi level exhibits a maximum and follows a power law behavior with an exponent of about -0.8, i.e. the tunneling rate is proportional to $(E_f\text{-}E_d)^{-0.8}$. This is very analogous to the Luttinger liquid case where the TDS vanishes at the Fermi level as a power law, so it provides an immediate starting point for the theoretical analysis for the semiconducting CNT situation.

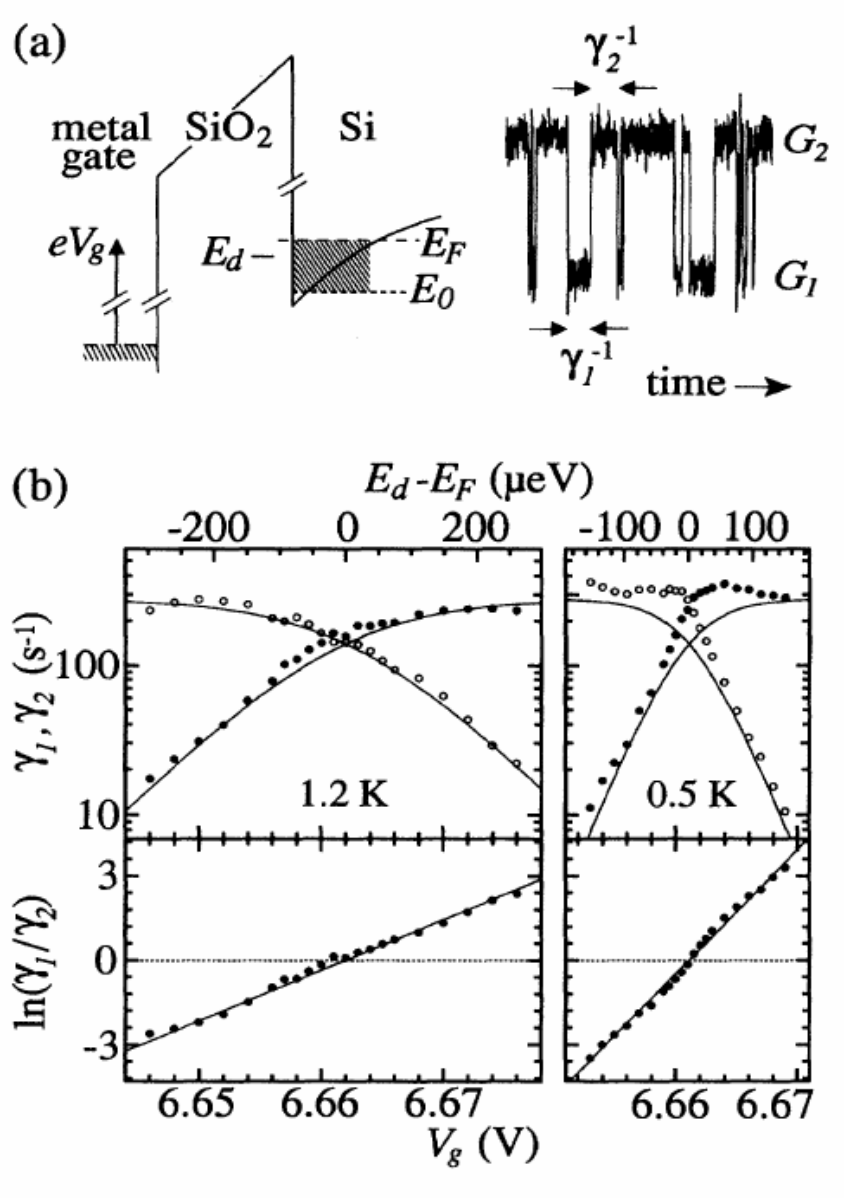

Figure 5-5. Previous RTS experiment. Taken from Cobden *et al.*[81] γ_1 and γ_2 are the rates for each state, E_d is the donor level and E_f is the Fermi energy. The upper left image depicts the effect of shifting the gate voltage on the relative energy between the defect and the Fermi energy and the semiconductor. The upper right image depicts the telegraph signal for a single gate voltage, the average time in each state is used to determine the transition rate. The data at the bottom depicts the rates for the switcher at two temperatures, as described in text.

In Fig. 5-5 the lower left plot shows the data for a device at 1.2 K. The detailed balance equation for a system at thermal equilibrium is

$$\frac{\gamma_1}{\gamma_2} = e^{\left[-\left(E_d - E_f\right)/kT\right]} \tag{5.3}$$

Here γ_1 and γ_2 are the rates for each state (the reciprocal of the mean lifetime for each telegraph state), E_d is the defect energy, E_f is the Fermi energy and T is the temperature. The straight line in the log plot shows the ratio of the rates for the two states, this indicates that the system is at thermal equilibrium with the defect and that the gate voltage is shifting the energy of the defect. Above this is the plot of the individual rates for each of the states.

$$\begin{aligned} \gamma_1 &= (2\pi/\hbar) D\Delta^2 f(E_d) \\ \gamma_2 &= (2\pi/\hbar) D\Delta^2 \left[1 - f(E_d)\right] \end{aligned} \tag{5.4}$$

Here D is the density of states and Δ is the tunneling matrix. The data is fit using Fermi statistics and Fermi's golden rule shown in Eq. 5.4. The lower right plot shows data at 0.5 K where the system is no longer obeying Fermi statistics and there is an enhancement of tunneling at the Fermi energy. This allows for the extraction of information about the amount of interaction of the electron system in the semiconductor by fitting the data to a theory for the behavior of electrons in a 2DEG. For nanotubes, I will insert a theory for tunneling into a Luttinger liquid in Chapter 7.

In CNTs telegraph signals have been observed by numerous groups[80, 82]. It is not essential that these traps are located in the oxide as depicted in the figure; they

could also be in contaminants adsorbed on the surface of the chip, although the field strength is perhaps circumstantial evidence suggesting that they are in the oxide. As suggested above there are two reasons to suggest that the tunneling is actually occurring between the CNT and the defect: first, the electric field is strongest closest to the CNT, and second, the sign of the hysteresis loop indicates tunneling to and from the CNT. In this experiment we observe gate voltage dependent tunneling rates that follow that predicted for transition of an electron between two states in thermal equilibrium.

To make this study we need a sample with a defect with energy close to the Fermi level of the CNT and only one such defect. If there are several active defects the switching will be amongst many states and become much more difficult to interpret.

To discover whether a fluctuator can be isolated the device is cooled to the base temperature, 1.2 K, where the fewest defects should be active and the gate voltage is swept slowly. As the potential of the gate, V_g is varied, the defect energy, E_d, is also varied with respect to the Fermi energy, E_f, of the CNT. At some gate voltage switching of the current between two discrete states may be observed, as seen in Fig. 5-6. These gate voltages cannot be chosen ahead of time since the technique relies upon defects that are intrinsic to the device; they are not designed by the experimenter.

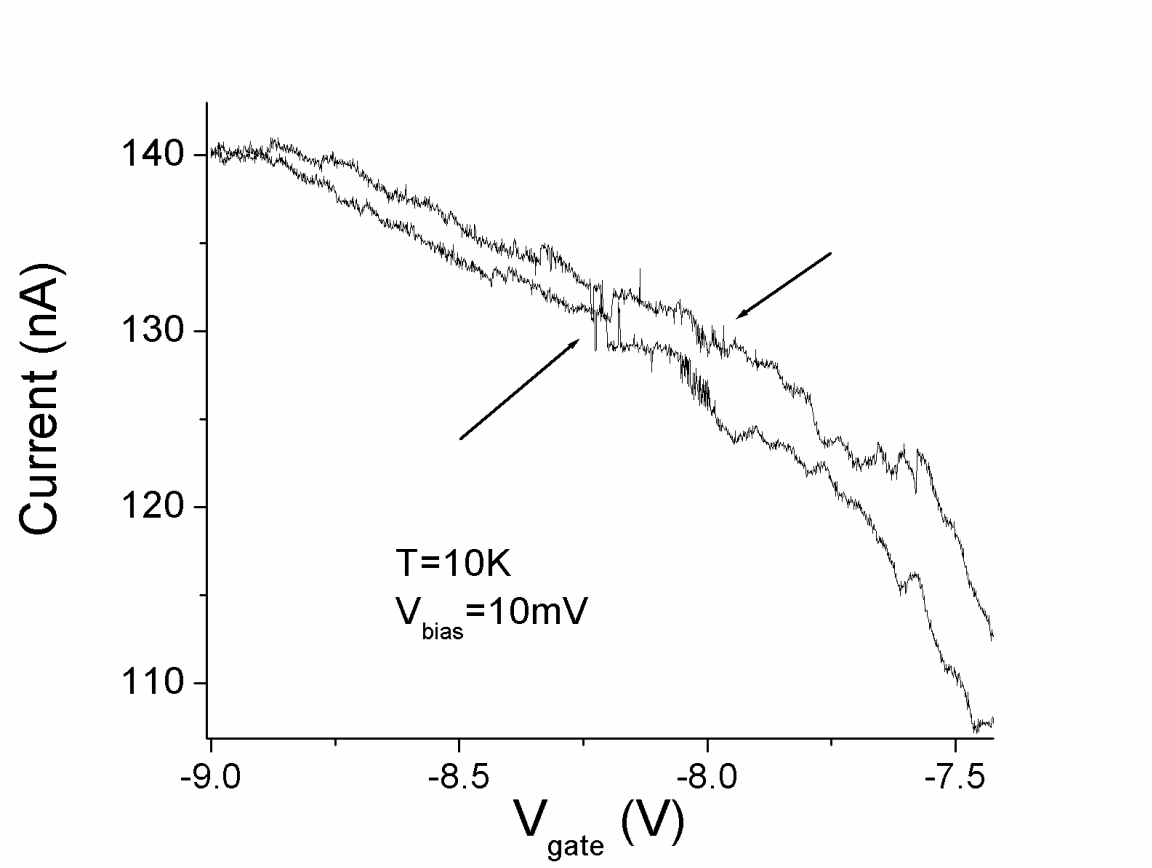

Figure 5-6. Segment of an I-Vg curve taken on a CNT FET. Since the device was swept in both directions the hysteresis is visible. There are two regions in the image indicated by the arrows where two-level switchers are active, the left one of these is further investigated in the later chapters.

Chapter 6 Random telegraph signals in carbon nanotubes and their use as a defect thermometer

This chapter will characterize random telegraph signals in CNTs and show that the signals may be used to extract the electron temperature in the CNT. The dependence of the electron temperature on bias voltage is used to extract the energy relaxation length l_ε in the CNT.

6.1 Random Telegraph Signals in Carbon Nanotube Transistors

The initial goal is to find a region of gate voltage in which the current displays clear switching between two and only two states; i.e. that appears to be influenced by only a single two-level fluctuator that can be studied in isolation over a range of bias voltages and hopefully temperatures. The best fluctuator I was able to find showed consistent two-level behavior from 1 mV to 100 mV in bias voltage and from temperatures from 1.2 K to over 80 K. This was on sample 1 from the $1/f$ noise section 4.5 and has a length of 3 μm and a diameter of 1.4 nm.

Fig. 6-1 depicts a section of an I-V_G curve indicating the presence of a two level fluctuator. At more negative V_g, it can be seen that the system prefers the high current state with occasional switching events to the low current state. At intermediate gate voltages ($-8.22 < V_g < -8.18$) both states are nearly equal in occupation probability. As the gate voltage is swept more positive the lower-current state is favored.

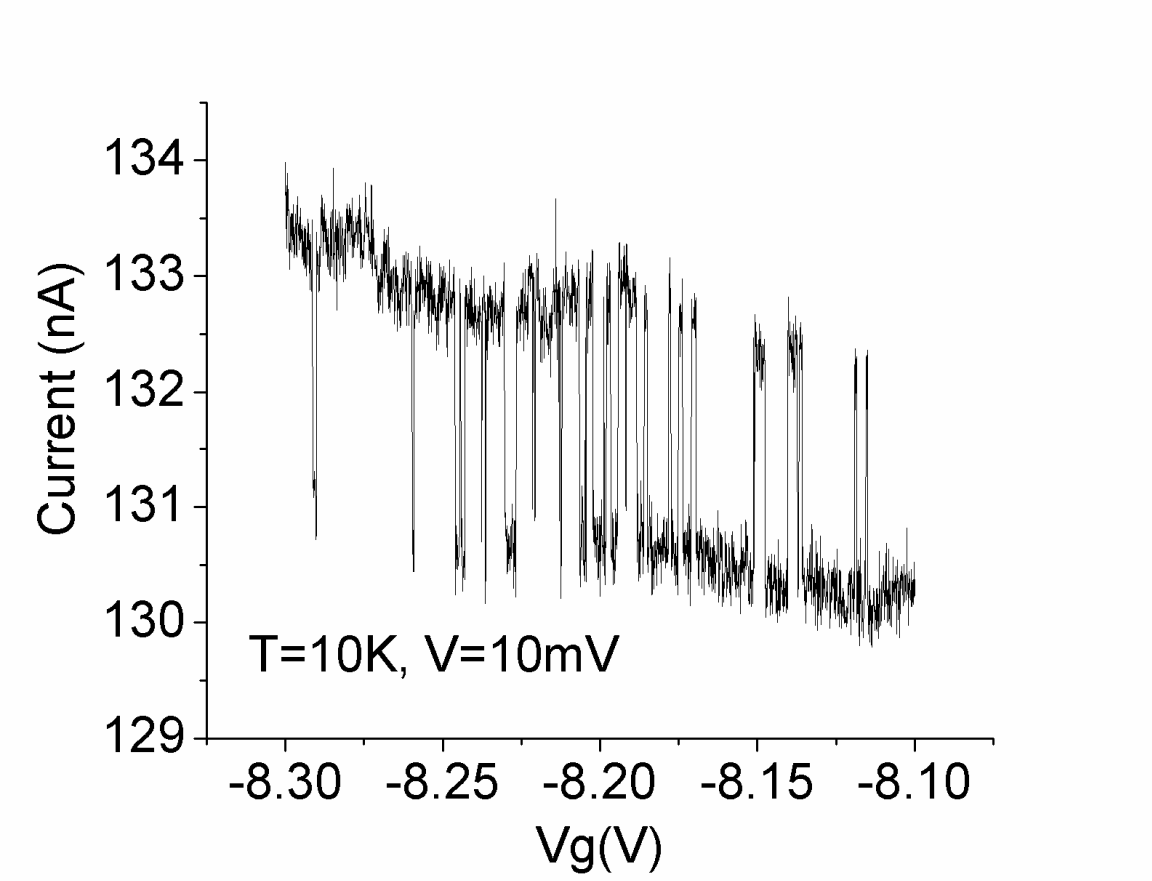

Figure 6-1. Small section of the current versus voltage curve for a two level fluctuator. To visualize how the data was taken would require a third axis for time to be shown at many of the gate voltage locations. It can obviously be seen that the system is switching from preferring one state to the other with a section in the center where both states are nearly equal in occupation probability.

This behavior suggests that the gate voltage controls the defect energy with respect to the Fermi energy of the CNT, which affects the probability of finding the system in one state or the other. This allows us to develop a model for the gated defect-CNT system, as depicted in Figure 6-2 A-C. In this model, the defect lies in

the gate dielectric between the CNT and gate electrode, close enough to the CNT for tunneling to occur. In Fig. 6-2A, when V_g is lowered (corresponding to higher electron energy, or a rise in Fig. 6-2A), the defect chemical potential E_d is raised relative to the CNT chemical potential E_F. Likewise, when the V_g is raised, E_d is lowered relative to E_F. Thus the gate electrode controls the difference in chemical potential of the defect and CNT:

$$E_d - E_f = -\eta e\left(V_g - V_{g0}\right) \tag{6.1}$$

where V_{go} is the gate voltage where E_d equals E_F and η is the dimensionless gate efficiency which represents the ability of the gate voltage to move the defect potential with relation to the Fermi level in the CNT. The gate efficiency is less than unity due to the capacitive coupling of the CNT and defect to the gate, source and drain.

Within this model, we identify the switching events between two states as the stochastic process of electron tunneling between the defect and CNT. We can analyze this process by recording the current as a function of time. Fig. 6-2D-F I shows data for the same RTS depicted in Fig. 1, but now the gate voltage is kept fixed while the current is recorded as a function of time. In Fig. 6-2D, V_g - V_{go} is negative, so the defect chemical potential is higher than the chemical potential of the CNT; this corresponds to the diagram in Fig. 6-2A. Here the time trace of the RTS shows that the system spends most of its time in the higher current state. Fig. 6-2E the defect is at the Fermi energy so the system spends an equal amount of time in both states. Fig. 6-2F shows the opposite situation of 2D where the system now spends more time in the other state since V_g - V_{go} is positive.

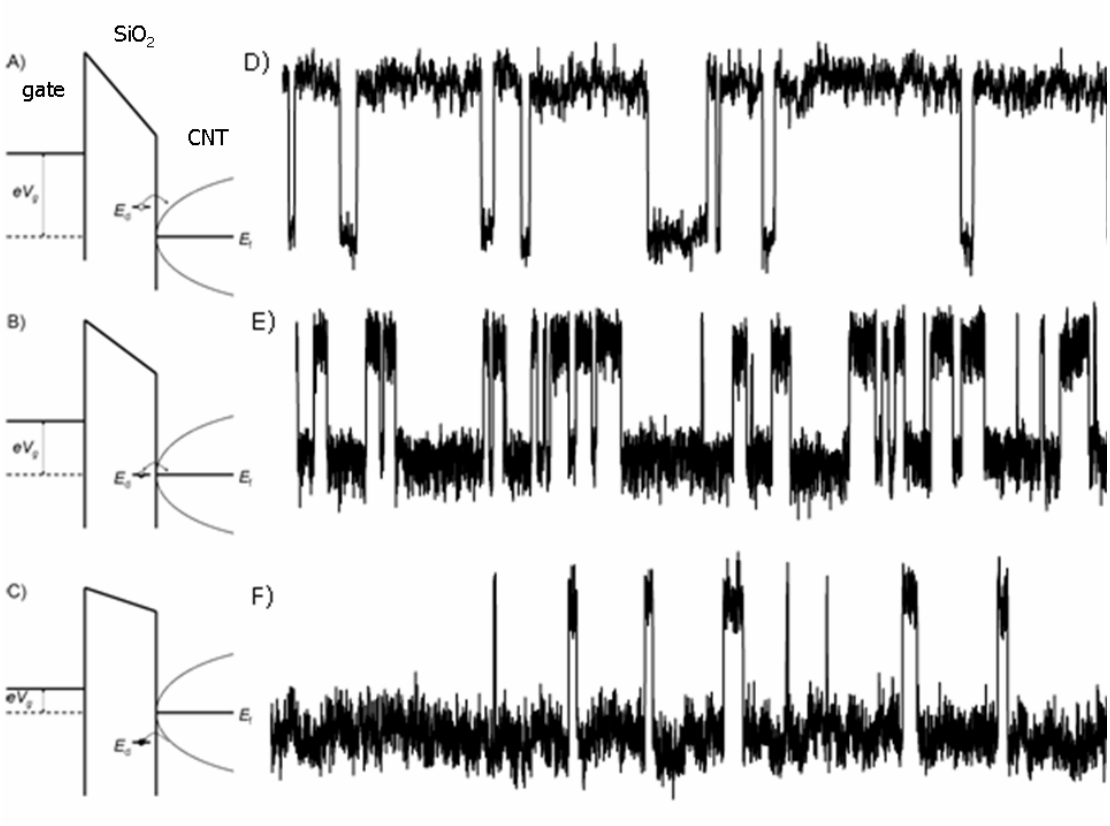

Figure 6-2. RTS schematic. (A-C) Schematic of the band diagrams for the semiconducting CNT, defect (in the SiO_2), and gate electrode, for the conditions (A) Ed - Ef > 0, (B) Ed - Ef = 0, and (C) Ed - Ef < 0. The defect is shown as being located in the oxide but that is not essential to the physics. The thin solid lines indicate the spectrum of excited states at zero temperature in a Lutinger liquid. The arrows indicate the direction of the largest tunneling rate. (D-F) Time series of the current through the CNT at three gate voltages which correspond to the diagrams (A-C). The current fluctuates between two discrete states. As the gate voltage is changed the relative tunneling rates between the two states change, resulting in the system spending more or less time in the respective states. This is reflected in the time series becoming more dominated by one current state or the other.

From time traces of the RTS as shown in Fig 2D-F, we can define two tunneling rates γ_1 and γ_2 corresponding to an electron tunneling into and out of the defect. We determine these rates by calculating the mean time spent in each state (high current or low current) $<t_1>$, $<t_2>$, then $\gamma_{1,2} = <t_{1,2}>^{-1}$.

The experimental procedure is as follows. Once an isolated RTS fluctuator is found, several time traces are taken. At a given temperature the voltage bias is set and then time traces of 30 to 150s are taken at a constant gate and bias voltage. Then the gate voltage is incrementally increased to take further time traces, with the fluctuator slowly changing from predominantly one state to the other. This entire process is then repeated at different bias voltages and different temperatures. As a reminder, the bias voltage, gate voltage and temperature are all constant while the data is being recorded. (This was also true for the 1/*f* noise experiments.) From the time traces the average times $<t_{1,2}>$ spent in each state are calculated, along with the number of switching events to gauge the statistical uncertainty. The reciprocal of the average times $<t_{1,2}>^{-1}$ determines the switching rates $\gamma_{1,2}$.

The first point to verify is whether the data satisfies the detailed balance condition for a two level system:

$$\frac{\gamma_1}{\gamma_2} = e^{\left[-\left(E_d - E_f\right)/kT\right]}, \tag{6.2}$$

,Using Eq. 6.1 above, we have:

$$\frac{\gamma_1}{\gamma_2} = e^{\left[\eta e\left(V_g - V_{g0}\right)/kT\right]}. \tag{6.3}$$

As will be shown below, once the gate efficiency, η, is known, Eq. 6-3 may also be used to determine the electron temperature of the system.

Figure 6-3 shows the natural logarithm of the ratio of the rates $\ln(\gamma_2/\gamma_1)$ as a function of gate voltage for the same RTS studied in Figs. 6-1 and 6-2. To compare with the exponential behavior predicted by Eq. 6.3, I plot the natural log of the ratio of the two rates. The linear behavior of $\ln(\gamma_2/\gamma_1)$ vs. V_g indicates Eq. 6-3 is obeyed. From the slope of $\ln(\gamma_2/\gamma_1)$ vs. V_g we extract the exponential prefactor $-\eta e/kT$.

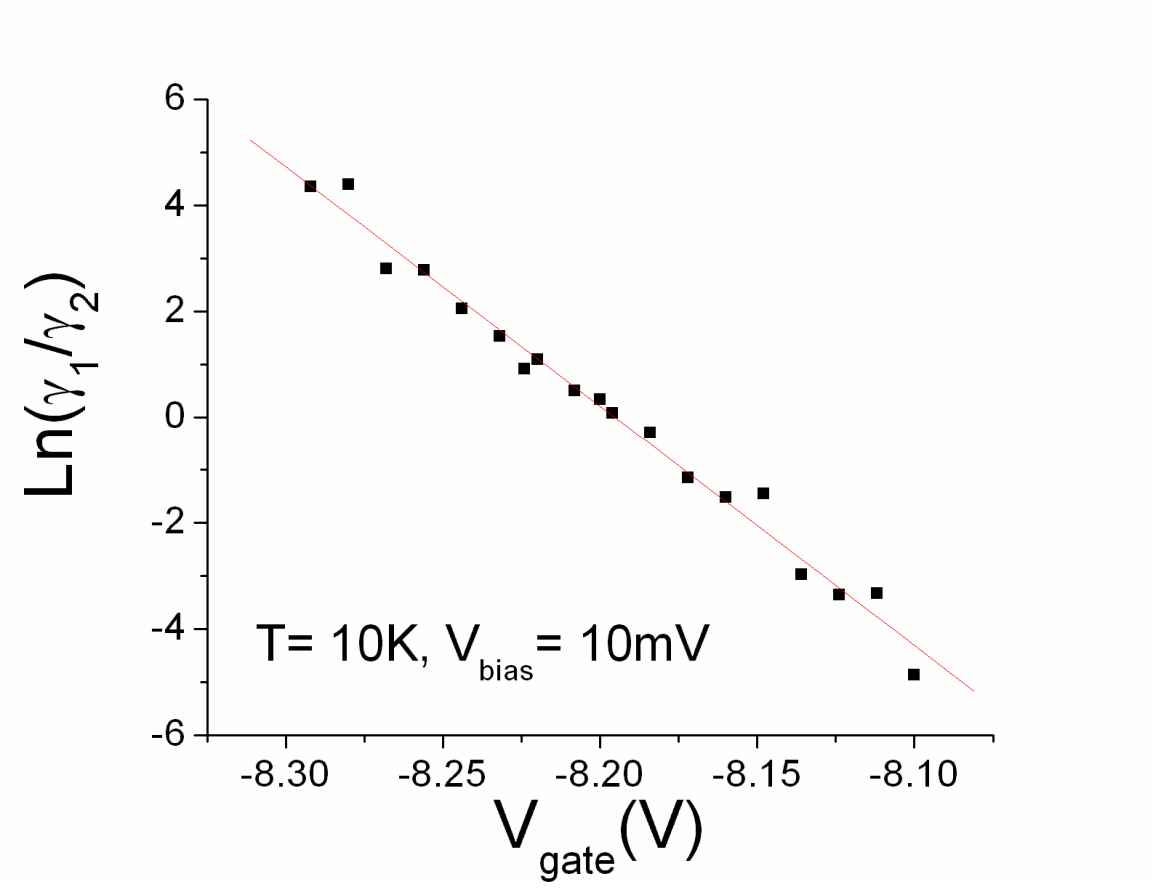

Figure 6-3. The natural log of the ratio of the tunneling rates versus gate voltage for the same RTS as Figs. 6-1 and 6-2.

$$\ln\left(\frac{\gamma_1}{\gamma_2}\right) = -\frac{\eta e}{kT}(V_g - V_{g0}) \tag{6.4}$$

It is tempting to simply use the base temperature of the cryostat as T, and therefore extract the gate efficiency η from the slope $-\eta e/kT$ in Figure 6-3. However, it is necessary to ensure that the electron gas is in thermal equilibrium with the substrate before performing this calculation. To measure whether the electrons are being heated by the bias voltage, the slope is measured at many different bias voltages and several base temperatures. At each bias voltage, I measure $\ln(\gamma_2/\gamma_1)$ vs. V_g and set the slope equal to $-\eta e/kT$ to extract a temperature T which I identify with the electron temperature of the CNT. The gate efficiency η is chosen such that the extracted T tends to the cryostat base temperature at low bias for cryostat temperatures of 20 K, 40 K, and 80 K; this determines $\eta = 0.053$. The electron temperature as a function of bias voltage is shown in Fig. 6-4. This demonstrates that it is indeed important to consider the effect of heating of the electron system by the bias voltage.

6.2 Defect thermometry

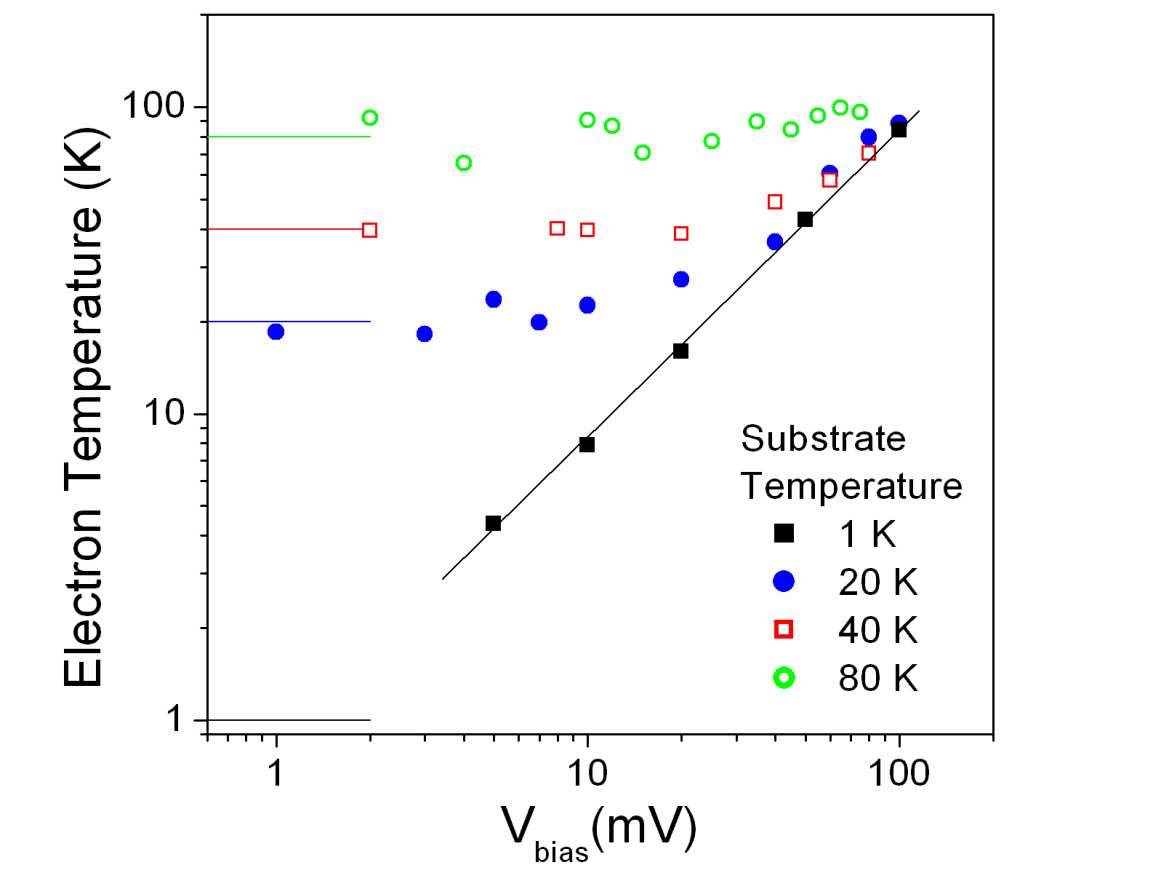

Figure 6-4. Electron temperature as a function of bias voltage at various substrate temperatures. Electron temperature is determined from the logarithmic slope of the tunneling rate ratio as a function of gate voltage as in Fig. 6-3. The gate voltage efficiency $\eta = 0.053$ is chosen such that the low-bias electron temperature extrapolates to the substrate temperature (solid colored lines). The rate of the switchers drops for lower electron temperature data, limiting the range where data can be taken.

As seen above in Fig. 6-4, the low-bias limit of the slope $-\eta e/kT$ taken at different temperatures can be used to extract the gate efficiency η. However, the

slope $-\eta e/kT$ at higher bias can be used to determine the rise in temperature of the electron system due to the influence of the bias voltage (and transport current). The RTS acts as a "defect thermometer"; such a thermometer has been used previously to study heating of the electron gas in metal wires under conditions of charge transport[83-85].

As the CNT electron temperature deviates from the substrate temperature, the main source of thermal resistance between the CNT electron system and the substrate can be determined. The CNT electrons equilibrate to the substrate through two effective thermal resistances in series: Λ_{ep}, the thermal resistance of the CNT electrons interacting with the phonons, and Λ_{sub}, the thermal resistance of the CNT phonons interacting with the substrate. Different behaviors will result if one resistance is dominant. For $\Lambda_{ep} < \Lambda_{sub}$, Joule heating of the CNT should cause the device temperature to rise above the substrate temperature, this should result in a $\Delta T \sim V^2$. However, as is typical in metals at low temperature, this behavior is not observed in Fig. 6-5; the slope of T vs. V on this log-log plot is 1, implying $T \propto V^1$. Interestingly, this indicates that the electrons do not achieve thermal equilibrium with the phonons in the CNT at moderate biases (~40 mV) even at high temperatures (40 K). This is an indication of the very small electron-phonon coupling in CNTs, which is partially due to their one-dimensional nature[86, 87].

This implies that the electron-phonon process is the bottleneck for thermal transport from the electron system to substrate (i.e. $\Lambda_{ep} > \Lambda_{sub}$); then the temperature dependence typically exhibits a power law in voltage[83]. The electrons will gain

energy from the electric field over a distance called the energy loss length, l_ε and Boltzmann transport theory predicts that the temperature of the electron system is[83]

$$kT = 0.780eEl_\varepsilon \tag{6.5}$$

at high electric field, i.e. $eEl_\varepsilon >> kT_{sub}$ where T_{sub} is the substrate temperature.

For constant energy relaxation length, the temperature rise of the electron system is linear in bias voltage. I can then use the slope of T vs. V in Fig. 6-5 to extract l_ε = 280 nm. I currently do not understand why the energy relaxation length is constant; typically the energy relaxation length varies as a power-law in the electron temperature $l_\varepsilon \propto T^a$, where p = 2, 3, or 4 has previously been calculated[88] depending on the dimensionality of the electron system (2 or 3) and phonon system (2 or 3). However, I am not aware of any calculations of the energy relaxation length for CNTs or other 1-D systems.

The energy relaxation length l_ε may be used to extract an energy relaxation time $\tau_\varepsilon = l_\varepsilon/v_F$, where v_F is the Fermi velocity. For a heavily doped semiconducting CNT, v_F approaches the value for a metallic CNT, 9.3 x 10^7 cm/s[29, 89, 90]. Then τ_ε ~ 300 fs. This time is an upper bound to the coherence time for electrons in the CNT (at least under the transport conditions probed in our experiment), so has implications for use of CNTs in any quantum-coherent applications.

Chapter 7 Coherence and correlations in carbon nanotubes studied using random telegraph signals

Chapter 5 described the previous work on Luttinger liquids (LL) and discussed the techniques that have been used to study the LL state in carbon nanotubes (CNTs) and similar correlations in other electron systems. Chapter 6 showed that random telegraph signals (RTS) in semiconducting CNT transistors result from tunneling of an electron between CNT and a defect, probably located in the gate dielectric. The gate voltage can be used to control the energy of this defect relative to the Fermi energy of the CNT. The ratios of the tunneling rates as a function of gate voltage were used to extract the electron temperature of the CNT using the detailed balance relation. In this chapter I will study the gate voltage dependence of the *individual rates* from random telegraph signals in CNTs and analyze the data to arrive at a value for the Luttinger liquid interaction parameter g.

7.1 1-D electron behavior

The previous chapter analyzed the RTS in a CNT and examined only the ratio of the tunneling rates as the gate voltage was swept. Here we will examine how the individual tunneling rates change with gate voltage, which will allow us to test whether the electrons are obeying Fermi gas behavior or if the electron system of one-dimensional CNTs is better described by Luttinger liquid theory.

Varying the gate voltage varies the energy difference between the defect level and the Fermi level of the nanotube, E_d - E_f according to Eq. 6.1. As the gate voltage alters this difference, the defect level acts as a probe of the occupation probability and tunneling density of states (TDS) of the system at that energy. The rates for tunneling into and out of the system predicted by Fermi gas theory combined with Fermi's golden rule are

$$\gamma_1 = (2\pi/\hbar)D\Delta^2 f(E_d)$$
$$\gamma_2 = (2\pi/\hbar)D\Delta^2 [1 - f(E_d)] \qquad (7.1)$$

where D is the tunneling density of final states, f is the Fermi function, and Δ^2 the overlap integral between initial and final states. D and Δ^2 are assumed not to vary with energy. I have shown previously in Chapter 6 (see Fig. 6.3) that E_d - E_f is linearly related to the gate voltage, i.e. $E_d - E_f = -\eta e(V_g - V_{g0})$.

Plotting the individual rates vs. gate voltage there is a simple way to check if Fermi statistics are being obeyed. Comparing the rates when the defect energy is near the Fermi energy of the nanotube and when the defect level is far away from the Fermi energy of the nanotube, we have for Fermi statistics

$$\gamma_1(E_d << E_f)/\gamma_1(E_d = E_f) = \gamma_2(E_d >> E_f)/\gamma_2(E_d = E_f) = 2 \qquad (7.2)$$

Stated in words, the rate of the switching at the edges of Fig. 6-1 should be twice the rate at the point where the two data sets cross (this is also where E_d - E_f).

However the data in Fig. 7-1 shows that the ratio clearly exceeds two. This indicates that Fermi statistics are not sufficient to explain the tunneling behavior into the CNT device. This indicates that the tunneling at E_d - E_f is suppressed compared to

its expected value, an indication that Luttinger liquid theory may better describe the phenomenon.

From the TDS at zero temperature one can create a corresponding tunneling rate for a Luttinger liquid at zero temperature[63]

$$\gamma_1 \sim \theta(E_f - E_d)(E_f - E_d)^{\alpha} \tag{7.3}$$

the tunneling exponent α differentiates the LL from the Fermi gas which has a uniform density of states just above the Fermi energy. This must be extended to finite temperature[88, 91]

$$\gamma_{1,2} = CT^{\alpha} \exp(\pm \frac{Ef - Ed}{2kT}) \frac{\left|\Gamma[(\alpha+1)/2 + i(Ed - Ef)/2\pi kT]\right|^2}{\Gamma(\alpha+1)} \tag{7.4}$$

where the sign in the exponential switches for the two different rates. By using $E_d - E_f = -\eta e(V_g - V_{g0})$ we have for the Luttinger case

$$\gamma_{1,2} = CT^{\alpha} \exp(\pm \frac{\eta e(V_g - V_{g0})}{2kT}) \frac{\left|\Gamma[(\alpha+1)/2 + i\eta e(V_g - V_{g0})/2\pi kT]\right|^2}{\Gamma(\alpha+1)}. \tag{7.5}$$

which is fitted to the data in Fig. 7-1, where the Luttinger fit provides a superior fit to the data. This is due to the ability of the Luttinger model to take into account the reduced tunneling rate for the situation where the defect energy is close to the Fermi energy of the CNT. The only undetermined parameter in the fit is the value of α; the temperature, T, and the gate efficiency, η, are determined by the fit to the natural logarithm of the ratio of the rates for the two states versus gate voltage as in Fig. 6-3 in chapter 6.

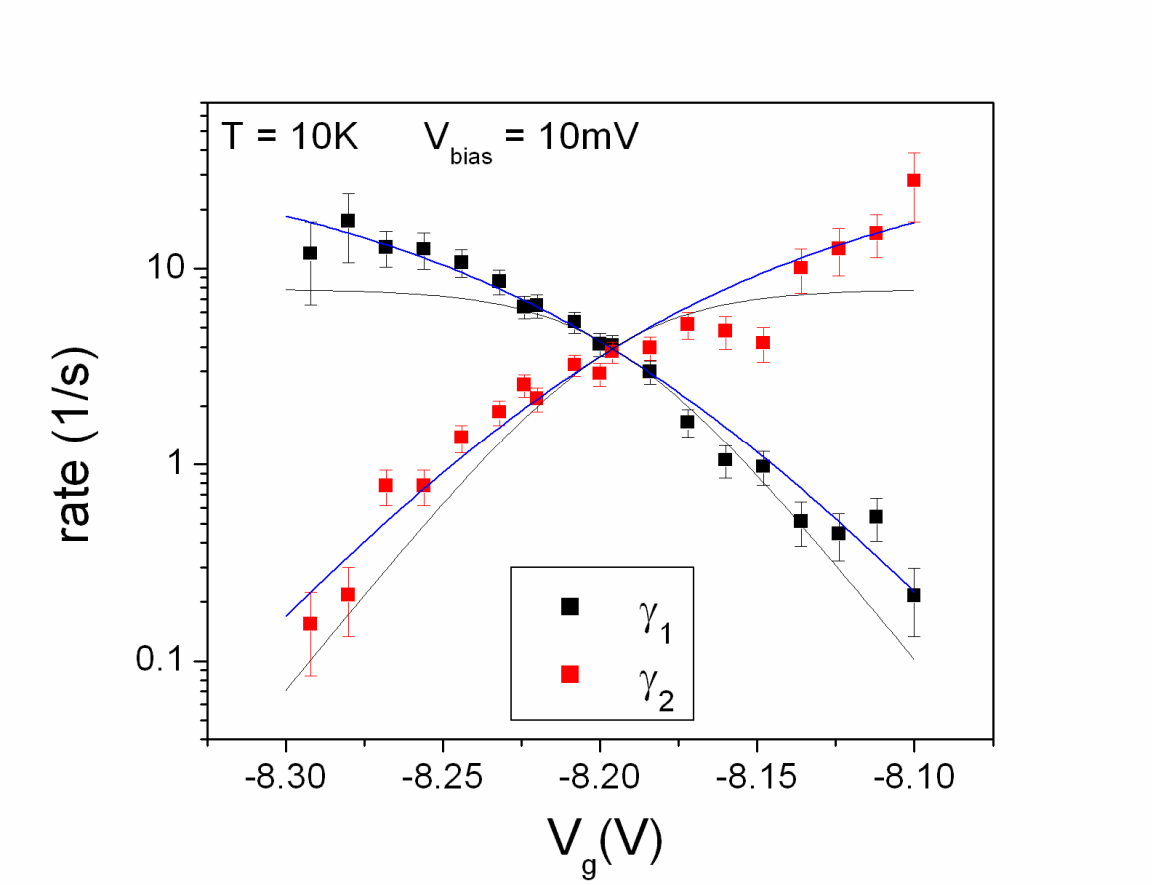

Figure 7-1. A typical plot of the individual transition rates versus gate voltage for a two-level RTS. The black curves are the fit to Fermi gas theory and the blue curves are the fit to the Luttinger liquid model described in text with $\alpha = 2$.

As discussed in chapter 5 α reveals the strength of the interactions of the electrons in the Luttinger liquid system. The relation between α and the LL parameter g should be

$$\alpha_{bulk} = \frac{\left(\frac{1}{g} + g - 2\right)}{8} \tag{5.1}$$

for our system, since the defect is tunneling into the bulk of the tube. The value for α is extracted for several fluctuators in the last section of this chapter. This value is called a_{rate} to indicate that the value is obtained at one temperature and bias voltage. Remember that g can range from 1 to 0 with smaller values indicating stronger interactions amongst the electrons in the system.

The value for α can also be calculated by taking the switching rate at the point where $E_f = E_d$ (equivalent to $V_g = V_{g0}$) and plotting it versus temperature. Eq. 7.5 becomes

$$\gamma\left(E_f = E_d\right) = CT^{\alpha}\frac{\left|\Gamma\left[(\alpha+1)/2\right]\right|^2}{\Gamma(\alpha+1)} \tag{7.6}$$

so that a plot of log rate vs. log temperature will yield the value of α as the slope. I will call this α_{temp}.

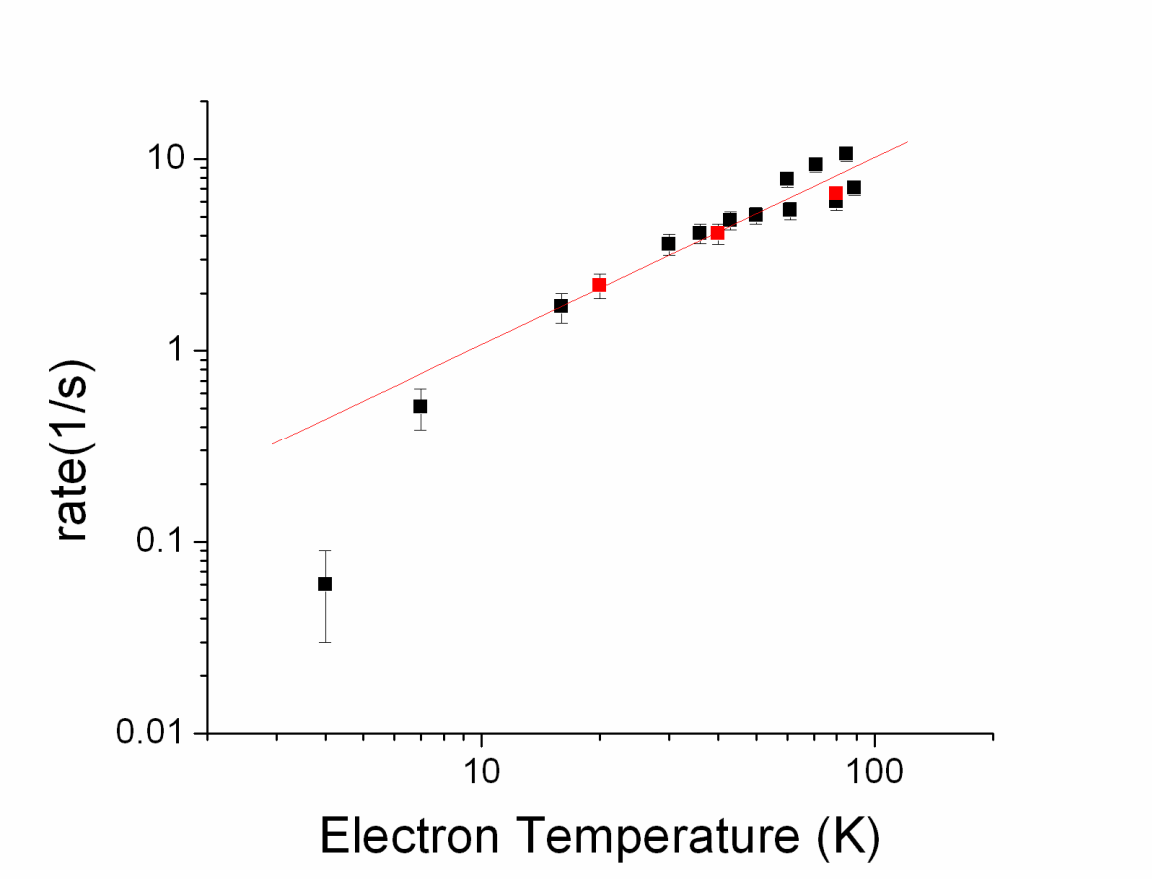

Figure 7-2. Degenerate rate vs. electron temperature. The rate of switching when the defect is at the Fermi energy vs. the temperature of the electron system. The temperature of the electron system is calculated using the detailed balance condition for the ratio of the rates. The power fit is used to give the value for α. Here α_{temp}=0.97. The red dots indicate points taken at low bias voltages, while the black points are from points where the tube is being heated by the bias voltage. (see Chapter 6 for details)

The temperature dependence follows a power law, with an exponent of α_{temp} = 0.97 ± 0.1. Analysis of the temperature dependence of another RTS gives a power law exponent of α_{temp} = 0.7 ± 0.1. Note that the expected behavior for tunneling into

a Fermi liquid would be an absence of temperature dependence; the strong temperature dependence in Figure 7-2 is in itself evidence for non-Fermi liquid behavior. The data of Figure 7-2 are poorly fit by an activated (Arrhenius) temperature dependence, and such a fit results in an unphysically low activation energy on order of 2 meV.

The theoretical value for g is given for any system by[69, 73, 74]

$$g = \left[1 + \frac{2U}{\Delta}\right]^{-1/2} \tag{7.7}$$

where U is the Coulomb charging energy and Δ is the single particle level spacing. For a semiconducting CNT the level spacing is a function of the Fermi energy. For a metal the calculation yields a theoretical value of g = 0.28 and therefore $\alpha_{bulk} = 0.24$ [71, 72]. Therefore we need to determine how the level spacing for the semiconducting CNT will vary versus gate voltage to replace the U/Δ ratio for the metallic nanotubes.

Since the charging energy will be the same for either metallic or semiconducting

$$U = \frac{e^2}{2C_g} \tag{7.8}$$

and the single particle level spacing is

$$\Delta = \frac{dE}{dn}\frac{\Delta N}{L} = \frac{1}{D(E)L} \text{ for } \Delta N = 1 \tag{7.9}$$

to find g all that is now needed is the density of states for the two systems. The energy of the electrons in a metallic CNT is $E = (\hbar v_f k)^2$, where $\hbar$ is Planck's constant, $v_f = 9\text{x}10^7$cm/s is the Fermi velocity and $k = \pi n/4$ is the wave vector, where n is the

number of carriers. So the density of states is $D(E) = dn/dE=(dE/dn)^{-1}=4/\pi\hbar v_f$. For a metal the calculation yields a theoretical value of g = 0.28 and therefore $\alpha = 0.24$. For the semiconducting case the bandgap must be taken into account, and the new dispersion relation is approximated as hyperbolic $E^2 = \delta^2 + (\hbar v_f k)^2$, where δ is the bandgap. This makes the density of states

$$D(E)_{semi} = \frac{16}{(\hbar v_f \pi)^2} \frac{\left(\delta^2 + (\hbar v_f \pi n/4)^2\right)^{1/2}}{n} \tag{7.10}$$

where the bandgap is 0.59eV for a tube with a diameter of 1.4nm. If I assume that the number of carriers is linear with the gate voltage, $n = C_g V_g/e$, I can plot how the parameters g and α should vary with gate voltage for a semiconducting CNT by using eqs. 5.1 and 7.10. This assumes that the only alteration required to Luttinger theory when switching from metallic to semiconducting CNTs is to take into account the new density of states.

Figure 7-3 plots the expected variation of the LL tunneling exponent α with gate voltage, as well as my experimentally-determined values of α from analysis of the gate-voltage dependence and temperature dependence of the individual tunneling rates. Fig 7-4 is the corresponding plot for the value of g assuming bulk tunneling. The values of α determined from experiment are significantly higher than the expected values. There are several possible explanations for this. First, it is quite possible that the simple analysis above overestimates g and underestimates α. A more careful analysis by Egger and Gogolin[73] gives $g = 0.18$ for a 3 μm length metallic CNT, corresponding to $\alpha = 0.46$, in good agreement with photoemission experiments on metallic CNTs[70]. This would result in a nearly doubled estimate of

the semiconducting α compared to the values plotted in Figure 7-3. Second, our analysis also neglected any interaction between the electron system and the defect itself, which seems reasonable, since the typical change in resistance upon charging and discharging the defect is on order several kOhms, corresponding to a change in transmission on order 1/2. However, the backscattering of electrons by the defect itself may cause correlations in the electron system (this is the essence of the work by Cobden *et al*.[81]). More theoretical work is needed to understand whether this is relevant in the CNT case. Third, the interactions in semiconducting CNTs may simply be stronger than expected, for reasons not yet elucidated.

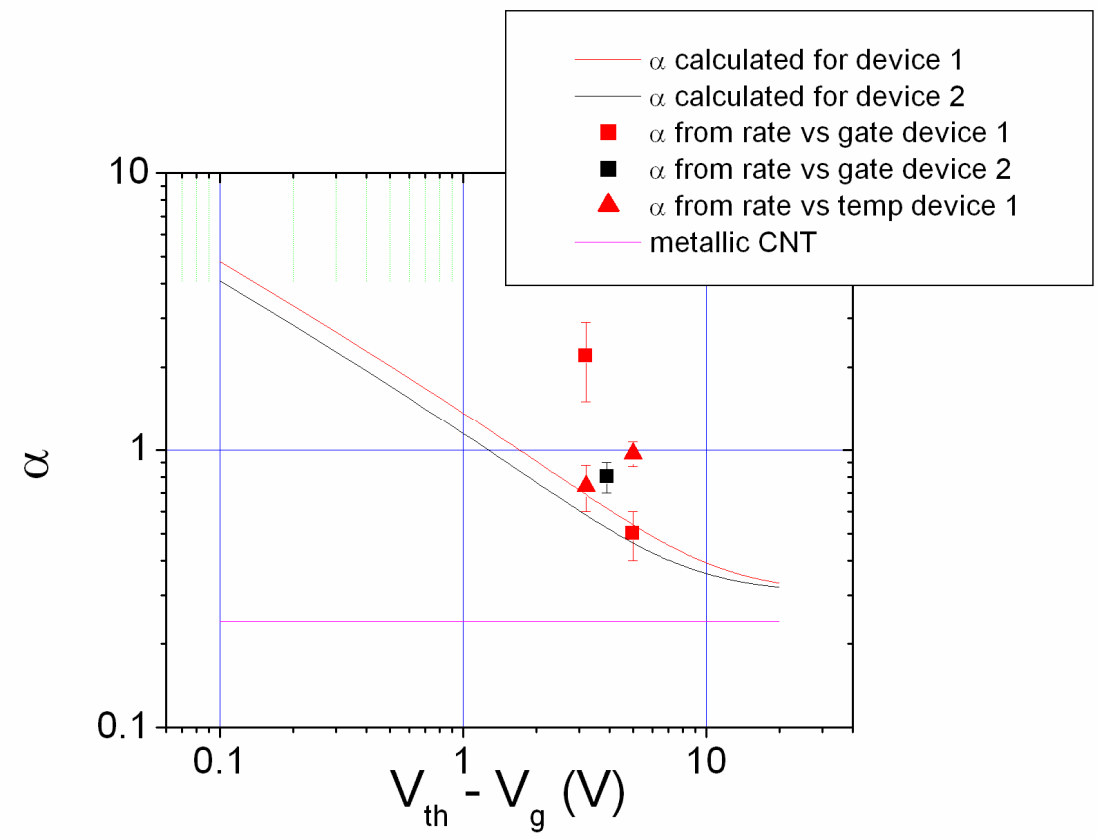

Figure 7-3. Depiction of the theoretical calculation of the Luttinger parameter α versus gate voltage. The red points are from two fluctuators on sample 1 and the black dot is from a fluctuator on sample 2. The squares indicate values obtained from fitting the individual rates vs gate voltage while the triangle points were obtained from fitting the rate vs. temperature. (both methods explained in text above) The details are given in the table below. The difference in the theoretical curves is due to the different diameters of the tubes, which results in a different band gap.

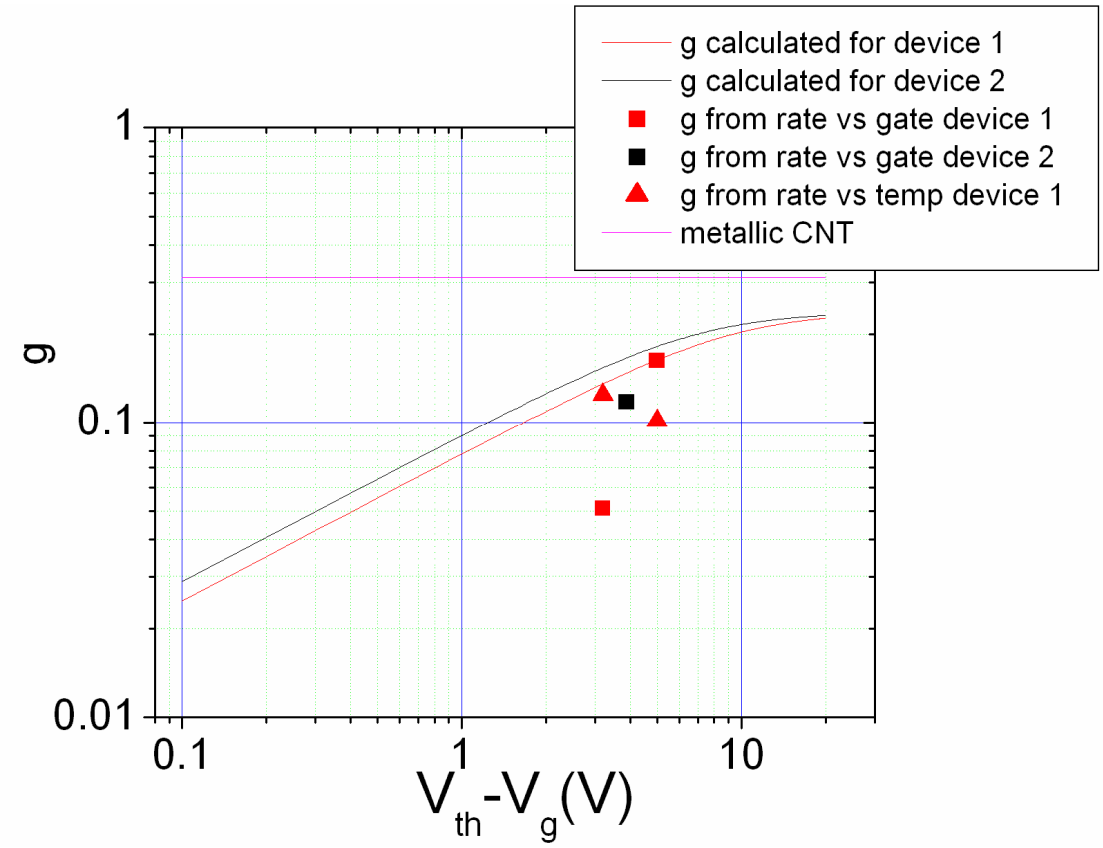

Figure 7-4. Depiction of the theoretical calculation of the Luttinger parameter g versus gate voltage. The red points are from two fluctuators on sample 1 and the black dot is from a fluctuator on sample 2. The squares indicate values obtained from fitting the individual rates vs gate voltage while the triangle points were obtained from fitting the rate vs. temperature. (both methods explained in text above) The horizontal line indicates the value for metallic CNTs. The difference in the theoretical curves is due to the different diameters of the tubes, which results in a different band gap.

Table 7-1. Luttinger parameter α for the three RTS.

Fluctuators	Diameter (nm)	$V_{threshold}$-V_{g0}	α_{rate}	α_{temp}
Sample 1	1.4	5.0	0.5 +/- 0.1	0.9 +/- 0.1
Sample 1	1.4	3.2	2.2 +/- 0.7	0.7 +/- 0.1
Sample 2	1.9	3.9	0.8 +/- 0.1	NA

Table 7-1 gives the details for the RTS signal studied in this chapter. The first two fluctuators are on the same device but at different gate voltages, with the first fluctuator having the largest range of observable fluctuations with respect to temperature. The last fluctuator was not stable over a wide enough range of temperatures to extract a fit for the change in rate vs. temperature.

In conclusion I have analyzed the temperature, bias voltage, and gate voltage dependence of the random telegraph signal resulting from an electron tunneling between a semiconducting carbon nanotube and a nearby defect. The RTS is used as a sensitive probe of the tunneling density of states of the Luttinger liquid state of the semiconducting CNT. We show that the tunneling rate is strongly suppressed at the Fermi level, consistent with Luttinger liquid theory confirming the more strongly interacting nature of electrons in semiconducting CNT relative to metallic CNT. Our value of $g<0.2$ indicates that the electrons in semiconducting CNTS are interacting more strongly than the electrons in metallic CNTs.

Abbreviations

1-D One dimensional

2DEG Two-dimensional electron gas

A/D Analog to digital

CAD Computer assisted drawing

CNT Carbon nanotube

CVD Chemical vapor deposition

DAQ Data acquisition

EBL Electron beam lithography

FET Field effect transistor

IPA isopropanol

LL Luttinger liquid

MIBK methylisobutylketone

MMA methylmethacrylate

MOSFET Metal-oxide-semiconductor field-effect transistor

PMMA polymethylmethacrylate

RTS Random telegraph signal

SEM Scanning electron microscope

TDS Tunneling density of states

UHV Ultra-high vacuum

Symbols

a	graphite lattice constant
a_1,a_2	graphene unit vectors
A	noise magnitude
β	correction to V^2 dependence of noise
C_G	gate capacitance
Δ	bandgap
$D(\ )$	density of states operator
d	CNT diameter
e	electron charge
E	energy
γ_0	tight-binding integral
γ_1, γ_2	rates into and out of an RTS system
$\hbar$	Planck's constant
I	current
$\mathbf{k}$	wave-vector
k_b	Boltzmann constant
$\mathbf{K}$	K point
f	frequency
n	density of electrons
N	number of electrons

q	wave vector from **K** point
R	rolling vector
R	resistance
S_I	current noise power
S_V	voltage noise power
T	temperature
τ	characteristic time of fluctuator
V	voltage
V_g	gate voltage
V_{sd}	source-drain voltage
Vth	threshold gate voltage (gate voltage where the device begins to conduct)
v_f	Fermi velocity
ω	angular frequency
z	exponent for $1/f^z$ noise (z close to 1)
ζ	Hooge noise parameter

Bibliography

[1] Iijima, S., Helical Microtubules of Graphitic Carbon. *Nature* **354**, 56-58 (1991).

[2] Dai, H., A.G. Rinzler, P. Nikolaev, A. Thess, D.T. Colbert, and R.E. Smalley, Single-wall nanotubes produced by metal-catalyzed disproportionation of carbon monoxide. *Chemical Physics Letters* **260**, 471-475 (1996).

[3] Thess, A., R. Lee, P. Nikolaev, H.J. Dai, P. Petit, J. Robert, C.H. Xu, Y.H. Lee, S.G. Kim, A.G. Rinzler, D.T. Colbert, G.E. Scuseria, D. Tomanek, J.E. Fischer, and R.E. Smalley, Crystalline ropes of metallic carbon nanotubes. *Science* **273**, 483-487 (1996).

[4] Bethune, D.S., C.H. Klang, M.S. de Vries, G. Gorman, R. Savoy, J. Vazquez, and R. Beyers, Cobalt-catalysed growth of carbon nanotubes with single-atomic-layer walls. *Nature* **363**, 605-607 (1993).

[5] Zheng, L.X., M.J. O'Connell, S.K. Doorn, X.Z. Liao, Y.H. Zhao, E.A. Akhadov, M.A. Hoffbauer, B.J. Roop, Q.X. Jia, R.C. Dye, D.E. Peterson, S.M. Huang, J. Liu, and Y.T. Zhu, Ultralong single-wall carbon nanotubes. *Nature Materials* **3**, 673-676 (2004).

[6] Hong, B.H., J.Y. Lee, T. Beetz, Y.M. Zhu, P. Kim, and K.S. Kim, Quasi-continuous growth of ultralong carbon nanotube arrays. *Journal of the American Chemical Society* **127**, 15336-15337 (2005).

[7] Miaudet, P., S. Badaire, M. Maugey, A. Derre, V. Pichot, P. Launois, P. Poulin, and C. Zakri, Hot-drawing of single and multiwall carbon nanotube fibers for high toughness and alignment. *Nano Letters* **5**, 2212-2215 (2005).

[8] Yakobson, B.I. and R.E. Smalley, Fullerene nanotubes: C-1000000 and beyond. *American Scientist* **85**, 324-337 (1997).

[9] Beyer, G., Flame retardancy of nanocomposites based on organoclays and carbon nanotubes with aluminium trihydrate. *Polymers for Advanced Technologies* **17**, 218-225 (2006).

[10] Baughman, R.H., A.A. Zakhidov, and W.A. de Heer, Carbon Nanotubes--the Route Toward Applications. *Science* **297**, 787-792 (2002).

[11] Hertel, T., R.E. Walkup, and P. Avouris, Deformation of carbon nanotubes by surface van der Waals forces. *Physical Review B* **58**, 13870 (1998).

[12] O. Breuer, U.S., Big returns from small fibers: A review of polymer/carbon nanotube composites. *Polymer Composites* **25**, 630-645 (2004).

[13] Collins, P.G., K. Bradley, M. Ishigami, and A. Zettl, Extreme oxygen sensitivity of electronic properties of carbon nanotubes. *Science* **287**, 1801-1804 (2000).

[14] Collins, P.G., M.S. Fuhrer, and A. Zettl, 1/f noise in carbon nanotubes. *Applied Physics Letters* **76**, 894-896 (2000).

[15] Banerjee, I.A., L. Yu, and H. Matsui, Location-Specific Biological Functionalization on Nanotubes: Attachment of Proteins at the Ends of Nanotubes Using Au Nanocrystal Masks. *Nano Lett.* **3**, 283-287 (2003).

[16] Kohli, P., C.C. Harrell, Z. Cao, R. Gasparac, W. Tan, and C.R. Martin, DNA-Functionalized Nanotube Membranes with Single-Base Mismatch Selectivity. *Science* **305**, 984-986 (2004).

[17] Hamada, N., S. Sawada, and A. Oshiyama, New One-Dimensional Conductors - Graphitic Microtubules. *Physical Review Letters* **68**, 1579-1581 (1992).

[18] Mintmire, J.W., B.I. Dunlap, and C.T. White, Are Fullerene Tubules Metallic. *Physical Review Letters* **68**, 631-634 (1992).

[19] Tans, S.J., A.R.M. Verschueren, and C. Dekker, Room-temperature transistor based on a single carbon nanotube. *Nature* **393**, 49-52 (1998).

[20] Odom, T.W., J.L. Huang, P. Kim, M. Ouyang, and C.M. Lieber, Scanning tunneling microscopy and spectroscopy studies of single wall carbon nanotubes. *Journal of Materials Research* **13**, 2380-2388 (1998).

[21] Postma, H.W.C., T. Teepen, Z. Yao, M. Grifoni, and C. Dekker, Carbon nanotube single-electron transistors at room temperature. *Science* **293**, 76-79 (2001).

[22] Durkop, T., S.A. Getty, E. Cobas, and M.S. Fuhrer, Extraordinary mobility in semiconducting carbon nanotubes. *Nano Letters* **4**, 35-39 (2004).

[23] Kane, C.L. and M.P.A. Fisher, Transport in a One-Channel Luttinger Liquid. *Physical Review Letters* **68**, 1220-1223 (1992).

[24] Bockrath, M., D.H. Cobden, J. Lu, A.G. Rinzler, R.E. Smalley, T. Balents, and P.L. McEuen, Luttinger-liquid behaviour in carbon nanotubes. *Nature* **397**, 598-601 (1999).

[25] Yao, Z., H.W.C. Postma, L. Balents, and C. Dekker, Carbon nanotube intramolecular junctions. *Nature* **402**, 273-276 (1999).

[26] Souza, A.G., A. Jorio, J.H. Hafner, C.M. Lieber, R. Saito, M.A. Pimenta, G. Dresselhaus, and M.S. Dresselhaus, Electronic transition energy E-ii for an isolated (n,m) single-wall carbon nanotube obtained by anti-Stokes/Stokes resonant Raman intensity ratio. *Physical Review B* **63**, 241404 (2001).

[27] Dresselhaus, M.S., G. Dresselhaus, and P.C. Eklund, *Science of fullerenes and carbon nanotubes*. 1996, San Diego: Academic Press.

[28] Saito, R., G. Dresselhaus, and M.S. Dresselhaus, *Physical properties of carbon nanotubes*. 1998, London: Imperial College Press.

[29] Wallace, P.R., The Band Theory of Graphite. *Physical Review* **71**, 622-634 (1947).

[30] Martel, R., T. Schmidt, H.R. Shea, T. Hertel, and P. Avouris, Single- and multi-wall carbon nanotube field-effect transistors. *Applied Physics Letters* **73**, 2447-2449 (1998).

[31] Ishigami, M., J.H. Chen, E.D. Williams, D. Tobias, Y.F. Chen, and M.S. Fuhrer, Hooge's constant for carbon nanotube field effect transistors. *Applied Physics Letters* **88**, 203116 (2006).

[32] Zhenhui, K., W. Enbo, M. Baodong, S. Zhongmin, C. Lei, and X. Lin, Obtaining carbon nanotubes from grass. *Nanotechnology* **16**, 1192 (2005).

[33] Kong, J., A.M. Cassell, and H.J. Dai, Chemical vapor deposition of methane for single-walled carbon nanotubes. *Chemical Physics Letters* **292**, 567-574 (1998).

[34] Kim, W., H.C. Choi, M. Shim, Y.M. Li, D.W. Wang, and H.J. Dai, Synthesis of ultralong and high percentage of semiconducting single-walled carbon nanotubes. *Nano Letters* **2**, 703-708 (2002).

[35] Tselev, A., K. Hatton, M.S. Fuhrer, M. Paranjape, and P. Barbara, A photolithographic process for fabrication of devices with isolated single-walled carbon nanotubes. *Nanotechnology* **15**, 1475 (2004).

[36] Brintlinger, T., Y.F. Chen, T. Durkop, E. Cobas, M.S. Fuhrer, J.D. Barry, and J. Melngailis, Rapid imaging of nanotubes on insulating substrates. *Applied Physics Letters* **81**, 2454-2456 (2002).

[37] Javey, A., J. Guo, Q. Wang, M. Lundstrom, and H. Dai, Ballistic carbon nanotube field-effect transistors. *Nature* **424**, 654-657 (2003).

[38] Zhang, J., A. Tselev, Y. Yang, K. Hatton, P. Barbara, and S. Shafraniuk, Zero-bias anomaly and possible superconductivity in single-walled carbon nanotubes. *Physical Review B (Condensed Matter and Materials Physics)* **74**, 155414 (2006).

[39] Gao, B., Y.F. Chen, M.S. Fuhrer, D.C. Glattli, and A. Bachtold, Four-Point Resistance of Individual Single-Wall Carbon Nanotubes. *Physical Review Letters* **95**, 196802-4 (2005).

[40] Dutta, P. and P.M. Horn, Low-frequency fluctuations in solids: 1/f noise. *Reviews of Modern Physics* **53**, 497 (1981).

[41] Hooge, F.N., 1/f noise is no surface effect. *Physics Letters A* **29**, 139-140 (1969).

[42] Hooge, F.N., 1/f noise sources. *Electron Devices, IEEE Transactions on* **41**, 1926-1935 (1994).

[43] Vandamme, L.K.J., L. Xiaosong, and D. Rigaud, 1/f noise in MOS devices, mobility or number fluctuations? *Electron Devices, IEEE Transactions on* **41**, 1936-1945 (1994).

[44] Machlup, S., Noise in Semiconductors: Spectrum of a Two-Parameter Random Signal. *Journal of Applied Physics* **25**, 341-343 (1954).

[45] Dutta, P., P. Dimon, and P.M. Horn, Energy Scales for Noise Processes in Metals. *Physical Review Letters* **43**, 646 (1979).

[46] Verleg, P.A.W.E. and J.I. Dijkhuis, Resistance fluctuations in hydrogenated amorphous silicon: Thermal equilibrium. *Physical Review B* **58**, 3904 (1998).

[47] Snow, E.S., J.P. Novak, M.D. Lay, and F.K. Perkins, 1/f noise in single-walled carbon nanotube devices. *Applied Physics Letters* **85**, 4172-4174 (2004).

[48] Ouacha, H., M. Willander, H.Y. Yu, Y.W. Park, M.S. Kabir, S.H.M. Persson, L.B. Kish, and A. Ouacha, Noise properties of an individual and two crossing multiwalled carbon nanotubes. *Applied Physics Letters* **80**, 1055-1057 (2002).

[49] Lin, Y.M., J. Appenzeller, J. Knoch, Z. Chen, and P. Avouris, Low-Frequency Current Fluctuations in Individual Semiconducting Single-Wall Carbon Nanotubes. *Nano Lett.* **6**, 930-936 (2006).

[50] Tersoff, J., Low-Frequency Noise in Nanoscale Ballistic Transistors. *Nano Lett.* **7**, 194-198 (2007).

[51] Kingrey, D., O. Khatib, and P.G. Collins, Electronic Fluctuations in Nanotube Circuits and Their Sensitivity to Gases and Liquids. *Nano Lett.* **6**, 1564-1568 (2006).

[52] Dumitrica, T. and B.I. Yakobson, Strain-rate and temperature dependent plastic yield in carbon nanotubes from ab initio calculations. *Applied Physics Letters* **84**, 2775-2777 (2004).

[53] Zhao, Q., M.B. Nardelli, and J. Bernholc, Ultimate strength of carbon nanotubes: A theoretical study. *Physical Review B* **65**, 144105 (2002).

[54] Ulbricht, H., R. Zacharia, N. Cindir, and T. Hertel, Thermal desorption of gases and solvents from graphite and carbon nanotube surfaces. *Carbon* **44**, 2931-2942 (2006).

[55] Tomonaga, S., *Prog. Theor. Phys* **5**, 544 (1950).

[56] Luttinger, J.M., Fermi Surface and Some Simple Equilibrium Properties of a System of Interacting Fermions. *Physical Review* **119**, 1153 (1960).

[57] Luttinger, J.M., An Exactly Soluble Model of a Many-Fermion System. *Journal of Mathematical Physics* **4**, 1154 (1963).

[58] Drude, P., *Annalen der Physik* **1**, 566 (1900).

[59] Ashcroft, N.W. and N.D. Mermin, *Solid State Physics*. 1976: Cornell University.

[60] Tinkham, M., *Introduction to Superconductivity*. 1975: Krieger Pub. Co.

[61] Landau, L.D., *Sov. Phys. JETP* **3**, 920 (1957).

[62] Pines, S., P. Nozieres, and W.A. Benjamin, *The Theory of Quantum Liquids I.* 1966, Menlo Park, California.

[63] Voit, J., One-dimensional Fermi liquids. *Reports on Progress in Physics* **58**, 977 (1995).

[64] Tarucha, S., T. Honda, and T. Saku, Reduction of quantized conductance at low temperatures observed in 2 to 10 [mu]m-long quantum wires. *Solid State Communications* **94**, 413-418 (1995).

[65] Yacoby, A., H.L. Stormer, N.S. Wingreen, L.N. Pfeiffer, K.W. Baldwin, and K.W. West, Nonuniversal Conductance Quantization in Quantum Wires. *Physical Review Letters* **77**, 4612 (1996).

[66] Milliken, F.P., C.P. Umbach, and R.A. Webb, Indications of a Luttinger liquid in the fractional quantum Hall regime. *Solid State Communications* **97**, 309-313 (1996).

[67] Chang, A.M., L.N. Pfeiffer, and K.W. West, Observation of Chiral Luttinger Behavior in Electron Tunneling into Fractional Quantum Hall Edges. *Physical Review Letters* **77**, 2538 (1996).

[68] Grayson, M., D.C. Tsui, L.N. Pfeiffer, K.W. West, and A.M. Chang, Continuum of Chiral Luttinger Liquids at the Fractional Quantum Hall Edge. *Physical Review Letters* **80**, 1062 (1998).

[69] Bockrath, M., D.H. Cobden, J. Lu, A.G. Rinzler, R.E. Smalley, L. Balents, and P.L. McEuen, Luttinger-liquid behaviour in carbon nanotubes. *Nature* **397**, 598-601 (1999).

[70] Ishii, H., H. Kataura, H. Shiozawa, H. Yoshioka, H. Otsubo, Y. Takayama, T. Miyahara, S. Suzuki, Y. Achiba, M. Nakatake, T. Narimura, M. Higashiguchi, K. Shimada, H. Namatame, and M. Taniguchi, Direct observation of

Tomonaga-Luttinger-liquid state in carbon nanotubes at low temperatures. *Nature* **426**, 540-544 (2003).

[71] Bockrath, M., D.H. Cobden, P.L. McEuen, N.G. Chopra, A. Zettl, A. Thess, and R.E. Smalley, Single-Electron Transport in Ropes of Carbon Nanotubes. *Science* **275**, 1922-1925 (1997).

[72] Tans, S.J., M.H. Devoret, H. Dai, A. Thess, R.E. Smalley, L.J. Geerligs, and C. Dekker, Individual single-wall carbon nanotubes as quantum wires. *Nature* **386**, 474-477 (1997).

[73] Egger, R. and A.O. Gogolin, Effective Low-Energy Theory for Correlated Carbon Nanotubes. *Physical Review Letters* **79**, 5082 (1997).

[74] Kane, C., L. Balents, and M.P.A. Fisher, Coulomb Interactions and Mesoscopic Effects in Carbon Nanotubes. *Physical Review Letters* **79**, 5086 (1997).

[75] Gao, B., A. Komnik, R. Egger, D.C. Glattli, and A. Bachtold, Evidence for Luttinger-Liquid Behavior in Crossed Metallic Single-Wall Nanotubes. *Physical Review Letters* **92**, 216804 (2004).

[76] Liang, W., M. Bockrath, D. Bozovic, J.H. Hafner, M. Tinkham, and H. Park, Fabry - Perot interference in a nanotube electron waveguide. *Nature* **411**, 665-669 (2001).

[77] Yaish, Y., J.Y. Park, S. Rosenblatt, V. Sazonova, M. Brink, and P.L. McEuen, Electrical Nanoprobing of Semiconducting Carbon Nanotubes Using an Atomic Force Microscope. *Physical Review Letters* **92**, 046401 (2004).

[78] Kanda, A., K. Tsukagoshi, Y. Aoyagi, and Y. Ootuka, Gate-Voltage Dependence of Zero-Bias Anomalies in Multiwall Carbon Nanotubes. *Physical Review Letters* **92**, 036801 (2004).

[79] Heinze, S., J. Tersoff, R. Martel, V. Derycke, J. Appenzeller, and P. Avouris, Carbon Nanotubes as Schottky Barrier Transistors. *Physical Review Letters* **89**, 106801 (2002).

[80] Fuhrer, M.S., B.M. Kim, T. Durkop, and T. Brintlinger, High-Mobility Nanotube Transistor Memory. *Nano Lett.* **2**, 755-759 (2002).

[81] Cobden, D.H. and B.A. Muzykantskii, Finite-Temperature Fermi-Edge Singularity in Tunneling Studied Using Random Telegraph Signals. *Physical Review Letters* **75**, 4274 (1995).

[82] Radosavljevic, M., M. Freitag, K.V. Thadani, and A.T. Johnson, Nonvolatile Molecular Memory Elements Based on Ambipolar Nanotube Field Effect Transistors. *Nano Lett.* **2**, 761-764 (2002).

[83] Arai, M.R., A fundamental noise limit for biased resistors at low temperatures. *Applied Physics Letters* **42**, 906-908 (1983).

[84] Chun, K. and N.O. Birge, Single-defect thermometer as a probe of electron heating in Bi. *Physical Review B* **49**, 2959 (1994).

[85] Roukes, M.L., M.R. Freeman, R.S. Germain, R.C. Richardson, and M.B. Ketchen, Hot electrons and energy transport in metals at millikelvin temperatures. *Physical Review Letters* **55**, 422 (1985).

[86] McEuen, P.L., M. Bockrath, D.H. Cobden, Y.-G. Yoon, and S.G. Louie, Disorder, Pseudospins, and Backscattering in Carbon Nanotubes. *Physical Review Letters* **83**, 5098 (1999).

[87] Ando, T., T. Nakanishi, and R. Saito, Berry's Phase and Absence of Back Scattering in Carbon Nanotubes. *Journal of the Physical Society of Japan* **67**, 2857-2862 (1998).

[88] Anderson, P.W. and G. Yuval, Exact Results in the Kondo Problem: Equivalence to a Classical One-Dimensional Coulomb Gas. *Physical Review Letters* **23**, 89 (1969).

[89] Souza Filho, A.G., A. Jorio, J.H. Hafner, C.M. Lieber, R. Saito, M.A. Pimenta, G. Dresselhaus, and M.S. Dresselhaus, Electronic transition energy E_{ii} for an isolated (n,m) single-wall carbon nanotube obtained by anti-Stokes/Stokes resonant Raman intensity ratio. *Physical Review B* **63**, 241404 (2001).

[90] Saito, R. and H. Kataura, *Optical Properties and Raman Spectroscopy of Carbon Nanotubes*, in *Carbon Nanotubes: Synthesis, Structure, Properties and Application*, M.S. Dresselhaus, G. Dresselhaus, and P. Avouris, Editors. 2001, Springer Berlin: Heidelberg. p. 213–247

[91] Ohtaka, K. and Y. Tanabe, Golden-rule approach to the soft-x-ray-absorption problem. III. The temperature dependence. *Physical Review B* **30**, 4235 (1984).